

Intelligent Roads

Project no. 012344

Specific Targeted Research Project
Sustainable Surface Transport, priority 1.6.2

D 2.1 – Model for Estimating Expectable Braking Distance

Due date of Deliverable: M15
Actual submission date: 02.07.2006

Start date of project: March 1 2005 Duration: 36 months

Project co-funded by the European Commission within the Sixth Framework Programme (2002-2006)		
Dissemination Level		
PU	Public	
PP	Restricted to other programme participants (including the Commission	X
RE	Restricted to a group specified by the consortium (including the Commission	
CO	Confidential, only for members of the consortium (including the Commission Services)	

Editors:

TASK LEADER AND MAIN EDITOR/CONTRIBUTOR

Minh-Tan Do
LCPC
Route de Bouaye – BP 4129
44341 Bouguenais – FRANCE
Tel: +33 (0) 2 40 84 57 95
Fax: +33 (0) 2 40 84 59 92
Email: minh-tan.do@lcpc.fr

WORK PACKAGE LEADER AND SECONDARY EDITOR/CONTRIBUTOR

Stefan Deix
Arsenal Research
TECHbase Vienna
Giefinggasse 2
1210 Vienna – AUSTRIA
Tel: +43 (0) 50550-6477
Fax: +43 (0) 50550-6599
Email: stefan.deix@arsenal.ac.at

SECONDARY EDITOR/CONTRIBUTOR:

Mattias Hjort
VTI
Olaus Magnus väg 35
581 95 Linköping- SWEDEN
Tel: +46 (0)13 20 42 91
Fax: + 46 (0)13 14 14 36

CONTRIBUTORS:

(in alphabetical order)
Stefan Deix (Arsenal research, Austria)
Yves Delanne (FEHRL/LCPC, France)
Minh-Tan Do (FERHL/LCPC, France)
Mattias Hjort (VTI, Sweden)
Pierre-Olivier Vandanjon (FEHRL/LCPC, France)

REVIEWED BY:

Peter Roe (TRL, Great-Britain)
Laurent Arnaud (ENTPE, France)
Sigvard Tim (VTI, Sweden)

Final control:				
Released by: Bengt Walivaara (VTI, Sweden) Signature: Date:				
Version	**Date**	**Prepared by**	**Checked by**	**Modifications**
1	01/06/2006	M.-T. Do	S. Deix, M. Hjort	1st draft outline
2	15/06/2006	All (phone meeting)		2nd draft outline
3	19/06/2006	All (phone meeting)		3rd draft outline
4	21/06/2005	S. Deix	M.-T. Do, M. Hjort	4th draft outline
5	21/06/2006	M.-T. Do	All	Version for peer reviewer + QM

Table of contents

Executive Summary (see separate document)

1 Context 8
2 Methodology and task organisation 9
3 Braking- and stopping distances 10
3.1 Stopping distance in four steps 11
3.2 Braking or stopping ? 11
3.3 Influence of vehicle type and braking system on braking distances 11
3.4 Tire/road friction and braking distance 13
3.4.1 Factors affecting braking distance 13
3.4.2 Road friction/braking distance relationship 13
4 Existing braking-distance models 15
4.1 AASHTO (Association of State Highway and Transportation Officials) model 15
4.2 Single-wheel model 15
4.3 Single-track model 16
4.4 Braking simulation 16
5 INTRO braking-distance model 17
5.1 Methodology and task organisation 17
5.2 Model implementation 20
5.3 Estimation of μ_{max} 22
5.3.1 μ_{max} from ROADSTAR 22
5.3.2 μ_{max} from BV12 24
5.3.3 μ_{max} from NIRA car (Audi A3) 27
5.3.3.1 Principle 27
5.3.3.2 Estimation of wheel slip (κ) 28
5.3.3.3 Estimation of slip slope, k-value 28
5.3.3.4 Estimation of μ_{max} 29
5.3.4 μ_{max} from Peugeot 406 30
5.3.4.1 Principle 30
5.3.4.2 Estimation of μ_{max} from front-wheel braking 30
6 Experiments 31
6.1 Summer 31
6.1.1 First campaign 31
6.1.2 Second campaign 33
6.2 Winter 34
7 Results 35
7.1 Deceleration curves 35
7.1.1 Deceleration curves from NIRA car (Audi A3) and Toyota Verso during “summer” tests (September 2005, Nantes, France) 35
7.1.1.1 Measurement Systems 36
7.1.1.2 Measurement assembly 36
7.1.2 Deceleration curves from NIRA car during winter tests (Arjeplog, Sweden) 37
7.1.3 Deceleration curves from Peugeot 406 car (September 2005, Nantes, France) 40
7.2 Summer tests (Nantes, France) 41
7.2.1 Braking distances 41
7.2.2 Estimation of “a”, “b” and “t_s” 42

7.2.3 Relationship between “a”, “b” and µRS 45
7.2.4 Comparison of measured-computed braking-distances 46
7.3 Winter tests (Arjeplog, Sweden) 47
7.3.1 Comparison of μ_{max} 47
7.3.2 Comparison of measured-computed stopping-distances 52
8 Conclusions 59
9 References 62
10 Appendices 64
10.1 Tire/ground relationship 64
10.1.1 Slip rate 64
10.1.2 Braking force and longitudinal friction coefficient 65
10.2 Vehicle dynamics during longitudinal braking 66
10.2.1 External forces 67
10.2.2 Dynamic model 68
10.3 Antilock Braking Systems 68
10.3.1 Principle 68
10.3.2 Hydraulic phases 69
10.3.3 ABS Electronic Control Unit 69
10.3.4 Simulation of ABS 69
10.4 Device descriptions 70
10.4.1 ROADSTAR 70
10.4.1.1 Principle of measurements 70
10.4.1.2 Measured data 72
10.4.2 BV12 73
10.4.2.1 The vertical load and the side slip angle 75
10.4.2.2 Force measuring system 75
10.4.2.3 Side slip angle and speed measuring system 76
10.4.2.4 On board vehicle water film application system for aquaplaning tests 76
10.4.2.5 VTI test vehicle BV12 specifications 77
10.4.2.6 Software for Measurement Control 78
10.4.2.7 Data acquisition and analysis 80
10.4.2.8 Contact 82
10.4.3 ADHERA 82
10.4.4 NIRA car (Audi A3) and Toyota Verso 83
10.4.4.1 Internal Sensors (Audi A3) 83
10.4.4.2 Applied (External) Measurement Systems (Audi A3 / Toyota Verso 83
10.4.5 Peugeot 406 84
10.4.5.1 Vehicle 84
10.4.5.2 System of measurement 85
10.4.5.3 Data acquisition 88
10.4.5.4 Estimation of wheel slip (κ) 88
10.4.5.5 Estimation of friction coefficient (µ) 89

Figure captions

Figure 1. Braking distance of vehicle on the LCPC test track [4] 12
Figure 2. Dry and wet surface braking distances [7] 12
Figure 3. Typical friction/slip curve 13
Figure 4. 3D friction map on an open graded bituminous concrete with 1mm water thickness 14
Figure 5. Friction map and braking 14
Figure 6. Four-wheel ABS (new vehicles) 17
Figure 7. Measured deceleration curve and approximation 18
Figure 8. Braking-distance model flowchart 19
Figure 9. Computation of braking-distance flow chart 20
Figure 10. VB express GUI 21
Figure 11. Tyres used for ROADSTAR in NANTES measurements 22
Figure 12. Plotted raw data 23
Figure 13. Three runs on surface 2 23
Figure 14. The VTI BV12 measurement vehicle for passenger tyre friction characterisation. 24
Figure 15. The VTI BV12 measurement vehicle from the rear. 24
Figure 16. Example of six consecutive brakings with the BV12 on snow at 20 km/h. 26
Figure 17. An average slip curve constructed from the six brakings in Figure 16 26
Figure 18. Schematic picture of slip curves (Gustafsson 1996) 28
Figure 19. Samples of μ and κ on dry asphalt (upper plots) and hard snow (lower plots) respectively circles and dots represent measurements on the left and right wheel respectively and the solid line is a straight line approximation (Gustafsson 1996) 29
Figure 20. Parameters used for μ_{max} calculation 30
Figure 21. LCPC test track (Nantes, France) 31
Figure 22. The VTI test vehicle BV12 in action at Colmis test track. 34
Figure 23. The ice track at Colmis test centre. 35
Figure 24. Test cars at NANTES test track Audi A3 (left) and Toyota Verso (right) .. 36
Figure 25. Setup for braking distance and deceleration measurements with Audi A3 and Toyota Verso 37
Figure 26. Deceleration curve (left) and braking distance diagram (right) for Audi with activated ABS and all season tire on surface 1. 37
Figure 27. The NIRA car with the Correvit sensor mounted at the front 38
Figure 28. Speed and deceleration curves obtained from braking on snow at 20 km/h. a) Unfiltered braking. b) Speed and acceleration filtered by a 3 Hz low pass filter. c) Filtered speed curves from three different brakings. d) Filtered deceleration curves from the same three brakings as in c). 39
Figure 29. Deceleration curves from Peugeot 406 40
Figure 30. Relationship between “a” factor and skid-resistance measured by ROADSTAR 45
Figure 31. Relationship between “b” factor and skid-resistance measured by ROADSTAR 46
Figure 32. The friction levels measured by the NIRA car on packed snow 47
Figure 33. The friction levels measured by the NIRA car on packed snow during brake tests from 20 km/h. 48
Figure 34. The friction levels measured by the NIRA car on packed snow during brake tests from various speeds 49
Figure 35. The friction levels measured by the NIRA car on ice 50
Figure 36. The slip curves on snow measured with the BV12 51
Figure 37. The slip curves on ice measured with the BV12 52

Figure 38. The measured velocity of the NIRA car during the ABS-braking phase... 54
Figure 39. Four different brakings with the NIRA car compared to an estimated curve 56
Figure 40. Slipping of the wheel 64
Figure 41. External forces applied on the wheel during braking 65
Figure 42. 3D braking curves 66
Figure 43. External forces acting on the braking longitudinal car..... 67
Figure 44. Basic structure for ABS control 70
Figure 45. Overview of the ROADSTAR 71
Figure 46. Skid resistance device 71
Figure 47. Calculation of friction coefficient µ..... 72
Figure 48. One tyre at one speed and slip, different surfaces..... 72
Figure 49. One surface, different tyres and speeds 73
Figure 50. One tyre, one surface, different slips and speeds..... 73
Figure 51. The VTI BV12 measurement vehicle for passenger tyre friction characterisation. 74
Figure 52. The VTI BV12 measurement vehicle from the rear. 75
Figure 53. Triaxial force measuring hub principle drawing. 76
Figure 54. The water nozzle supplying the water film for wet measurements..... 77
Figure 55. The main menu of the measuring program. 78
Figure 56. Menu for setting parameters for the brake/turn wheel measuring sequence. 79
Figure 57. Graphs of forces, speeds, and wheel angles shown after completion of the measuring sequence..... 80
Figure 58. Example of six consecutive brakings with the BV12 on snow at 20 km/h.81
Figure 59. An average slip curve constructed from the six brakings in Figure 58. 81
Figure 60. View of ADHERA 2 device and example of data recording..... 82
Figure 61. NIRA Car (Audi A3) with external Sensors 83
Figure 62. The Toyota Verso with mounted external measurement device 84
Figure 63. Peugeot 406..... 84
Figure 64. Inertial system Crossbow VG700AA-201..... 85
Figure 65. Correvit Datron DLS1..... 86
Figure 66. Encoder 10 000 pulses/turn Hengstler RI-58 87
Figure 67. Torque sensor 87
Figure 68. Laser sensor for tyre radius measurement 88
Figure 69. PC with Labview..... 88
Figure 70. Braking without ABS at 40 km/h – Analysis of encoders signal just after braking 90
Figure 71. Braking with ABS at 40 km/h – Analysis of encoders signal just after braking 91
Figure 72. Braking without ABS at 80 km/h – Analysis of encoders signal just after braking 91
Figure 73. Braking with ABS at 80 km/h – Analysis of encoders signal just after braking 92

1 Context

Pavement skid-resistance is an essential factor of road safety. It is defined as the maximum value of the coefficient of friction between a wheel and the pavement surface, denoted as μ_{max}. Typically, this friction coefficient ranges from 0,05-0,20 on ice to 0,6-1,2 on dry asphalt roads, with packed snow exhibiting intermediate values of 0,2-0,5. It would be beneficial both for the driver, but also for the vehicle, to obtain information about the attainable friction levels. As the friction coefficient itself may be a concept which is too abstract for the driver to grasp during driving, it would be desirable with a more intuitive measure of the available grip between tyres and road. Thus, a stopping distance model based on skid-resistance data has been developed and tested.

It has been the purpose of INTRO Task 2.2, to link pavement skid-resistance to vehicle stopping-distance. The field measurements required for determining parameters and for validation of the model, were performed within INTRO Task 2.1. It should be noted that even if the relationship between skid-resistance and stopping distance is intuitive, its quantification is not straightforward. Actually, stopping distance depends on many factors other than pavement skid-resistance: vehicle type, braking system, tyre, etc. A realistic model had then to be developed. It should be nevertheless simple enough to be easily implemented in a warning system.

Pavement skid-resistance is usually measured by monitoring devices, which comprise a vehicle equipped with a 5th wheel. This practice, widely employed by road administrators, has one drawback since monitoring devices are (or can) not always be present on roads to deliver real-time information, especially when weather conditions are bad. An alternative solution would be to estimate the pavement skid-resistance using normal vehicles as “friction probes” although these will not be as accurate as using a standard 5th wheel.

This leads to three different ways an ordinary “non-probe” vehicle may receive and process the information thus made available by the road/tyre skid-resistance measuring devices (5th wheel as well as car probes).

- The vehicle may receive skid-resistance data from the standard monitoring devices employed by road administrators. In order to process this data, information regarding the receiving vehicles´ own tyres, ABS-brakes, weight (including passengers and load) must be factored in to estimate the attainable skid-resistance for this particular car.
- The vehicle may receive skid-resistance data from probe vehicles driving on the road, equipped with a skid-resistance measuring system. All these skid-resistance measuring vehicles will report skid resistance values that are affected by the specific tyres and weights of these probe vehicles. In order to process this data, information regarding the receiving vehicles´ own tyres, ABS-brakes, weight (including passengers and load) must be factored in to estimate the attainable skid-resistance for this particular car.
- The vehicle may receive skid-resistance data from its own skid-resistance measuring system. Then, only information regarding the vehicles´ own braking system is needed for estimating the attainable skid-resistance for this particular car.

The first two methods require that skid-resistance data measured by a different vehicle (or vehicles) need to be translated into valid skid-resistance values relevant for the receiving vehicle. For that, information about this vehicles´ own tyres, weight and braking system need to be taken into account, and in practice this means that the entire vehicle needs to be tested together with the reference monitoring device(s) or probe vehicle(s) on surfaces with various friction levels in order to determine true conversion parameters. However, for such a method to be useful, one must be able to change tyres of the car and it must be possible to use worn tyres, without having to redo these tests.

The third method does not suffer from problems with different tyres or tyre wear. Whether it is affected by changing the number of passengers or load is not clear, but that should depend on the particular algorithm used for the friction estimation. Presently there are no commercial systems available for the private consumer, and the accuracy of such systems under development is unclear. The main drawback of method 3 is that no information about friction levels on the road ahead of the vehicle is received.

One can argue that method 3 is outside the scope of INTRO, as it does not involve intelligent roads. However, the method is interesting since it may be combined with Method 1 or 2. Such a combination may solve the apparent problems of the first two methods, as an onboard friction measurement system continuously will aid in finding the true conversion parameters regardless of the particular tyres on the car.

In this study we have focused on the first two methods, using the Arsenal ROADSTAR and the VTI BV12 measurement vehicles as standard monitoring devices. The probe vehicles driving on the road, equipped with a skid-resistance measuring system is represented by a solution from a Swedish Company, NIRA Dynamics AB. The test vehicle itself was represented by four different vehicles: a Renault Clio, a Peugeot 306, a Peugeot 406 and a NIRA dynamics equipped Audi A3. Due to the restricted budget of the INTRO Task 2.1 we could only use one kind of tyre for the braking tests We chose an all season tyre, the Vredestein Quatrac.

This deliverable deals with the model development and its validation through two test campaigns performed on test tracks. The work reported is strongly relying on the results from task 2.0 [1] dealing with the system assembly and methods of friction estimation from sensor-equipped cars (also called probe cars), and task 2.1 [2] comprising the test campaigns in Nantes (summer conditions) and Arjeplog (winter conditions).

2 Methodology and task organisation

One major effort within INTRO WP2 deals with creating models for translating the skid resistance due to water, snow or ice into a useable parameter, vehicle stopping distance. The stopping distance model has two components “summer” and “winter”. Both models must use the same input: the pavement skid-resistance, which may be provided using two possible methods:

- monitoring devices, which represent today’s way of obtaining pavement skid-resistance through yearly recurring measurement campaigns (“static data”)..

- sensor-equipped light vehicles, called also “probe vehicles”, which represent the future vision of obtaining up-to-date real-time information on pavement skid-resistance (“dynamic data”).

Within the frame of WP2, it is not possible to validate general stopping distance model valid for all monitoring devices and all car types. The limitations are:

- Provision of a “static data” solution, using input from ROADSTAR from Arsenal and BV12 from VTI used for summer and winter conditions respectively;
- Provision of a “dynamic data” solution, using input from two cars (Audi A3 from Arsenal and VTI) equipped with a prototype friction-estimation method developed by a Swedish Company, NIRA Dynamics AB. This method provides maximum tyre/road friction from the knowledge of wheel slip and friction forces mobilised during car movements. Both cars are referred to as “NIRA cars” further in this report;
- Model is based on use of one tyre type.

As complementary to the above, the following additional investigations were also performed in conjunction to the field trials:

- Arsenal assessed the influence of tyre type and tyre wear on stopping-distance. This was achieved using a fully instrumented Toyota Verso;
- LCPC assessed the performance of an alternative friction-estimation method by using a fully instrumented Peugeot 406;
- LCPC assessed the performance of a French monitoring device, called ADHERA, in measuring the full friction-slip curve.

The task organisation was:

- LCPC were in charge of the model development, the linking with ROADSTAR measurements and its validation through comparisons with measured stopping-distances in Nantes. Tests with ADHERA and Peugeot 406 were also included in the responsibility of LCPC.
- Arsenal was in charge of the test with ROADSTAR, Audi NIRA-car and Toyota Verso. Pre-processing of data was also included in Arsenals´ responsibility.
- VTI was in charge of the adaptation of the model to winter conditions and the conduction of winter-test with BV12 and the NIRA-car.

3 Braking- and stopping distances

In addition to what is mentioned in the previous chapter, stopping distance and braking is chosen as a describer, because it is the most current reaction of drivers to unanticipated events on the road. In such situations road users take suddenly conscience of the effectiveness of their braking system and of the limits set by the available friction. Friction and adherence are concepts that are not really understood by the common driver. Even in the road technical world confusion remains. So many indices are used and their relationship is not clearly known [3][4], and besides their relationship to the actual potential of a vehicle is not straightforward. Stopping distance seems to be an understandable concept by road users even if they have some difficulties to get the real sense of this performance (referring to their behaviour in vehicle lines).

3.1 Stopping distance in four steps

The effective stopping distance of a vehicle depends on:

1. the time, the driver requires to become aware of a critical situation, to process this awareness mentally and to then move his foot from the accelerator to the brake pedal,
2. the time period starting from when the driver first touches the brake pedal and start to press the pedal
3. the time the brake pressure builds up to the final value that the driver gives to the brakes. In this time, the wheel brakes eliminate the remaining kinetic energy of the vehicle up to a full braking effect (load transfer),
4. the time of effective deceleration during the full braking effect phase until the car stop.

The car runs on during the two first phases at almost starting speed, only the drag torque from the engine and drive train and the tyres rolling resistance have a slight decelerating effect. Drivers use up about ¾ of second, in the best case (paying full attention), to react to an emergency and start hitting the brakes to a complete action, but time over 1 second is a more realistic time used. The effective stopping distance is the addition of distances cover for these four phases. It is clear that one of the most important factors affecting braking distance is car speed. The distance covers during the full braking depends on the braking equipment technology and braking system.

3.2 Braking or stopping ?

At this stage, it is quite important to differentiate “braking” and “stopping” senses:

- “stopping” consists of four steps as described in 3.1, where the first one is the reaction one;
- “braking” comprises steps 2 to 4, starting when the driver touches the brake pedal, and ending when the vehicle is completely stopped.

Actually, the model employed in this report does not take into account the driver reaction: we model only the braking distance. In the rest of this report, the word “braking” is then used.

3.3 Influence of vehicle type and braking system on braking distances

In 2002, LCPC carried out an experiment on its test track (unpublished results), the objective was the recording of the speed curve up to stop for different vehicles as input data for a vehicle line simulation. Each vehicle in its state was driven by the same person and the operating command was an emergency full push down of the brake pedal without any movement of the driving wheel.

The curves on Figure 1 correspond to different vehicles: cars (mainly), 2 vans, and one light lorry. Shorter braking distances were obtained with car fitted with ABS and the longest braking distance was obtained with the lorry (locked wheels) on a wet bituminous concrete section.

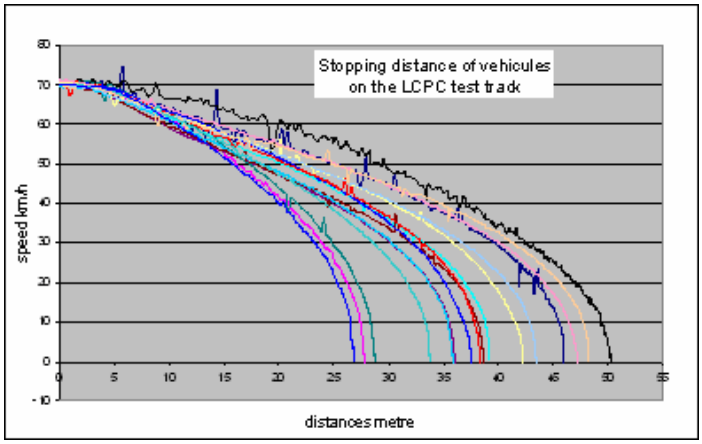


Figure 1. Braking distance of vehicle on the LCPC test track [4]

Recent passenger vehicles equipped with a four wheel sensors anti lock system give almost similar braking distances (27/29m).

A comparison of performances of passenger cars equipped with ABS for different manoeuvres including braking, on was carried out in the USA [5][6][7]. Some results are directly relevant to the question addressed in this report. For instance, braking distances for 10 vehicles with 4 wheel speed sensors ABS at 100 km/h on a dry bituminous concrete vary from 43m to 61m, ranking of vehicle on wet surfaces was different but approximately correlated (Figure 2) [7].

Considering that temperature of the brake discs and pads and tire were similar in all cases, the differences in braking distance for these vehicles are mainly explained by:

- the braking system technology
- the wear of the brake pads
- the front/rear brake balance
- the slip/friction of the tire/road couple

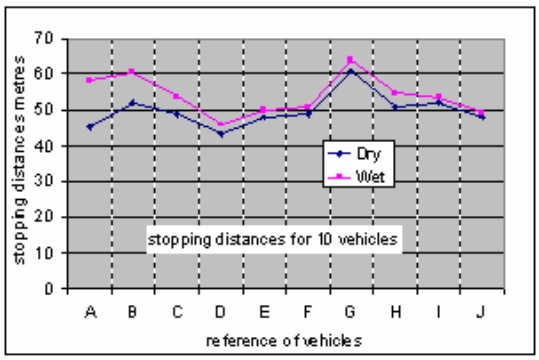


Figure 2. Dry and wet surface braking distances [7]

3.4 Tire/road friction and braking distance

3.4.1 Factors affecting braking distance

Various experiments have shown that the total braking distance depends on the following factors:

- the type of braking system, brake pad material, brake alignment, brake bias (balance)
- tyre pressures, tyre tread and grip (which depends on the road characteristics and condition)
- vehicle weight, suspension system, the braking technique applied by the driver,
- wind speed,
- slope of road, surface smoothness.

3.4.2 Road friction/braking distance relationship

Brakes applied to the wheels transfer their effort to the road surface through tyre contact where tangential longitudinal forces are generated. It is customary to describe the longitudinal friction performance of a tyre / road couple by the slip coefficient of friction curve as shown in Figure 3 (see 10.1.1 for slip definition).

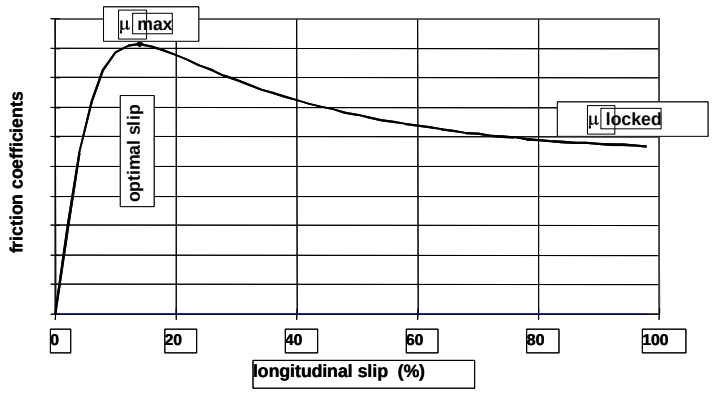


Figure 3. Typical friction/slip curve

The friction/slip curve varies for different speeds. The influence of the load can be considered as negligible. A 3D map (Figure 4) is a more correct way to describe the longitudinal forces that can be generated on the tire road contact patch.

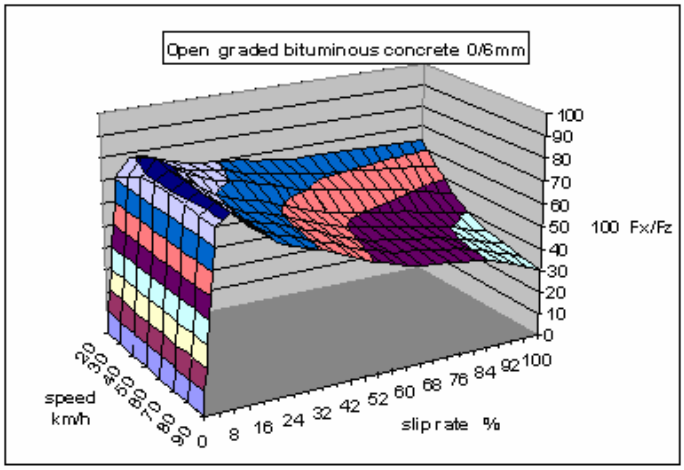


Figure 4. 3D friction map on an open graded bituminous concrete with 1mm water thickness

Figure 5 aims at illustrating the difference between ABS braking and locked wheel. For a vehicle without ABS the generated longitudinal force corresponds to the magenta line. For a panic braking manoeuvre, it takes less than 1second to follow the path from 0 to 100% slip rate, then the slip rate remain at 100% and the friction force is directly dependent on skidding performances of the tire/road couple versus speed.

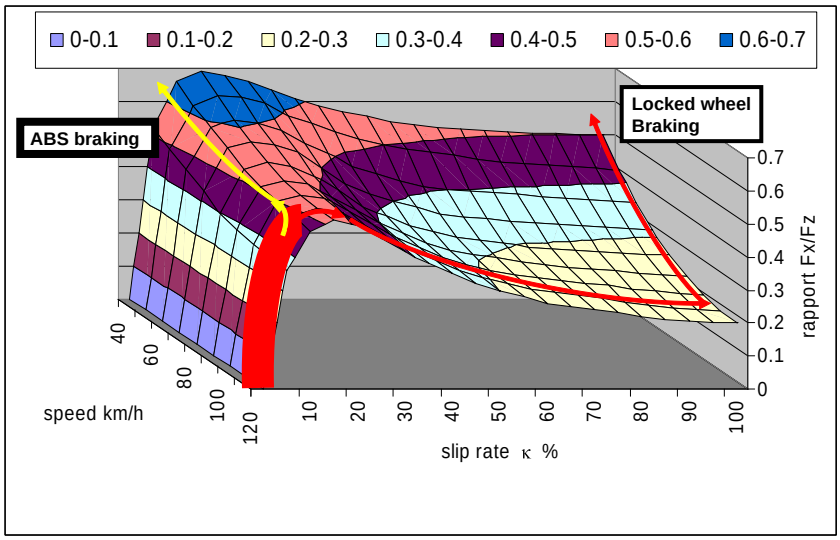


Figure 5. Friction map and braking

For cars with ABS, as the ECU (Electronic Control Unit, see 10.3) seeks to continually optimise the slip to generate the maximum deceleration the targeted path is as close as possible to the ridge of the 3D map (red line on Figure 5). The path really followed depends on the controller algorithm and on the response of the braking system.

4 Existing braking-distance models

Different models are presented hereafter from the simplest to the more complex implemented in vehicle dynamics simulation programs.

4.1 AASHTO (Association of State Highway and Transportation Officials) model

This model is a point kinematics model based on the work/energy theorem stating that the initial amount of total mechanical energy (total initial mechanical energy plus the work done by external forces is equal to the final amount of total mechanical energy) yielding:

$$(1)\quad d = \frac{V^2}{2g(\mu - G)}$$

where V: vehicle speed before the braking [m/s];
μ: friction coefficient independent of speed;
G: road surface gradient [%];
g: acceleration of gravity [m/s²].

This rather simple model is used in accident reconstruction and road design. This model has been improved in taking into account the transient phase previously described.

4.2 Single-wheel model

$$(2)\quad X(t) = \int_0^t V(t)dt$$

$$(3)\quad V(t) = V_o + \int_0^t \gamma_t dt$$

$$(4)\quad \gamma(t) = \mu(\kappa(t), V(t))g$$

where μ: coefficient of friction;
$\kappa(t)$: tire slip, which is equals to $\frac{V(t) - \omega(t)R_{eff}}{V(t)}$;
$\omega(t)$: angular speed;
R_{eff}: effective rolling radius.

This model is a simplified version of the following model which takes into account more external forces:

$$(5)\quad SD = M\int_0^V \frac{VdV}{F_{aero} + F_{rr} + F_{grade} + F_{friction}}$$

The single wheel model does not take into account the weight transfer and the front/rear brakes balance (or bias).

4.3 Single-track model

The main difference from the previous model the introduction of the front and rear friction force which depends on:

- the actual load (weight transfer);
- the rear/front balance;
- the friction available which depends on the instantaneous slip of the wheels and on the vehicle speed.

Other factors as grade and air and rolling resistance can be taken into account in adding complementary terms to the instantaneous deceleration. This deceleration is speed dependent for the aerodynamic and the rolling resistance.

For the calculation of wheel vertical forces, taking:

- M: vehicle mass
- E: wheel base
- « a »: distance from cog « G » to the front wheel axle unit
- « b »: distance from cog « G » to the rear wheel axle unit
- H: height of cog (ground reference)
- $F_{zG} = m \times g$
- F_{zr} , F_{zf}: vertical forces, r for rear, f for front
- γ : longitudinal deceleration
- θ: slope angle

and assuming there is no cross slope, we have:

$$(6)\quad F_{zf} = m \times g \times \frac{b}{E}\cos\theta + m \times g \times \frac{H}{E} \times \left(\frac{\gamma(\kappa(t), V(t))}{g} \pm \sin\theta \right)$$

$$(7)\quad F_{zr} = m \times g \times \frac{a}{E}\cos\theta + m \times g \times \frac{H}{E} \times \left(\frac{\gamma(\kappa(t), V(t))}{g} \pm \sin\theta \right)$$

So the friction forces will be:

$$(8)\quad F_{fricf}(t) = F_{zf} \times \gamma(\kappa(t), V(t))$$

$$(9)\quad F_{fricr}(t) = F_{zr} \times \gamma(\kappa(t), V(t))$$

One key point for this model is the estimation of the friction coefficient that means tracking the slip rate. The question is addressed in the next paragraph.

4.4 Braking simulation

To simulate the ECU, we need a correct longitudinal friction curves. We assume that the first part of the 3D map, i.e. until the vicinity of the maximum friction coefficient is

independent of the longitudinal speed then, a rather simple model[1] can be used with the three following elements:

- longitudinal stiffness K_x
- the maximum friction μ_{peak} and the corresponding slip.

The main question and difficulty is to build up a connection between the vehicle tire slip curve and the measurement carried out with a skid resistance device. This problem had been addressed and solved few years ago in Netherland by TNO [8][9][10]. The solution implemented was a scaling of the “Magic Formula” (Pacejka’s model) parameters from skid and texture measurement. Braking distances are computed with vehicle dynamic simulation software including four independent braking controls for modern car with ESP (Figure 6).

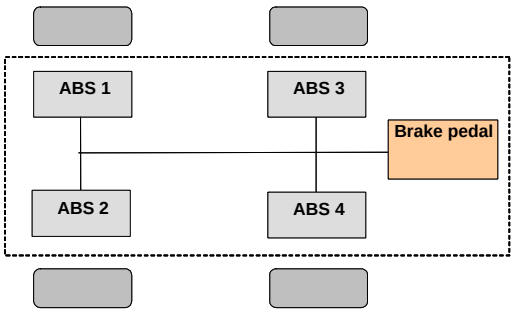


Figure 6. Four-wheel ABS (new vehicles)

5 INTRO braking-distance model

5.1 Methodology and task organisation

It has been proved that the speed dependent deceleration during a brake test with locked wheel correlates well to the speed-dependent skid-resistance coefficient (locked wheel) in the shape and altitude [8]. This is not as simple as that for ABS braking. The most sophisticated method, the braking simulation using a vehicle dynamics simulation package with a tire/road friction model is not applicable to the INTRO program. The single track model needs further information, for example brake balance, which cannot be measured on line.

The most adapted solution is to exploit directly the deceleration curve, expressing the temporal variation of deceleration during a braking manoeuvre, in its two parts: transient and quasi stabilised regions (Figure 7). This method has been more or less set forth for in [11] for accident reconstruction to assess the speed at the onset of braking from skids marks.

[1] Dugoff, Rado for exemple [18]

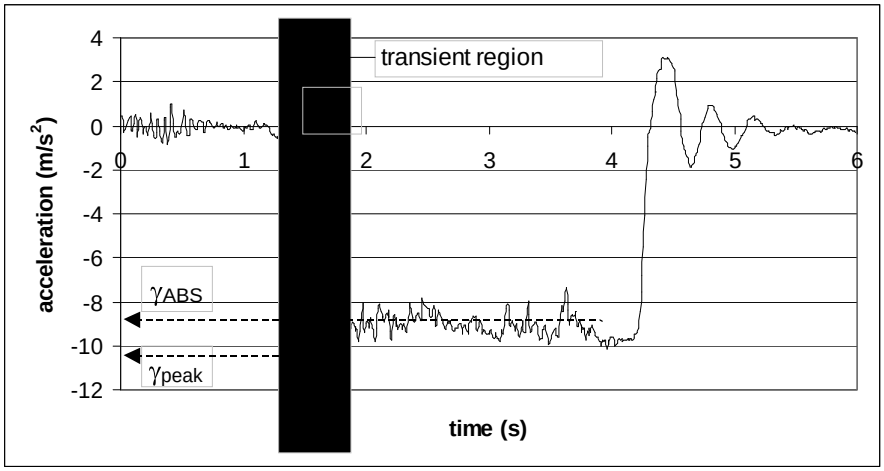


Figure 7. Measured deceleration curve and approximation

In the transient region, the deceleration can be expressed as:

(10) $$\gamma(t) = \frac{\gamma_{peak}}{t_s} t$$

where t_s: time at which deceleration becomes (quasi)stabilised.

From t_s to stop, the deceleration can be expressed as:

(11) $$\gamma(t) = \gamma_{ABS} .$$

We admit that γ_{peak} and γ_{abs} are somehow related to the maximum friction coefficient μ_{max} (Figure 3). So:

(12) $$\gamma_{peak} = a\mu_{max} g$$

and

(13) $$\gamma_{abs} = b\mu_{max} g$$

where a, b: weighting coefficients.

The coefficients *a* and *b* are not identical, as *a* describes the maximum deceleration and *b* describes the average deceleration during the quasi-steady phase. As the deceleration is negative both *a* and *b* are negative, with absolute values smaller than one. The absolute value of *a* is also larger than the absolute value of *b*.

μ_{max} can be any friction value measured by friction devices at a speed of the order of the initial vehicle speed; the best solution would be μ_{max} at the speed reached after the transient phase. $\gamma(t)$ is integrated twice in order to compute the braking time. If b

is constant, the integration is readily done and yields to an analytical solution [2].

The INTRO braking model is then based on the modelling of deceleration curves, which require four parameters:

- "a" and "b" factors, which should be related to vehicle braking-system;
- "t_s", which should be related to speed and also to vehicle braking-system;
- "μ_{max}", which is related to pavement skid-resistance.

INTRO WP2 deals with slippery risks due to water, snow or ice. The model has then two components: "summer" and "winter". Theoretically, both components must use the same inputs. However, their development is executed as two separate sub-tasks for at least two reasons:

- physical phenomena during tire/wet-road and tire/snowy- or icy-road contacts are not the same. This difference can have significant consequences on "a", "b" and "t_s" determination;
- μ_{peak} might not be provided by the same vehicle, mostly in the case where values come from monitoring devices.

The last point creates a supplementary difficulty in the model development, since the aim of INTRO is to predict braking distances using two μ_{peak}-measuring possibilities:

- monitoring devices, which represent the "short-term" solution;
- sensor-equipped light cars, called also "probe cars", which represent the "long-term" solution.

Since there is no evidence regarding the relationship between these two possibilities, we must also verify that their μ_{peak} are the same, or at least related each to the other.

The general organisation of the braking-distance model development is shown in Figure 8.

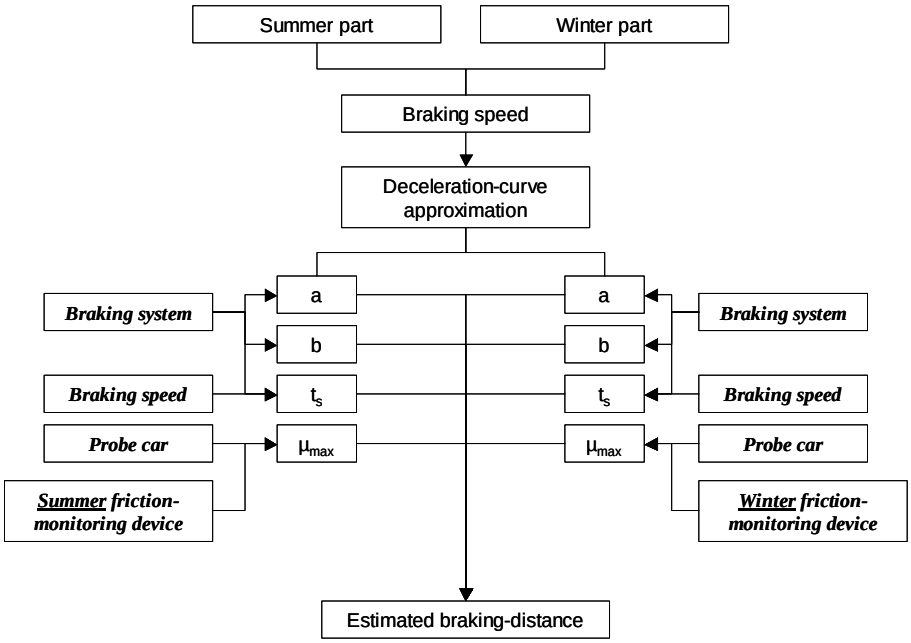


Figure 8. Braking-distance model flowchart

5.2 Model implementation

The Figure 9 explains the algorithm written in Visual Basic.Express edition [2].

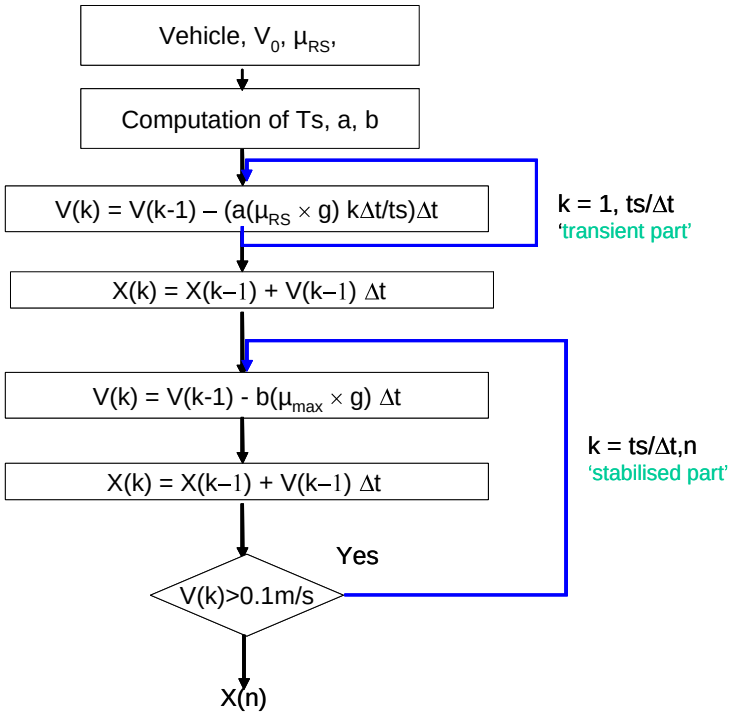


Figure 9. Computation of braking-distance flow chart

The example is shown for "summer" component, in which:

- μ_{max} is represented by friction-coefficient value provided by ROADSTAR "μ_{RS}".
- V_0 is the vehicle speed at which the driver starts to brake.
- k is an increment which varies from 1 to $t_s/\Delta t$ during the transient part and from $t_s/\Delta t$ to the end of this algorithm during the stabilised part.
- Δt is the time step, which is 0.001 second in the current algorithm.

At the beginning of this study, the model aimed to take into account the speed-dependency of friction. With this additional feature, the deceleration integration can not be done analytically. Analysis of experimental data shows that the speed-dependency assumption does not increase significantly the accuracy of the braking-distance prediction. In this case, it is straightforward to integrate the deceleration two times to calculate the braking distance. However, the general algorithm is maintained here in order to have later the possibility to complicate the model if necessary.

[2] Free download from Microsoft time (1 year limited usage)

For winter conditions, *b* may not necessarily be constant during the quasi-stabilised phase; it can be time- and speed dependent. There are at least two reasons for assuming that *b* would not be constant during braking on snow and ice:

- Water could be formed between the tyre and the road surface as a result of the heat generation during the braking, and thus leading to a lowering of the attainable friction with time as the braking proceeds. This effect has been observed for fully locked wheel braking on ice in the VTI Stationary Tyre Test Facility [12]. However, for ABS braking we do not expect any water build up, unless the temperature is very close or above zero degrees Celcius.
- If μ_{peak} is strongly speed dependent, this may be represented by introducing a speed dependence in *b*, while keeping μ constant. This actually allows for b to grow larger than one during the braking process.

It is also a well known phenomenon that ABS brakes perform poorly on loose surfaces like gravel or really loose snow. In this case braking distances twice the length compared to non ABS braking distances have been reported [13]. In such a scenario *b* takes a small value and its time dependence is unclear.

The Graphic User Interface (“summer” component example) is shown Figure 10.

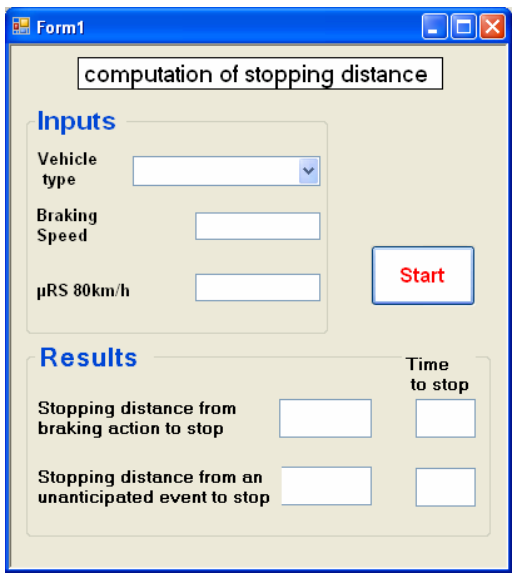


Figure 10. VB express GUI

Inputs to run the program (click “Start”) are:

- select the vehicle in the list box
- type the speed before braking
- type the ROADSTAR coefficient µRS (European notation : 0,785 : with a comma).

Let us note that the inputs needed for the calculation will either be provided by the INTRO system - µRS from the Server and the parameters a, b from the onboard

system as they are car, tyre, etc. dependent. For the development phase in this task the program uses manual inputs.

5.3 Estimation of μ_{max}

As it was stated in the paragraph 5.1, the input μ_{max} can be provided by probe cars or friction-monitoring devices. Since the friction measuring- or estimation principles are not identical, a brief description is given in this paragraph for all apparatus involved in INTRO program.

5.3.1 μ_{max} from ROADSTAR

The actual measurements were carried out with different constant slip of 18 %, 37.5 %, 50 % and 75 % to cover the upper part the μ-slip-curve starting from μmax at 18 % slip. A water film thickness of 0.5 mm and speeds of 40 km/h, 60 km/h, 80 km/h and 100 km/h were chosen. To cover the full spectrum of nowadays tyres for summer conditions, five different types of tyres were used – see Figure 11:

- All season (Vredestein Quatrac) – 18 %, 37.5 %, 50 %, 75 % (1)
- Summer new (Dunlop SP9) – 18 % (2)
- Summer worn (Dunlop SP9, 1.6 mm profile depth) – 18 % (3)
- PIARC ribbed standard tyre – 18 % (4)
- PIARC smooth standard tyre – 18 %, 37.5 %, 50 %, 75 % (5)

It should be noted that only results from Vredestein tyres are used for the braking model.



Figure 11. Tyres used for ROADSTAR in Nantes measurements

The measurements were carried out on six different surfaces (see description in Chapter 6.1). A wheel load of 3500 N was used. Two or three runs with each slip ratio and each tyre on each surface and speed were done, resulting in a total of 350 measurements.

Each measurement run covered three different surfaces. To ensure good measurement repeatability, a lane with a width of one meter was marked on the surfaces. This lane had to be followed with the measurement wheel. Each beginning and end of a surface was marked during the measurement by the operator (see Figure 12).

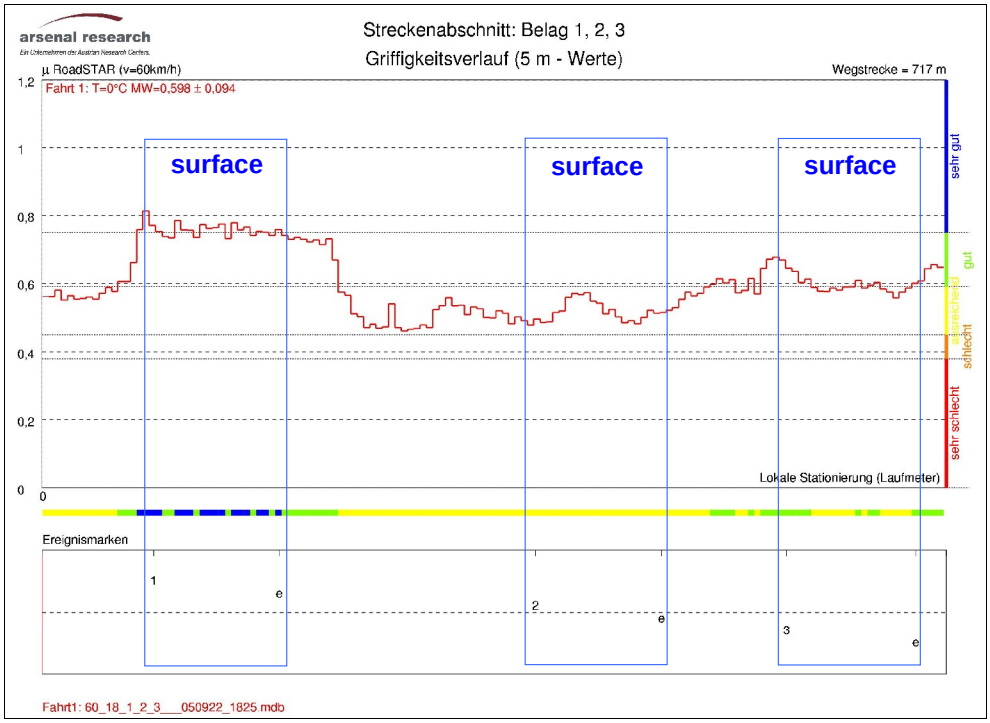


Figure 12. Plotted raw data

After the measurements, the different surface sections were cut out and saved as separate files. The different runs on each surface were compared (see Figure 13) and due to plausibility checks a characteristic run for further analysis was chosen.

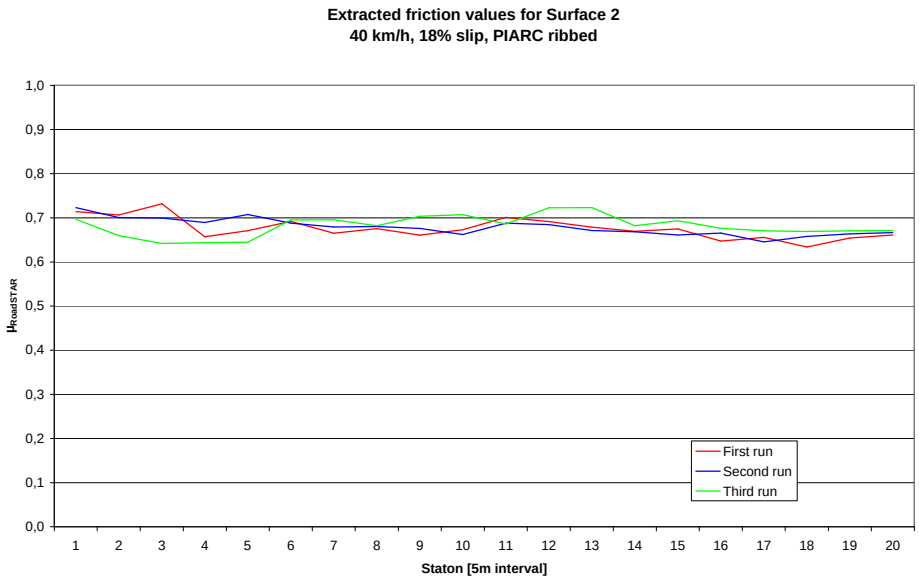


Figure 13. Three runs on surface 2

5.3.2 μ_{max} from BV12

The VTI friction test vehicle BV12 shown in Figure 14 and Figure 15 is a specially equipped truck with a test wheel suspension for passenger car wheels. The test wheel can be braked by a hydraulic disc brake connected to the wheel via a cardan shaft. This allows the braking slip to be continuously varied between 0-100%. (Slip is usually given in percent and is defined as 100 times the ratio between the difference between the free rolling rotational velocity (w_r) and the rotational velocity during braking (w_b) and the free rolling velocity (Slip = 100 (w_r - w_b)/ w_r).



Figure 14. The VTI BV12 measurement vehicle for passenger tyre friction characterisation.



Figure 15. The VTI BV12 measurement vehicle from the rear.

The vertical load can be controlled by a double acting air spring cylinder, and the side slip angle is set by an electric steering cylinder which is controlled from a PC program. For the INTRO project, only straight brakings with zero slip angles have been considered.

Forces acting on the wheel in all three directions are measured by rear mounted force measuring hub constructed at VTI. The system contains standard Bofors KG1 force transducers for longitudinal and transversal forces, while the vertical force is measured by a standard Bofors KIS 1 cylindrical shear force transducer, sensitive to forces only in one direction.

The side slip angle is measured both relative to the vehicle and relative to the ground.
The angle relative to the vehicle is measured by a potentiometer with a spring-loaded wire/pulley actuation system. The wire is attached to the cylindrical rotating upper end of the steering shaft (see figure). The angle relative to the ground is measured by a fifth wheel with a potentiometer connected to the vertical suspension hinge

The speed of the vehicle is measured by means of a digital pulse encoder at the left front wheel of the truck. A similar device is used for measuring the rolling speed of the test wheel.

Signals are measured at 200 Hz, and are filtered by a 25 Hz analog low pass filter.

In the INTRO project the data collected from the measuring program was further treated using Matlab to extract the interesting combinations of variables. Typically, 4-6 complete brakings with zero slip angle were carried out during each test run. By performing two test runs per speed and load, about 10-12 separate slip curves was recorded for each setting. Due to mainly variations of the vertical load during a measurement, but also from variations of the surface friction, this is typically the number of slip curves needed to produce a good average slip curve. The effect of vertical load oscillations is illustrated in Figure 16, where six consecutive brakings are presented. The average of these six curves is shown in Figure 17. This average was constructed by dividing the x-axis into small segments and for each segment calculating the vector average of all measurement points contained in the segment. This averaging method was used in the INTRO project with no measurement curve, nor measurement point, excluded from the average process for each set of measurement condition.

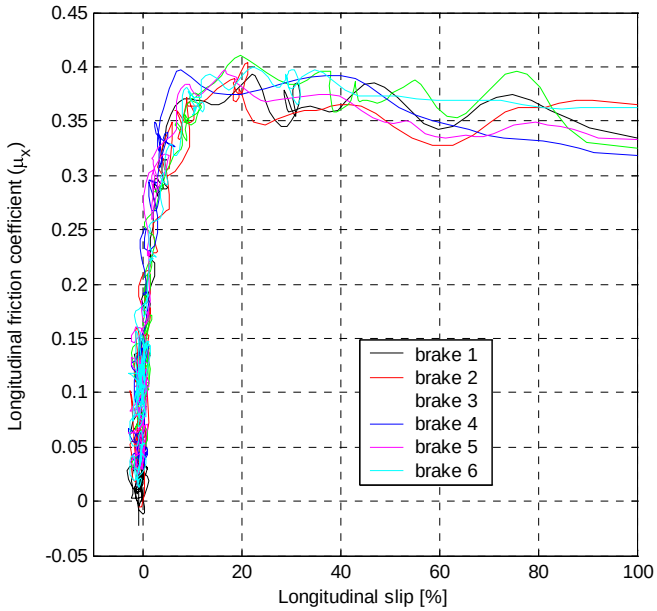


Figure 16. Example of six consecutive brakings with the BV12 on snow at 20 km/h.

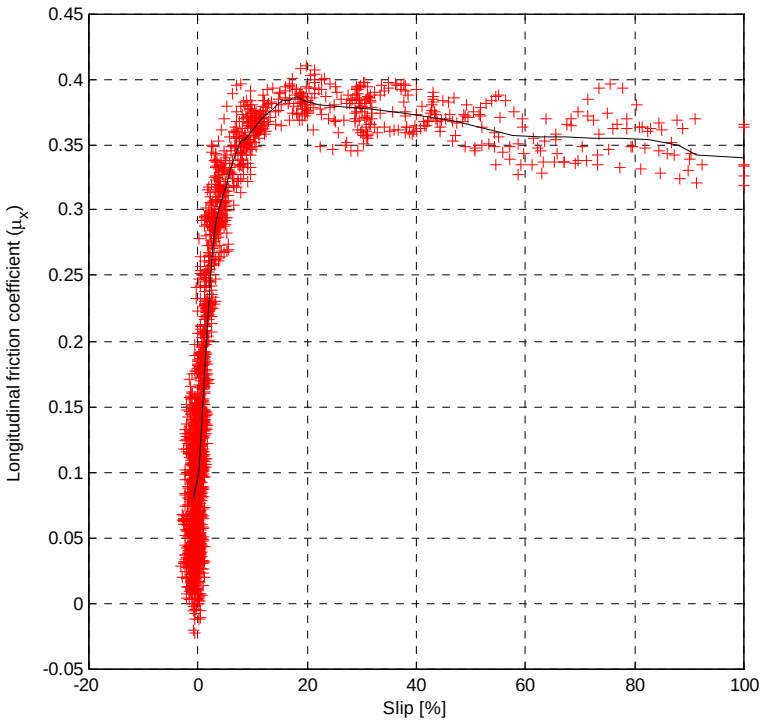


Figure 17. An average slip curve constructed from the six brakings in Figure 16

5.3.3 μ_{max} from NIRA car (Audi A3)

The NIRA car is equipped with a micro slip measurement system to estimate the maximal traction force μ_{max}. The system is based on sensor signals dedicated to the ESP system of the NIRA car and sampled from the CAN-Bus. The estimation is based on the different micro slip behaviour of different surfaces (Figure 18).

5.3.3.1 Principle

The following section describes the basic principles for µ-estimation system and is based on a technical report by Fredrik Gustafsson published in 1995 [14]. Although following the general description in this chapter, the final µ-estimation system implemented by NIRA Dynamics may deviate from the system described below.

The basic principle of the NIRA system is to continuously measure the small variations in the slip ratio (slip ratios <0.1), i.e. the differences in angular velocity between the driven and non-driven wheels occurring when the motor momentum is large enough. These slip variations are compared with the normalised traction force (µ) exerted on the driving wheels when the engine exerts more thrust (e.g. in uphill slopes or during acceleration).

The assumption in the report was that the relationship between slip and traction force contains enough information to predict the maximum friction values (μ_{max}) between the tyre and thereby enabling classification of road surface into classes with different μ_{max} asphalt, snow and ice surfaces (see diagram below). As described in the report by Gustafsson gravel surfaces were considered more difficult to distinguish from asphalt or ice and suggested surface texture as an independent qualifier.

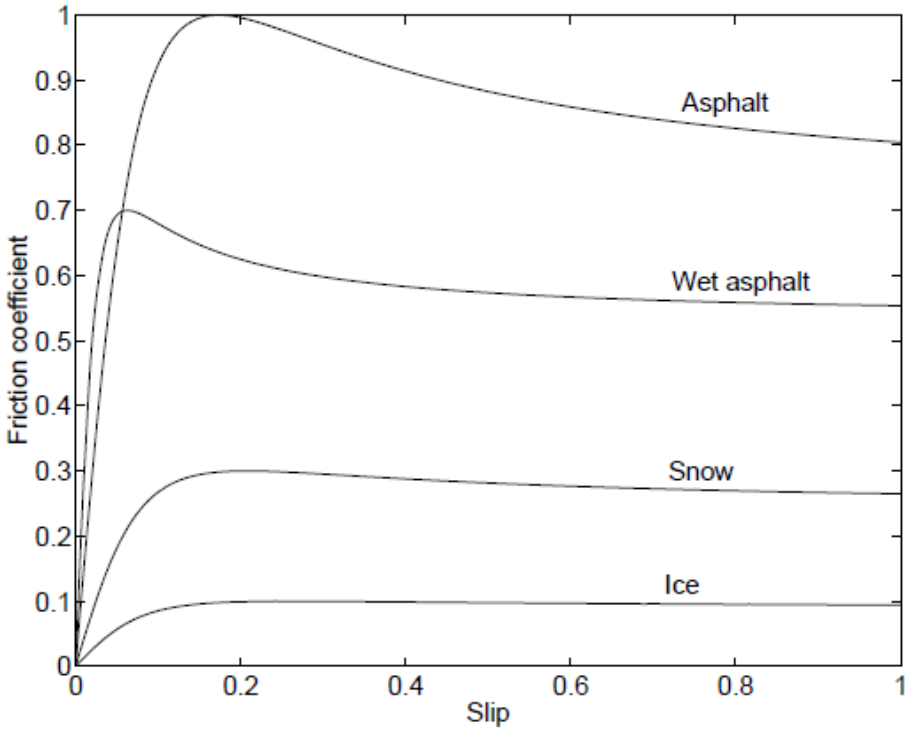


Figure 18. Schematic picture of slip curves (Gustafsson 1996)

5.3.3.2 Estimation of wheel slip (κ)

Wheel slips is calculated using difference of angular velocities between driven and non driven wheel (see paragraph 10.1.1).

The NIRA system calculates the wheel slips sampled from the wheel speed signals on the CAN-Bus with a high sample rate. The forwarded wheel speed signals for measurement logging purpose (see chapter 10.4.4) have a rather low sample rate.

5.3.3.3 Estimation of slip slope, k-value

When the normalised traction force values (μ) are plotted against the wheel slips, a linear relation may be assumed close to μ=0, a linear slope defined as the “k-value” or “slip slope” may be obtained. The k-value is also referred as to the “longitudinal stiffness” and is a tyre specific property. A tyre with high longitudinal stiffness gives rise to a high k-value.

In order to be able to derive a stable k-value of good quality there need to be a certain variation in the slip values and the corresponding μ values. If all points are collected only at a certain slip value, a “swarm” of measurement points is obtained around one point in the diagram and the estimated slope may take any direction giving rise to a large uncertainty.

This indicates the need of a rather high number of μ - κ pairs in a practice.

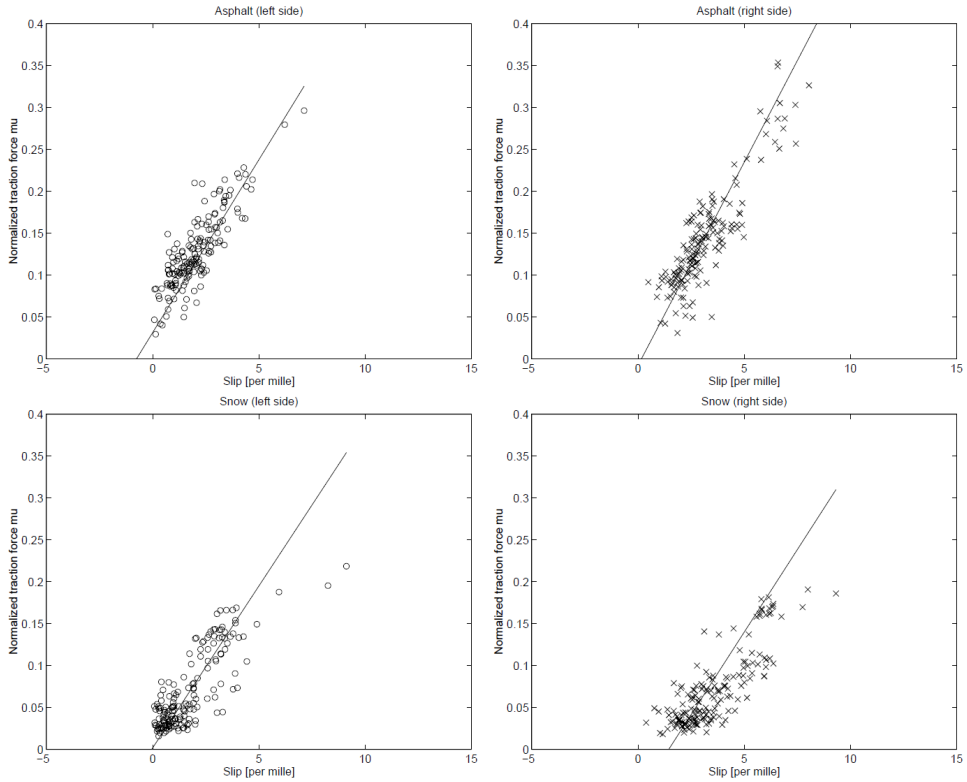


Figure 19. Samples of μ and κ on dry asphalt (upper plots) and hard snow (lower plots) respectively circles and dots represent measurements on the left and right wheel respectively and the solid line is a straight line approximation (Gustafsson 1996)

5.3.3.4 Estimation of μ_{max}

As the actual algorithm for predicting μ_{max} from k-values is proprietary to NIRA Dynamics we can only refer to the classification methods described by Gustafsson where different approximate maximum friction levels (high μ> 0.7, slippery μ≈0.4 and very slippery μ<0.3) were estimated by using the k-values and the estimated surface texture γ which is proportional to the variation of difference between left and right wheel angular velocity. This classification is appropriate for a specific tyre - surface interaction and therefore needs to be adapted.

In practice real braking curves were used to generate input for the NIRA software and adapt this classification. The following procedure was used in order :

- Full ABS Brakings at least four times was performed before starting measurements these should be a variety of surfaces, high and low friction,
- File with calibration values was stored for future use and loaded into the GUI before starting next measurement.

During the summer tests at Nantes the NIRA system failed to distinguish between the different test surfaces. One possible reason for this could be the relatively short test tracks for measurements on wet surfaces giving the NIRA algorithm not enough values for a good estimation. As this algorithm is knowledge belonging to the subcontractor NIRA it is not possible to verify this assumption.

5.3.4 μ_{max} from Peugeot 406

5.3.4.1 Principle

μ_{max} can be estimated by two ways:

- by performing front-wheel braking (currently employed method);
- by constructing the friction-slip curve (exploratory method).

Only the first method is described here. Some results related to the construction of friction-slip curve are shown in paragraph.

5.3.4.2 Estimation of μ_{max} from front-wheel braking

Front-wheel braking tests are performed with and without ABS activation (Figure 20). Decelerations are recorded between two speeds V_1 and V_2, and then the brake is released. Generally, the difference ($V_1 - V_2$) is equal to 20 km/h.



Figure 20. Parameters used for μ_{max} calculation

Friction is estimated from the average deceleration by the following formula:

$$\mu = \frac{M\left(\left[\frac{V_1^2 - V_2^2}{2 \cdot d}\right] - \left[A + B \cdot \left(\frac{V_1 + V_2}{2}\right)^2\right]\right)}{Z_{av} + M \cdot \left(\frac{V_1^2 - V_2^2}{2 \cdot d}\right) \cdot \frac{h}{L}} \quad (14)$$

Where μ: estimated friction;
M: vehicle mass;
d: braking distance;

V_i (i = 1, 2): test speed;
Z_{av}: load on the front axle;
h: height of the vehicle center of gravity (Figure 20);
L: vehicle wheelbase (Figure 20).
A, B: rolling-resistance coefficients (rolling-resistance force = $M \cdot \left[A + B \cdot \left(\frac{V_1 + V_2}{2} \right)^2 \right]$).

The estimation is μ_{peak} (respectively μ_{locked}) for braking with ABS (respectively without ABS). The associated speeds are the mean of the speed range: 80 km/h for braking between 90 km/h and 70 km/h for instance.

6 Experiments

6.1 Summer

6.1.1 First campaign

During 19-30 September 2005, friction measurements were made by LCPC and Arsenal at LCPC test tracks. The purpose of these tests were:

Borttaget: (To be completed)

- to assess the NIRA friction-estimation system on asphalt surfaces;
- to compare NIRA method to other friction-estimation methods;
- to compare NIRA-equipped cars to friction-monitoring devices;
- to provide data for a validation of the stopping distance model.

Five vehicles participated in the test program:

- NIRA car, identified as “F1” (Arsenal);
- ROADSTAR, identified as “F2” (Arsenal);
- Toyota Verso, identified as “F3” (Arsenal);
- Peugeot 406, identified as “F4” (LCPC);
- ADHERA, identified as “F5” (LCPC).

The test track is shown in Figure 21.

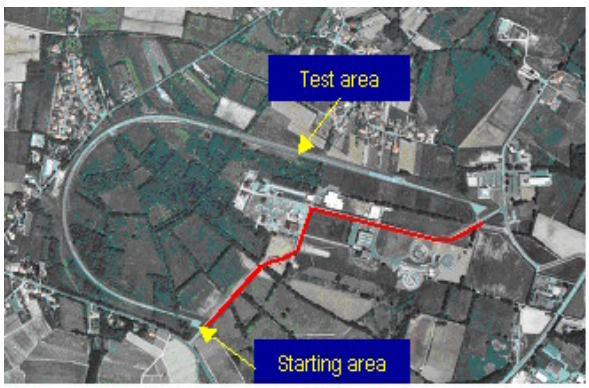
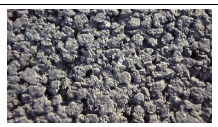
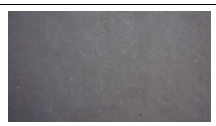


Figure 21. LCPC test track (Nantes, France)

The test area comprises 6 surfaces. They are 200m-long and 3m-wide; test sections are 100-meter long. Surface description is given in TABLE 1.

TABLE 1. TEST SURFACES

ID	Type (min/max aggregate size in mm)	Surface picture
FR1	Surface dressing (0.8/1.5)	
FR2	Bituminous Concrete (0/10)	
FR3	Very Thin Asphalt Concrete (0/6)	
FR4	Epoxy	
FR5	Sand Bituminous Concrete	
FR6	Porous Asphalt (0/10)	

Five test series compose the test program:

- Series 1: Tests on dry surfaces under stabilized-speed maneuver (only instrumented cars).

Speed (km/h)	Vehicle	Tire	Surface
40, 100	F1, F4	Vredestein	All

- Series 2: Tests on dry surfaces under acceleration maneuver (only instrumented cars).

Speed (km/h)	Vehicle	Tire	Surface
30 to V_{max}	F1, F4	Vredestein	All

- Series 3: Tests on wet surfaces under stabilized-speed maneuver.

This series comprises two sub-series:

- Series 3.1: series involving monitoring devices, surfaces are wetted by device water tanks.

Speed (km/h)	Vehicle	Tire	Slip ratio for ROADSTAR (%)	Surface
40, 60, 80, 100	F2	Vredestein, PIARC, summer new, summer worn	18 (all speeds), 75 (40 km/h), 50 (60 km/h), 37.5 (80 km/h)	All
40, 60, 80, 100	F5	Vredestein, PIARC		All

- Series 3.2: series involving instrumented cars, surfaces are wetted by sprinklers (external wetting).

Speed (km/h)	Vehicle	Tire	Surface
40, 100	F1, F4	Vredestein	All

- Series 4: Tests on wet surfaces under acceleration maneuver (only instrumented cars).

Speed (km/h)	Vehicle	Tire	Surface
30 to Vmax	F1, F4	Vredestein	All

- Series 5: Tests on wet surfaces under braking maneuver (only instrumented cars).

Speed (km/h)	Vehicle	Tire	ABS	Surface
40 to 0, 80 to 0	F1	Vredestein	Yes	All (except FR4 at 80 km/h)
40 to 0, 80 to 0	F3	Vredestein, summer new and worn	Yes, No	All (except FR4 at 80 km/h)
40 to 0, 80 to 0	F4	Vredestein	Yes, No	All (except FR4 at 80 km/h)

Regarding braking tests, it should be emphasized that NIRA- and Toyota cars performed four-wheel braking, whereas Peugeot 406 performed front-wheel braking.

6.1.2 Second campaign

Actually, the braking-model principle, consisting of exploiting the deceleration-time curve (see paragraph 5.1), was chosen after the Nantes campaign. Since the relevance of this approach had to be confirmed, the idea is to test the model first on LCPC cars, then to extend it to other participating cars.

A second campaign was then launched on December 2005. The test program comprises:

- the same surfaces as those of the September-campaign, except the epoxy;
- three vehicles: Peugeot 406, and two cars from LCPC (Peugeot 307 and Renault Clio);
- four-wheel ABS braking at two speeds: 70-0 km/h and 90-0 km/h. Three runs are performed at each speed.
- only wet condition: the wetting is performed by sprinklers.

The main drawback of this campaign is the tyres: Peugeot 406 is equipped with Vredestein tyres, whereas Peugeot 307 and Clio are equipped with existing tyres.

6.2 Winter

During 13-16 Mars 2006 friction measurements were made by VTI at Colmis test centre outside Arjeplog in northern Sweden. The purposes of these tests were to collect enough experimental data to validate the theoretical model for the braking distance on winter roads, as well as to obtain values of the parameters of this model on snow and ice. Deceleration curves from braking with the NIRA car were measured on ice and snow using different velocities. Parallel to the deceleration tests, complete slip curves of longitudinal braking were measured on the same surfaces with the VTI test vehicle BV12, using the same sort of tyre as on the NIRA car. In addition to these tests, measurements were also made for WP 2.5.

At Colmis we had access to snow tracks on a frozen lake which were sufficiently long and wide, see Figure 22. The tracks were prepared daily so that a surface of slightly loose snow on top of the packed snow was formed. The ice track had a smooth surface and was approximately 200 metres long, see Figure 23. As the ice track was embedded in the snow track, loose snow was partly moved on to the ice surface during the tests, but the amounts were small and did not affect the measurements.



Figure 22. The VTI test vehicle BV12 in action at Colmis test track.



Figure 23. The ice track at Colmis test centre.

The tests were divided into two different blocks, where the first one included deceleration tests with the NIRA car and slip measurements with BV12 using the same tyre load as the NIRA car. The second test block consisted of BV12 slip measurements with other loads in order to characterize the test tyre.

Main Block:
BV12: straight braking with different velocities: 10, 15, 20, 50, 70 km/h: 2 repetitions with 6 brakings per velocity. The wheel load was 3300 N, which was comparable to the NIRA car wheel load.
NIRA: Measure the friction value using the NIRA algorithm.
NIRA: Full brakings from 20, 50, 70 km/h;. 3 repetitions per velocity. A Correvit sensor was used to record the continuous change of velocity during the brakings.
(BV14: Measure friction value at different velocities: 20, 50, 70 km/h; 3 repetitions / velocity. – part of WP2.5)

BV12 block:
Straight braking with different loads and velocities: (2000, 3300, 5000 N) x (10, 20, 50 km/h):
2 repetitions with 6 brakings per velocity and load.

The main block was repeated twice on snow, and one time on ice. Typically, the BV12 block was carried out one time on snow and one time on ice.

7 Results

7.1 Deceleration curves

7.1.1 Deceleration curves from NIRA car (Audi A3) and Toyota Verso during "summer" tests (September 2005, Nantes, France)

The measurement system for braking distance and deceleration curves is developed to be used in different cars. The main purpose is to have an easy to mount setup to

be used in the Audi A3 (NIRA car) as well as in the Toyota Verso (Figure 24). The distinction between these cars is on the one hand the NIRA system in the Audi A3 for micro slip measurement, and on the other hand the capability to deactivate the ABS system.



Figure 24. Test cars at Nantes test track Audi A3 (left) and Toyota Verso (right)

7.1.1.1 Measurement Systems

- Capacity triaxial-accelerometer Typ 8393A2 (Kistler)
- Correvit L-CE CORRSYS Datron optical velocity Sensor
- DT BNC-Box USB of DT 9800-EC (A/D-conversion)
- Signal amplifier for accelerometer
- Laptop

7.1.1.2 Measurement assembly

For the braking distance measurement and logging of the deceleration curve the sensors are attached to the vehicle (Audi A3/Toyota Verso). The accelerometer is fixed inside the car to avoid movements of the sensor due to hard braking. The coordinates of the accelerometer has to be adjusted to the coordinates of the test vehicle. The optical velocity sensor (Correvit) is attached to the front seat passenger door. The maximum distance between sensor and surface must not exceed 40 cm to ensure good results.

The data acquisition is accomplished with an easy to use USB-Box and a standard laptop. The connection of each sensor direction to the USB-Box is shown in Figure 25. The digital signal is connected to the Laptop via the USB - interface.

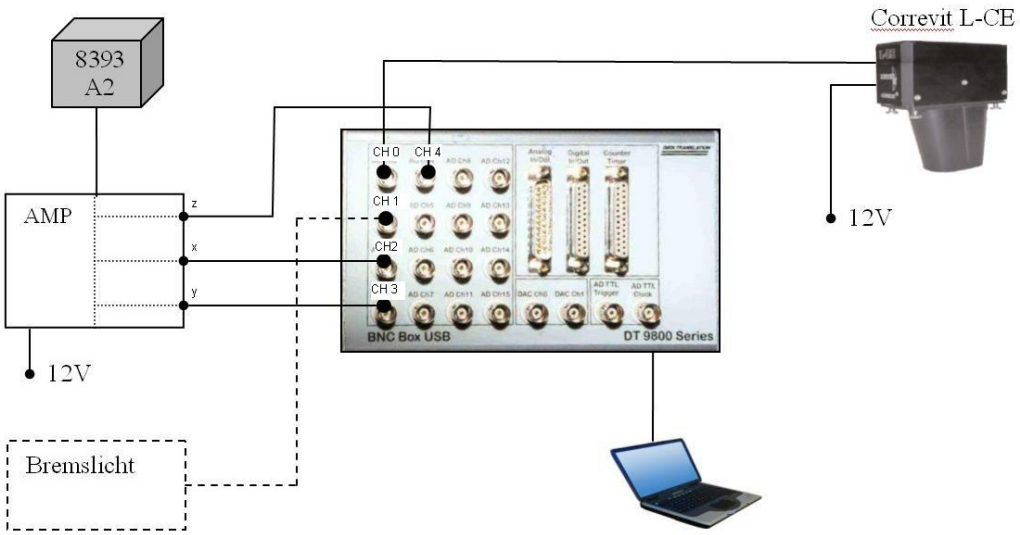


Figure 25. Setup for braking distance and deceleration measurements with Audi A3 and Toyota Verso

After each measurement the deceleration curves and the preliminary results where used for plausibility checks. All recorded datasets for each measurement are analysed in the post process. The signal is filtered with a 10 Hertz low pass filter in the post processing for visual control.

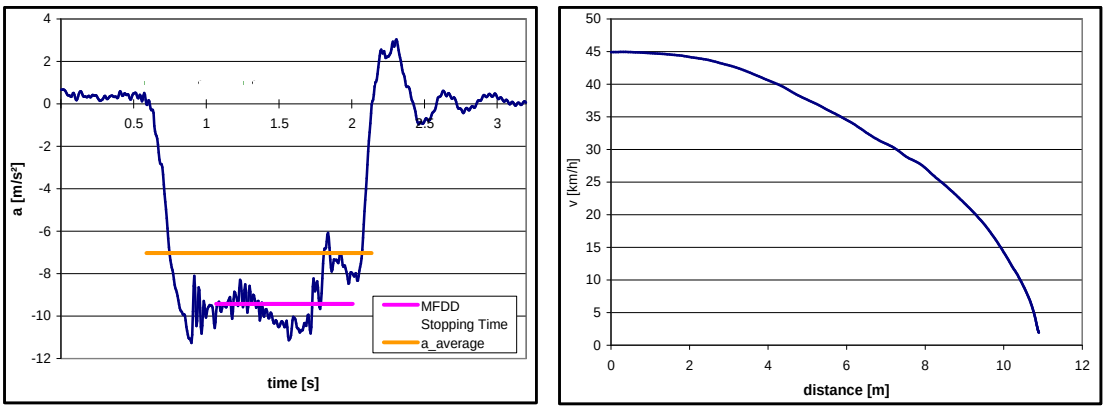


Figure 26. Deceleration curve (left) and braking distance diagram (right) for Audi with activated ABS and all season tire on surface 1.

7.1.2 Deceleration curves from NIRA car during winter tests (Arjeplog, Sweden)

The NIRA car was equipped with a Leitz Correvit-L digital one-axis optical sensor at the front of the car, see Figure 27. This sensor can measure the speed (always positive) of the vehicle continuously at 50 Hz, at speeds between 3-200 km/h. This

sensor has proven to work well on snow and ice. The measuring accuracy of this device is supposed to be better than ±0,5%, which corresponds to less than ±0,5 km/h in our tests. However, due to the oscillations of the sprung mass during braking, spurious oscillations were induced in the measured velocity during the brake tests, as shown below.



Figure 27. The NIRA car with the Correvit sensor mounted at the front.

A signal from the brake was also retrieved to indicate the start of a braking. In all the graphs below the time zero seconds has been used to mark the start of a braking. A typical braking on snow from 20 km/h is shown in Figure 28a. The velocity data has not been filtered, and it is clear that both noise and artefacts from car oscillations are present in the measured signal. At the very end of the braking procedure, when the velocity is about 2-3 km/h, the deceleration is rapidly diminishing, resulting in large pitch angle oscillations. These oscillations are the cause of the apparent increase of the measured speed between 1,5 and 2,5 seconds. This phenomenon, together with the fact that the Correvit sensor is not reliable below 3 km/h, makes it impossible to use the experimental data from the very end of the brakings. This is however not a problem since the vehicle speed is low, and assuming a constant deceleration at the end of the braking will not introduce large errors in the calculated braking distance. It is practical to “cut” the measured signals when the speed has gone below 1 m/s. The additional braking distance from 1 m/s to stand still will then, with the assumption of constant deceleration, be $1/a$, where a denotes the absolute value of the deceleration.

The large oscillations of the vehicle during the braking process can be seen in Figure 28b, where the velocity and the acceleration from Figure 28a has been filtered[3] with a 3 Hz digital low pass filter. The filter, a 4^{th} order Butterworth filter, was applied without phase shift so that no time delay of the measured signals would occur. As with all filters however, the curves will always be broadened. This effect can clearly be seen at the beginning of the acceleration curve, where the deceleration seems to start before the braking, which is indicated by time equals zero. Thus, heavily filtered curves will not be used to obtain parameters for the braking distance model, but can be very useful for clarification of the braking process.

[3] The entire signal, which begins approximately one second before the braking, was filtered.

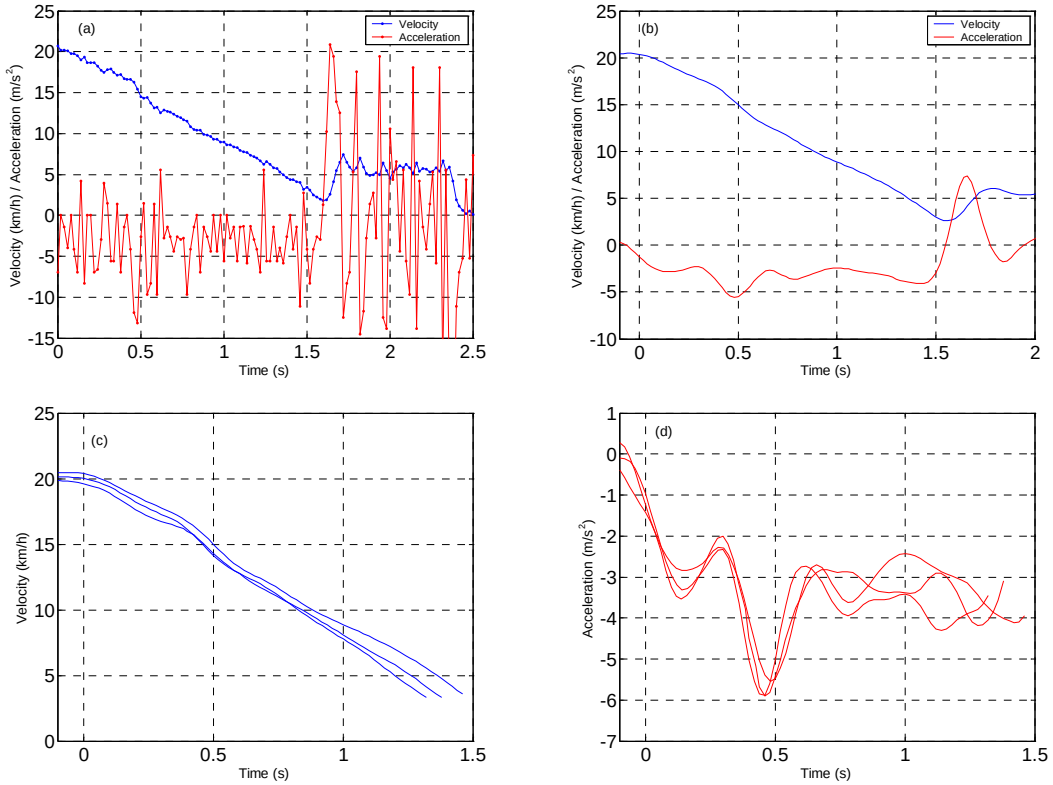


Figure 28. Speed and deceleration curves obtained from braking on snow at 20 km/h. *Figure title detail: a) Unfiltered braking. b) Speed and acceleration filtered by a 3 Hz low pass filter. c) Filtered speed curves from three different brakings. d) Filtered deceleration curves from the same three brakings as in c).*

In Figure 28c and Figure 28d, the filtered curves of three different brakings on snow from 20 km/h are shown. The presented data has been cut at a speed of 1m/s, as described above. It is evident from the figures that the car oscillates in a repeatable way. One can argue that these oscillations of the measured speed are just sinus functions with various frequencies superimposed to the real speed. Furthermore, the amplitude of these oscillations should decrease exponentially with time due to the vehicles damping system. Hence, it is not implied that the effect of the oscillations will cancel out when the measured speed is integrated to obtain the travelled distance. However, it is quite clear from Figure 28c that the amplitude of these oscillations are small and their effect on the calculated distance (the area under the graphs) is negligible in comparison with changes of the obtainable friction during the braking. The last effect is demonstrated in Figure 28c, in which the curves start to diverge when the speed goes below 10 km/h.

Based on the above conclusions, the braking distance from the measurements could be determined with an acceptable margin of error by integrating the unfiltered measured speed using the assumption of constant deceleration when the speed is below 1 m/s. Furthermore, finer details of the braking process, such as a possible speed dependent friction level, can not be identified from single measurements. Instead, an average speed versus time diagram must be constructed from several measurements to detect possible deviations from the simplest braking distance

model. It can, however, be argued that small details in the model are pointless from a practical point of view, if the deviation between the measured distances during identical conditions are large enough.

7.1.3 Deceleration curves from Peugeot 406 car (September 2005, Nantes, France)

The deceleration is delivered by the inertial system (crossbow) (see 10.4.5 for a full description of the sensors). Of course, this signal includes some delay. This can disturb the physical analysis of the system when we have to mix this signal with others providing by various sources like encoders, laser sensors, etc. in order to compute, for example, slip rate.

This delay can be removed in post processing by comparing the signal with the acceleration computed numerically using the encoder data sets. For further analysis on the time delay of the different systems the following signals are compared (see Figure 29):

- acceleration computed from Correvit
- encoders,
- inertial system
- raw accelerometer (added for this special calibration test)

Figure 29 shows the different curves obtained from these various sources during a braking maneuver. This shows the interest of crossing the information delivered by different sensors and so the interest of a fully equipped vehicle like the LCPC car. The signals are filtered very low in order to guess the delay between them. This is not the same filtering process as the one applied in order to get information on the braking curve (this last process is described in the paragraph 5.3.4). As far as the delays of the different signals are concerned, the measurement system of the 406 delivers also the signal of the brake pressure. However, this signal is not plotted because there is also some delay between the increasing of pressure and the deceleration.

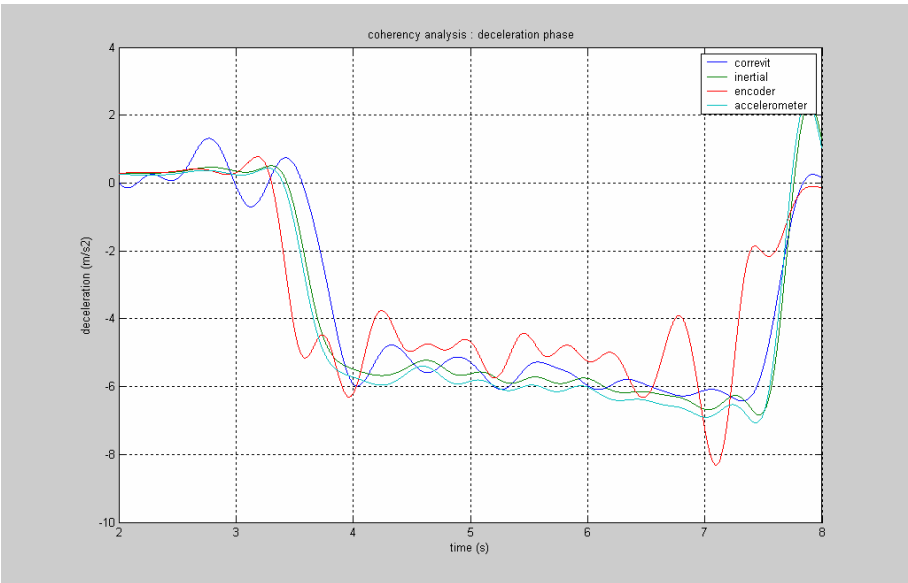


Figure 29. Deceleration curves from Peugeot 406

7.2 Summer tests (Nantes, France)

It should be emphasized that the word “summer” is used for convenience to relate the test campaigns to the two model components. As it was stated in 6.1.2, the summer component is currently validated using results from an extra braking-test campaign involving three cars: Peugeot 406, Peugeot 307 and Renault Clio. Analyses presented in the following paragraphs are based on this campaign. For a first validation of the model, only results at 90 km/h will be investigated.

7.2.1 Braking distances

Braking distances are presented in TABLE 2

TABLE 2. BRAKING DISTANCES FROM SECOND NANTES-CAMPAIGN

	Vehicle					
	307		Clio		406	
Surface	Speed (km/h)	Braking distance (m)	Speed (km/h)	Braking distance (m)	Speed (km/h)	Braking distance (m)
FR1	65,6	18,8	68,3	20,8	66,1	20,5
	66,3	17,5	71,1	21,6	67,1	20,7
	66,6	19,1	70,9	21,0	67,2	20,5
	87,3	30,0	90,1	34,5	86,1	32,8
	86,4	28,3	93,8	36,6	86,6	32,8
	85,9	29,2	90,3	34,4	86,8	32,8
FR2	67,4	20,1	71,0	26,2	66,3	25,4
	66,5	20,4	73,2	29,1	66,5	25,3
	66,3	20,5	71,4	27,9	66,7	25,6
	86,5	35,0	92,9	44,9	85,8	40,2
	87,1	36,4	91,0	44,2	86,7	40,7
	86,6	36,0	91,5	43,3	87,2	42,1
FR3	68,4	20,2	68,4	33,0	66,4	21,4
	69,1	20,4	92,0	25,3	66,7	21,6
	85,4	30,5	70,9	24,6	66,9	21,3
	86,6	31,2	89,1	37,3	85,7	34,1
	84,9	30,5	88,3	37,1	86,2	35,9
	86,0	30,8	87,1	36,4	86,4	36,2
FR5			70,8	24,4		
			73,7	25,4		
			70,5	24,6		
			87,5	36,5		
			80,1	38,2		
			88,0	38,8		
FR6	66,4	22,6	89,2	39,3	66,6	23,6
	66,9	21,0	72,1	30,6	67,5	24,1
	66,6	21,3	73,9	31,1	67,8	24,0
	86,3	36,7	87,9	45,4	85,1	38,3

	84,7	33,8	88,6	45,7	86,5	37,6
	86,1	35,0	85,8	42,0	86,6	37,9

7.2.2 Estimation of "a", "b" and "t_s"

From each deceleration curve, three parameters are first calculated (Figure 7): t_s, γ_{peak} and γ_{ABS}. The calculations are done "manually": γ_{peak} represents de maximum of deceleration, t_s is the corresponding time, and γ_{ABS} is the average value of the stabilised part. Using the ROADSTAR friction coefficient at 18% slip and 80 km/h (closest value to the studied speed), denoted as µRS80, and equations (12) and (13), "a" and "b" factors can be calculated.

Values are presented in TABLE 3 and TABLE 4.

TABLE 3. VALUES OF γ_{peak}, t_s AND a

		FR1			FR2			FR3			FR5			FR6		
Vehicle	Run	γ_{peak}	t_s	a	γ_{peak}	t_s	a	γ_{peak}	t_s	a	γ_{peak}	t_s	a	γ_{peak}	t_s	a
406	1	-9,96	0,21	1,22	-10,30	0,31	1,45	-11,33	0,3	1,37	-10,32	0,25	1,15	-10,33	0,25	1,53
406	2	-10,51	0,27	1,28	-9,81	0,44	1,38	-10,77	0,24	1,31	-10,39	0,26	1,16	-10,44	0,21	1,54
406	3	-10,48	0,25	1,28	-10,10	0,18	1,42				-10,56	0,16	1,17	-10,33	0,18	1,53
Mean 406		-10,32		1,26	-10,10		1,42	-11,05		1,34	-10,42		1,16	-10,36		1,53
307	1	-11,56	0,16	1,41	-9,91	0,1	1,39	-10,30	0,15	1,25				-11,40	0,12	1,68
307	2	-11,65	0,14	1,42	-9,67	0,1	1,36	-12,14	0,17	1,47				-9,00	0,12	1,33
307	3	-11,31	0,14	1,38	-10,03	0,12	1,41	-11,28	0,12	1,37				-9,44	0,17	1,39
Mean 307		-11,51		1,40	-9,87		1,39	-11,22		1,36				-9,77		1,44
Clio	1	-10,91	0,1	1,33	-9,69	0,15	1,36	-9,91	0,17	1,20	-9,87	0,15	1,10	-9,727	0,14	1,44
Clio	2	-11,75	0,17	1,43	-10,94	0,15	1,54	-10,44	0,17	1,27	-10,16	0,16	1,13	-9,477	0,14	1,40
Clio	3	-10,87	0,24	1,33	-10,17	0,13	1,43	-10,41	0,16	1,26	-10,64	0,17	1,19	-9,441	0,14	1,39
Mean Clio		-11,18		1,36	-10,27		1,44	-10,25		1,24	-10,22		1,14	-9,55		1,41
µRS80		0,84			0,73			0,84			0,92			0,69		

TABLE 4. VALUES OF γ_{ABS} AND b

		FR1		FR2		FR3		FR5		FR6	
Vehicle	Run	γ_{abs}	b	γ_{abs}	b	γ_{abs}	b	γ_{abs}	b	γ_{abs}	b
406	1	-8,86	1,08	-8,92	1,25	-9,76	1,18	-9,21	1,03	-8,91	1,32
406	2	-9,15	1,12	-8,39	1,18	-8,96	1,09	-9,03	1,01	-8,83	1,30
406	3	-8,96	1,09	-8,88	1,25		0,00	-9,12	1,02	-8,72	1,29
Mean 406		-8,99	1,10	-8,73	1,23	-9,36	1,14	-9,12	1,02	-8,82	1,30
307	1	-9,87	1,21	-8,21	1,15	-8,88	1,08			-7,98	1,18
307	2	-9,87	1,21	-8,15	1,15	-8,84	1,07			-7,90	1,17
307	3	-10,12	1,24	-8,12	1,14	-8,98	1,09			-7,61	1,12
Mean 307		-10,00	1,22	-8,14	1,15	-8,91	1,08			-7,88	1,16
Clio	1	-9,05	1,11	-7,56	1,06	-8,36	1,01	-8,19	0,91	-6,65	0,98
Clio	2	-9,50	1,16	-7,45	1,05	-8,43	1,02	-7,78	0,87	-6,75	1,00
Clio	3	-9,10	1,11	-7,46	1,05	-8,16	0,99	-7,79	0,87	-6,64	0,98
Mean Clio		-9,22	1,13	-7,49	1,05	-8,32	1,01	-7,92	0,88	-6,68	0,99

7.2.3 Relationship between "a", "b" and µRS

From TABLE 3, relationship between "a" factor and µRS can be assessed. The regression equations are (Figure 30):

(15) a 406 = - 1,49 μ_{RS} + 2,54
(16) a 307 = - 0,41 μ_{RS} + 1,72
(17) a Clio = - 1,20 μ_{RS} + 2,29

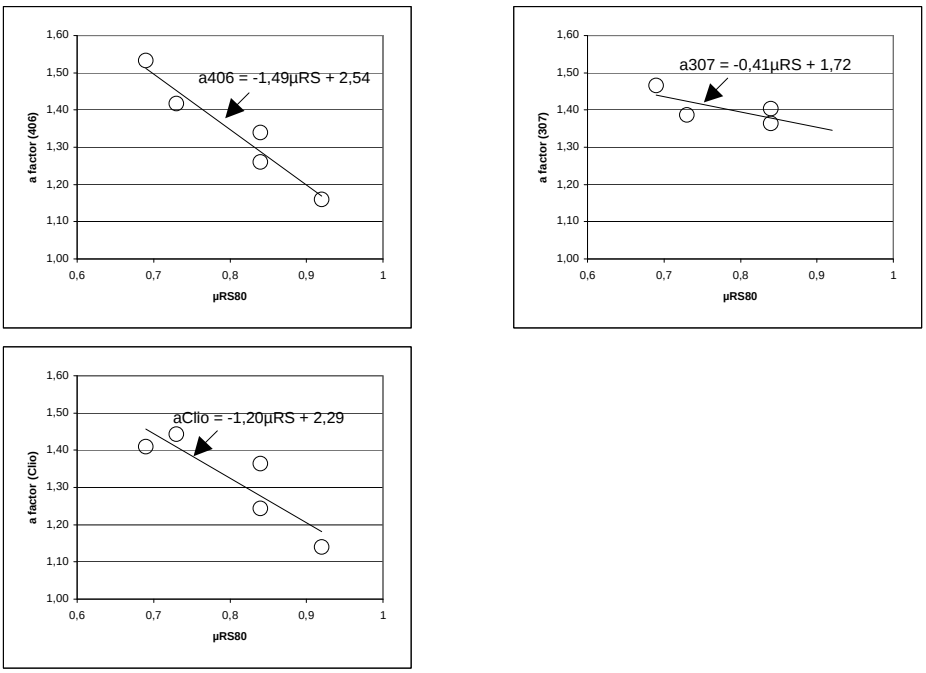


Figure 30. Relationship between "a" factor and skid-resistance measured by ROADSTAR

From TABLE 4, relationship between "b" factor and µRS can be assessed. The regression equations are (Figure 31):

(18) b 406 = - 1,21 μ_{RS} + 2,12 *
(19) b 307 = - 0,02 μ_{RS} + 1,17
(20) b Clio = - 0,32 μ_{RS} +1,27

**: in this case, the point corresponding to surface FR3 (small "circle" in the first graph of Figure 31) was discarded for the regression calculation.*

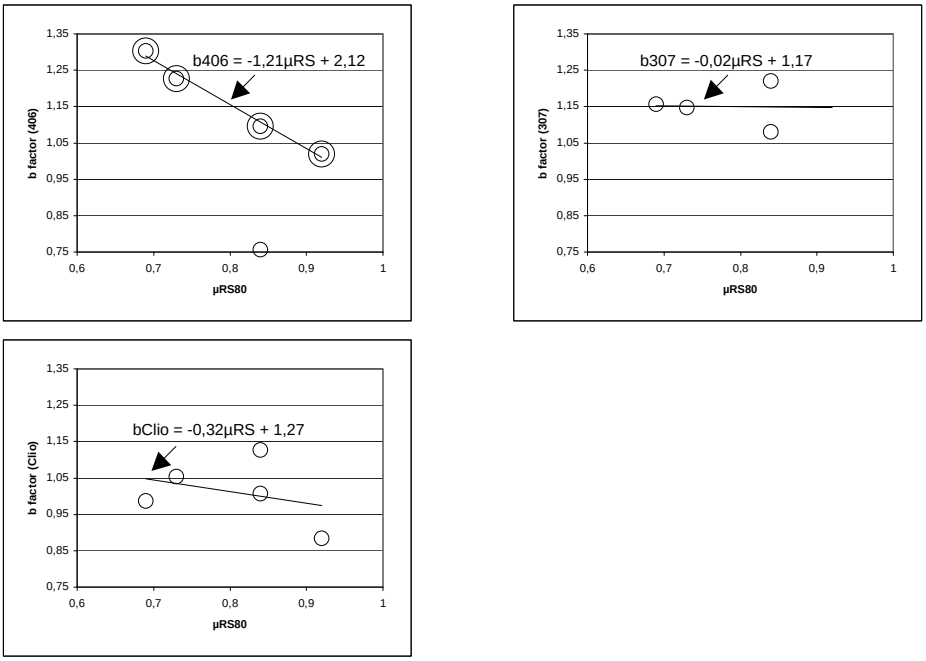


Figure 31. Relationship between “b” factor and skid-resistance measured by ROADSTAR

Transient times are evaluated as:

(21) Peugeot 406 $t_s = 0{,}0022 \times$ Speed (in km/h)
(22) 307 and Clio $t_s = 0{,}0014 \times$ Speed (in km/h).

7.2.4 Comparison of measured-computed braking-distances

Comparison between measurements and computed results are given in TABLE 5.

TABLE 5. COMPARISON MEASURED/COMPUTED BRAKING-DISTANCE

Surface	307			Clio			406		
	Speed (km/h)	Braking distance (m)		Speed (km/h)	Braking distance (m)		Speed (km/h)	Braking distance (m)	
		Meas.	Calcul.		Meas.	Calcul.		Meas.	Calcul.
FR1	87,3	30,0	33,2	90,1	34,5	36,6	86,1	32,8	37,0
	86,4	28,3	32,3	93,8	36,6	39,7	86,6	32,8	37,7
	85,9	29,2	31,3	90,3	34,4	40,2	86,8	32,8	38,3
FR2	86,5	35,0	37,4	92,9	44,9	47,7	85,8	40,2	39,0
	87,1	36,4	37,9	91,0	44,2	46,2	86,7	40,7	38,5
	86,6	36,0	38,2	91,5	43,3	46,2	87,2	42,1	37,0
FR3	86,6	31,2	34,8	89,1	37,3	40,6	85,7	34,1	36,3
	84,9	30,5	36,6	88,3	37,1	39,6	86,2	35,9	37,4
	86,0	30,8	33,4	87,1	36,4	39,4	86,4	36,2	
FR5				87,5	36,5	33,3			

				80,1	38,2	41,8			
				88,0	38,8	43,1			
FR6	86,3	36,7	38,5	87,9	45,4	49,0	85,1	38,3	36,8
	84,7	33,8	37,4	88,6	45,7	48,1	86,5	37,6	37,5
	86,1	35,0	41,0	85,8	42,0	46,0	86,6	37,9	37,1

Except few cases, braking distances are estimated with a precision of 10%, which in the order of the known variance for braking measurements (see Figure 1). The case of Peugeot 406 on surface FR1 needs further investigation.

7.3 Winter tests (Arjeplog, Sweden)

7.3.1 Comparison of μ_{max}

The friction levels of the packed snow and the ice were measured with the NIRA car during the Arjeplog main measurement block. Before the brake tests, the NIRA car was driven back and forth along the test track at speeds up to 70 km/h. A typical measurement on snow is shown in 0. From the figure it is clear that the test track, 700 metres long, was measured five times, with a friction coefficient ranging from 0,27-0,32 (not counting the anomalous behaviour around 2000 m). There is no apparent correlation between the measurement speed and the friction coefficient.

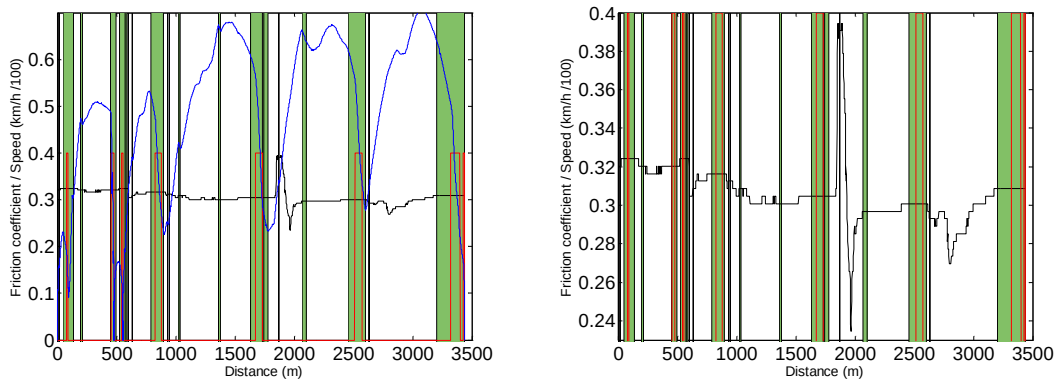


Figure 32. The friction levels measured by the NIRA car on packed snow

Figure title detail: The graph to the right is a close up of the left graph. The friction coefficient is plotted with black colour, and ranges between 0,27 and 0,32. The vehicle speed, shown by the blue line, ranges between 10 – 70 km/h. The red line indicates whenever the brake pedal was active, using a step. The green areas represent intervals when a flag was activated which indicates that the measured friction value is not reliable (see Sec. 5.3.3).

It was also possible to measure the NIRA friction coefficient during the brake tests. An example of this is shown in Figure 33, where the friction measured during 7 brakings on snow at 20 km/h is displayed. Compared to the measured friction without brakings, the friction coefficient is much more unstable, ranging from 0,32-0,46. Moreover, the friction coefficient seems to converge toward the highest value during

the measurement, reaching a stable level after about 5 brakings. A possible explanation could be that the calibration data is altered during the brakings (the NIRA system uses the last 8 brakings for calibration), which would happen if the friction is highly dependent on the vehicle speed and if a different speed is used for the brakings compared to the speed used during the original calibration. However, from inspection of the k-value (which is independent of the calibration) during the brakings, we conclude that this is not the case. The k-value is almost identical to the friction value, apart from a factor.

Another explanation could be that the available friction between the tyres and the snow on the test track is changed by the brakings. This is however not supported by the braking distance measurements, which indicate a rather constant friction during the tests. Nor do the friction measurements with the BV12 exhibit any notable changes of the friction with time. Thus, we conclude that the apparent increase of the friction, most likely is the result of a slowly converging k-value. This phenomenon shows up a few times during the Arjeplog measurements, and it is still not clear why it occurs.

In Figure 34, NIRA friction values during two separate measuring blocks on snow are displayed. Three different speeds were used: 20, 50 and 70 km/h. The friction is somewhat higher in the later measurements (the right column), which is also consistent with the BV12 measurements, and can be explained by a lower temperature.

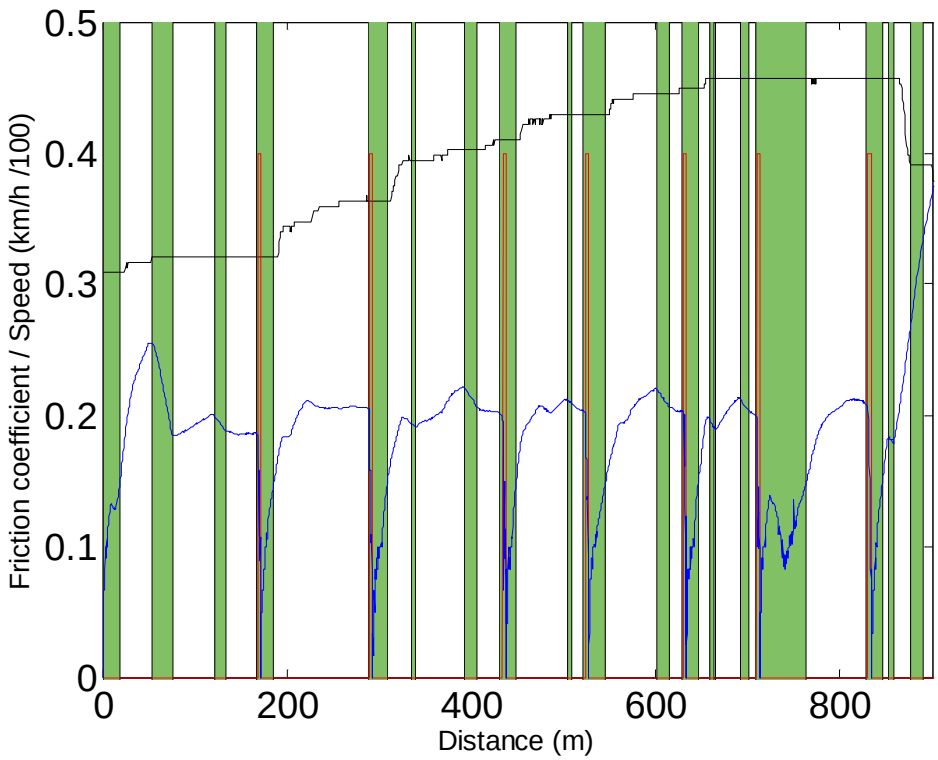


Figure 33. The friction levels measured by the NIRA car on packed snow during brake tests from 20 km/h.

Figure title detail: The same notation as in 0 was used.

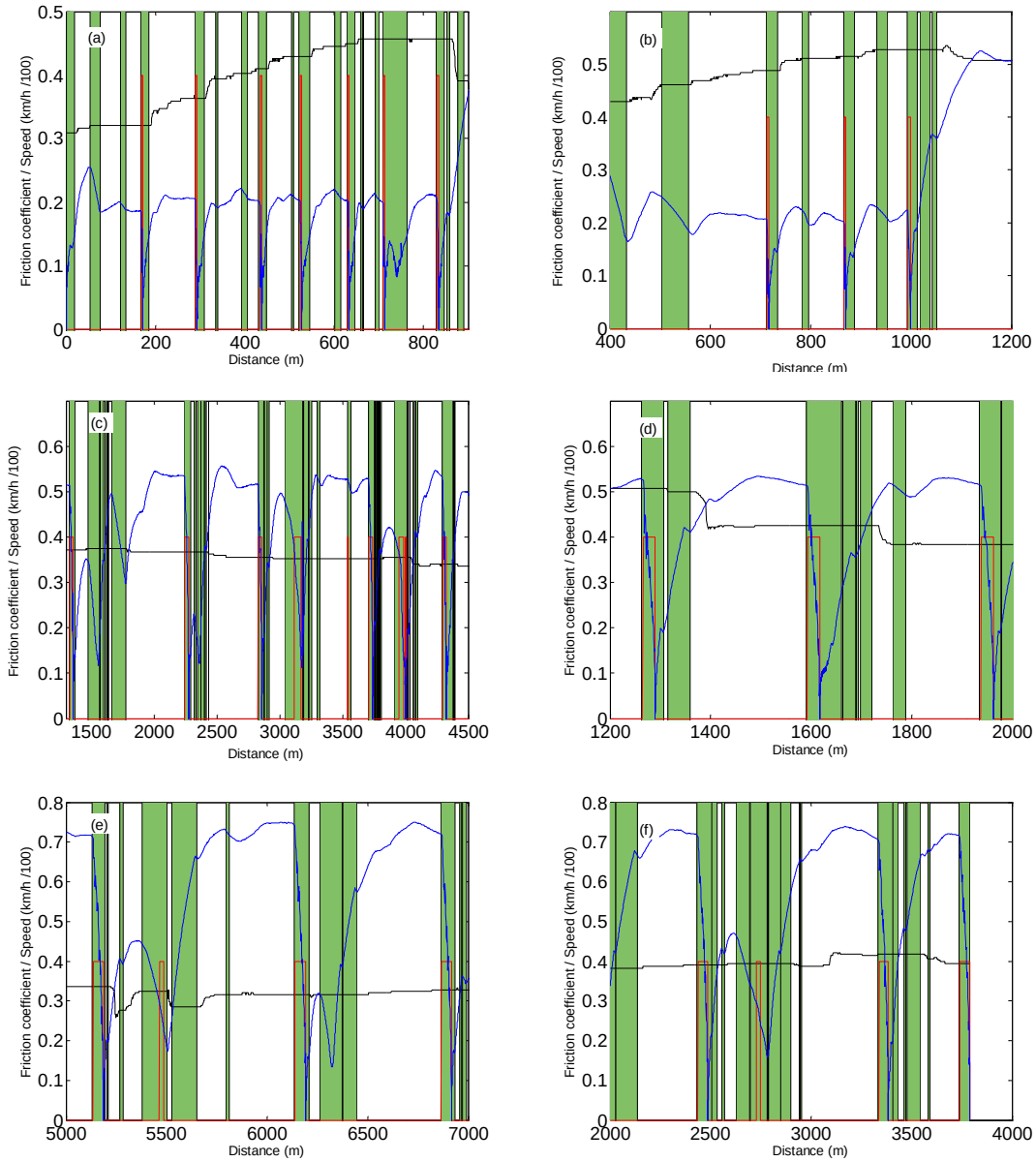


Figure 34. The friction levels measured by the NIRA car on packed snow during brake tests from various speeds

Figure title detail: The friction levels measured by the NIRA car on packed snow during brake tests from 20 km/h (a and b), 50 km/h (c and d), and from 70 km/h (e and f). The measurements displayed by a, c and e were carried out in one test block, while those displayed by b, d and f were carried out in another test block, six hours later. The same notation as in 0 was used.

Measuring the friction on the ice with the NIRA car was difficult because of the limited length of the ice track. Accelerating to the desired speed had to be done on the snow

track, and only the braking part could be performed on the ice track. Hence, no measurements of the ice friction during the brakings were recorded. Driving the NIRA car back and forth along the ice track would result in speeds up to 30 km/h, which is shown in Figure 35. From the figure it is clear that the test track, 200 metres long, was measured three times, with a friction coefficient ranging from 0,28-0,33. There is no apparent correlation between the measurement speed and the friction coefficient. It is rather surprising that the friction coefficient is almost identical to the similar measurement on snow presented in 0.

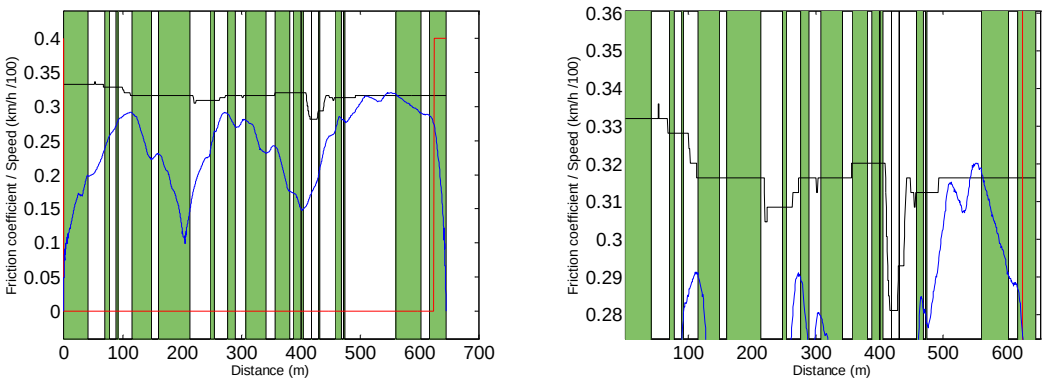


Figure 35. The friction levels measured by the NIRA car on ice

Figure title detail: The graph to the right is a close up of the left graph. The same notation as in 0 was used.

Complete braking slip curves were measured with the BV12 on both snow and ice at 10, 15, 20, 50 and 70 km/h. The vertical load on the test tyre was 3300N, which is the expected load on the tyres of the NIRA car. The same air pressure, 2,2 bar, was used on both test vehicles.

Average slip curves, calculated as described in Sec. 5.3.5.1, for measurements on snow during two different measuring blocks are shown below in Figure 36. From the figure it is clear that the friction reaches a maximum at approximately 20% slip, and stays more or less constant for higher slip values. In contrast to the NIRA friction levels, the BV12 maximum friction values exhibits no obvious speed dependence, and the friction at 20% slip ranges between 0,35-0,40. Assuming that the ABS brakes operates between 10-20% slip, the attainable friction levels during ABS braking would oscillate between 0,35-0,40, with an average friction of approximately 0,38 based on the measurement in the left graph of Figure 36. The measurements carried out 6 hours later, presented in the right graph of the figure shows a somewhat lower ABS friction, oscillating between 0,33-0,38, with an average friction of 0,36. This behaviour is also different from the NIRA friction measurements, where a slight increase of the friction could be noticed for all speeds during the later measurement.

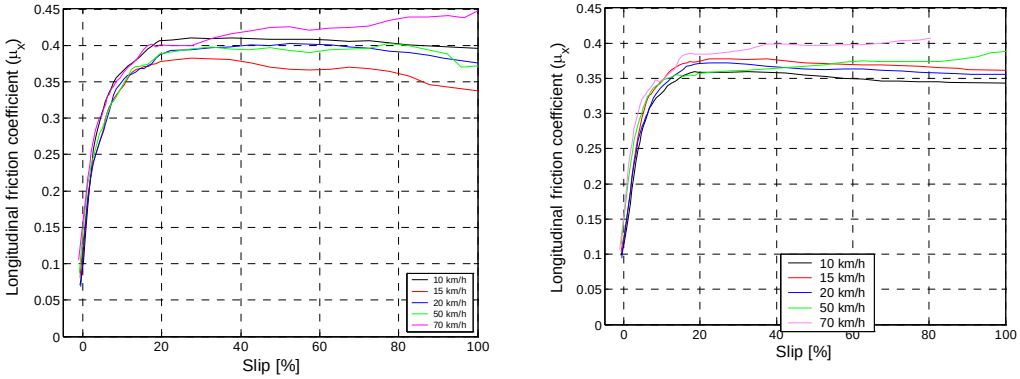


Figure 36. The slip curves on snow measured with the BV12

Figure title detail: The slip curves on snow measured with the BV12 at different speeds, using the same wheel load as the NIRA car, 3300 N. The two graphs display two different measurement blocks, where the measurements presented in the right graph were carried out 6 hours later than those presented in the left graph.

BV12 measurements on ice are shown in Figure 37. The slip curves are not as smooth as those for snow, and the reason for this is twofold. First, the short track length did not allow for enough number of brakings per measurement at the higher speeds. Time constraints did not allow for enough extra measurements to make up for this. Then, as can be seen for the lower speeds 10 and 15 km/h (where most curves were obtained), the friction coefficient exhibits a sharp peak which is extra sensitive to wheel load variations during the measurement. Thus, this kind of slip curves need an additional number of measured curves to produce a good average where no detail is lost in the process, compared to e.g. snow slip curves. However, perfect curves are not crucial for our application, and from our measurements we can conclude that the attainable ABS friction value ranges between 0,09-0,12, with a possible average of 0,11. This value is very different from the NIRA friction value, which was around 0,30.

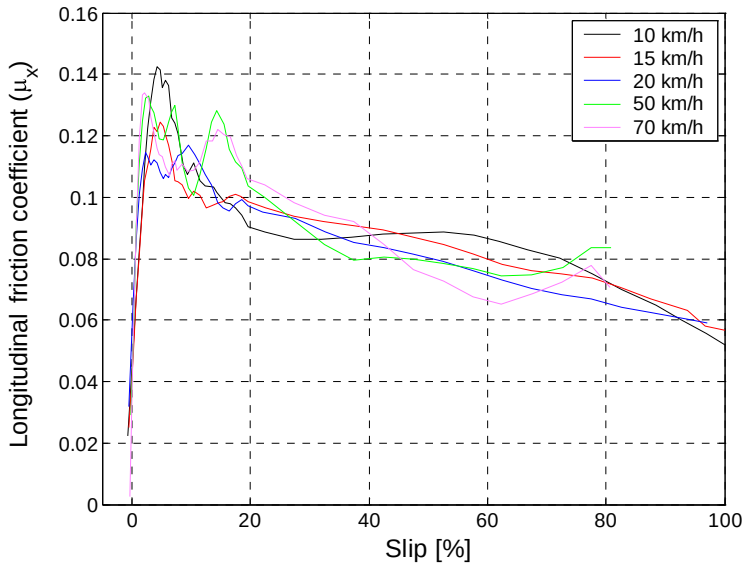


Figure 37. The slip curves on ice measured with the BV12

Figure title detail: The slip curves on ice measured with the BV12 at different speeds, using the same wheel load as the NIRA car, 3300 N.

In addition to the BV12 friction measurements with 3300N wheel load, complete slip curves using wheel loads 2000N and 5000N were recorded on both ice and snow. As it turns out that the statistical spread of the measured braking distances is too large for the braking distance model to benefit from load dependent friction data, the results of these friction measurements were omitted in this report. Instead we refer to the CD containing all the INTRO Task 2.1 measurement results [15].

7.3.2 Comparison of measured-computed stopping-distances

In this section the stopping distance measurements of the Arjeplog campaign, described in Section 6.2, are analysed using our relatively simple braking-distance model. The resulting friction values are compared to those measured by the NIRA car, as well as to those measured by the BV12. We then argue whether a more advanced model is possible, and if there are any merits of such a model.

Snow and ice are difficult surfaces for friction measurements since the friction may change notably Before applying the model to the measured data, it is important to understand what differences of the measured braking distance that could be expected between similar brakings (same speed and surface). As the driver can not obtain identical speeds before each braking, differences in initial speed will lead to different braking distances. We performed brakings from three different initial speeds: 20, 50 and 70 km/h. It is reasonable that the test driver obtained initial speeds in the following intervals: 19-21 km/h, 48-52 km/h and 68-72 km/h. Assuming that the surface is not changing, and thus a constant friction level, between brakings with similar speeds, equation (1) (reference to the AASHTO model, section 4.1) can be used to calculate the expected width of the resulting braking distance intervals. For the 19-21 km/h interval, the higher speed results in a 22% longer braking distance

compared to the lower speed. Similarly, 52 km/h results in 17% longer braking distance compared to 48 km/h, while 72 km/ increases the braking distance by 12% when compared to 68 km/h.

In TABLE 6, the measured braking distance for all the brakings in the Arjeplog campaign is presented. From the data in this table it can be concluded that the spread of the measured braking distances falls well into the above percentages for all categories but one. The exception is category 4 - “braking on ice from 20 km/h”, where the ratio between the longest and the shortest braking distance is 1,52, which is well above the 1,22 (22%) that can be explained by variations of the initial speed. Instead, this large ratio can only be explained by local changes of the friction on the ice surface, or by changes of the ice/tyre-friction between each test run.

TABLE 6. BRAKING DISTANCE AND DECELERATION FROM ARJEPLOG CAMPAIGN

Table title detail: The measured braking distance and the estimated deceleration during the quasi steady region for all the brakings perfomed with the NIRA car in the Arjeplog campaign. The measurements can be divided into 8 categories, where the first three (id: 65–79) comprise the first test block on snow, the next two (id: 81-86) represent the test block on ice, while the last three (id: 90-97) are the second test block on snow.

Attempted Speed (km/h)	Surface	Measurement id	Measured braking distance (m)	Estimated ABS deceleration (m/s^2)
20	Snow	65	4,97	-3,27
20	Snow	66	4,55	-3,45
20	Snow	68	4,48	-3,75
20	Snow	69	4,95	-3,48
50	Snow	71	29,4	-3,37
50	Snow	73	31,6	-3,26
50	Snow	74	33,9	-3,20
50	Snow	75	32,1	-3,26
70	Snow	76	56,2	-3,49
70	Snow	77	59,2	-3,50
70	Snow	78	54,5	-3,61
70	Snow	79	56,2	-3,43
20	Ice	81	11,3	-1,17
20	Ice	82	17,2	-0,98
20	Ice	83	14,1	-1,01
50	Ice	84	86,7	-1,03
50	Ice	85	78,7	-1,16
50	Ice	86	90,7	-1,01
20	Snow	90	4,80	-3,40
20	Snow	91	4,45	-3,54
20	Snow	92	5,37	-3,47
50	Snow	93	27,1	-3,72
50	Snow	94	26,1	-3,75
50	Snow	95	27,3	-3,60
70	Snow	96	53,7	-3,64
70	Snow	97	48,8	-3,82

The average deceleration during the ABS-braking phase could be estimated by linear regression of the measured speed data. The ABS-braking phase was assumed to begin within 0,3 seconds after the start of the braking, and then continue until the vehicle is at stand still. For measurement technical reasons, explained in Section 7.1.2, speed data could only be measured until the vehicle reaches a speed below 1 m/s. A typical linear regression fit is shown in Figure 38.

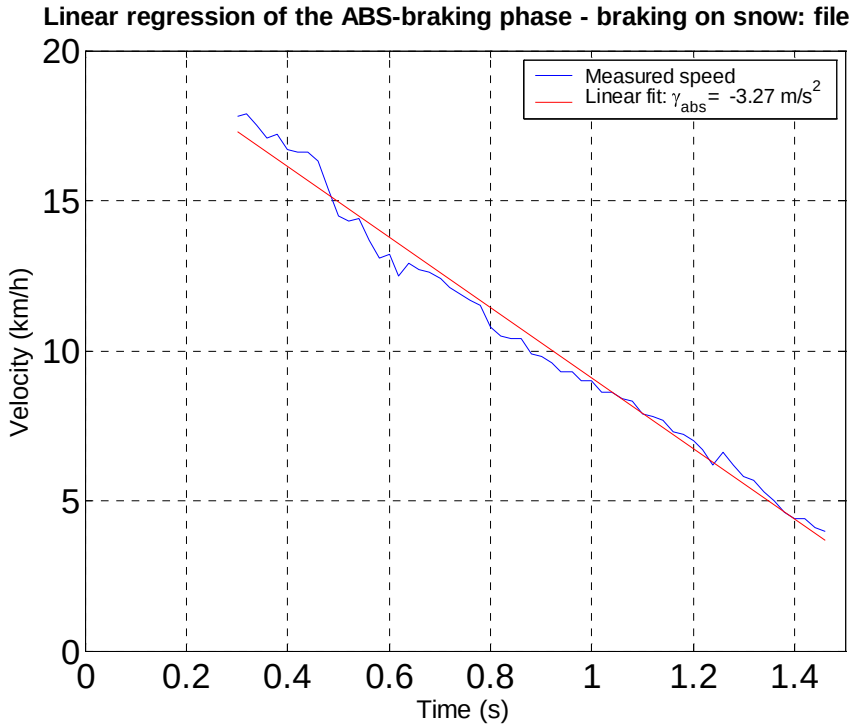


Figure 38. The measured velocity of the NIRA car during the ABS-braking phase

Figure title detail: The measured velocity of the NIRA car during braking on snow from 20 km/h, during the ABS-braking phase, which is assumed to begin before 0,3 seconds after the start of the braking. A linear regression fit to the data is also shown, where the slope of this line represents the estimated deceleration during the ABS phase.

The estimated ABS deceleration for all brakings is presented in TABLE 6. Averages of the estimated ABS decelerations within each measurement category are presented in TABLE 7. The averaged γ_{abs} values can be directly compared to the measured friction levels from the BV12, shown in Figure 37, multiplied by the factor *g*=9,81. There is a very good correspondence between deceleration- and friction data. On snow, a slip interval of 7-13% seems to include all deceleration averages, regardless of vehicle speed. On ice, the slip interval is larger, but it is still centred around 10% slip. Just as with the BV12 measurements, the deceleration estimates with the NIRA car does not indicate a typical speed dependence of the friction (apart from 70 km/h which exhibits a slightly higher friction than the lower speeds for all measurements). Hence, we conclude that γ_{abs} should be speed independent in our braking distance model. Furthermore, from inspection of the all linear fitting, no time dependence of γ_{abs} could be seen.

TABLE 7. AVERAGES AND STANDARD DEVIATIONS FROM THE MEASUREMENTS PRESENTED IN TABLE 6.

Surface	Speed	γ_{abs} - average	γ_{abs} - standard deviation
Snow	20	-3,49	0,20
Snow	50	-3,27	0,07
Snow	70	-3,51	0,08
Ice	20	-1,05	0,10
Ice	50	-1,07	0,08
Snow	20	-3,47	0,07
Snow	50	-3,69	0,08
Snow	70	-3,73	0,13

The model that will be used to describe the braking distance during winter conditions will then be identical to the one used for summer conditions. The braking process will be described by the three parameters t_s, γ_{peak} and γ_{abs}, where the two latter parameters are speed independent. After these parameters have been determined from the braking measurements, γ_{peak} and γ_{abs} can be coupled to a friction coefficient μ_{ref} via the constant parameters *a* and *b*. This friction coefficient μ_{ref} may be measured by a micro slip car like the NIRA, or by skid resistance measuring devices, like the ROADSTAR or the BV12.

Although the friction may differ between subsequent brakings, the general behaviour of the stopping process is the same for all brakings. This is illustrated in Fig. 40, where the travelled distance versus speed is plotted for the measurements within the category having the largest standard deviation, category 1 – braking on snow from 20 km/h during test block 1. In the figure the velocity/distance curves are shifted so that they end up in the same point. Several brakings can then be compared simultaneously, although different start speeds may have been used. As a comparison the expected stopping distance from 20 km/h during constant deceleration -µg is also indicated in the figure. In this case µ=0,34 produces a curve that is very similar to the measured ones.

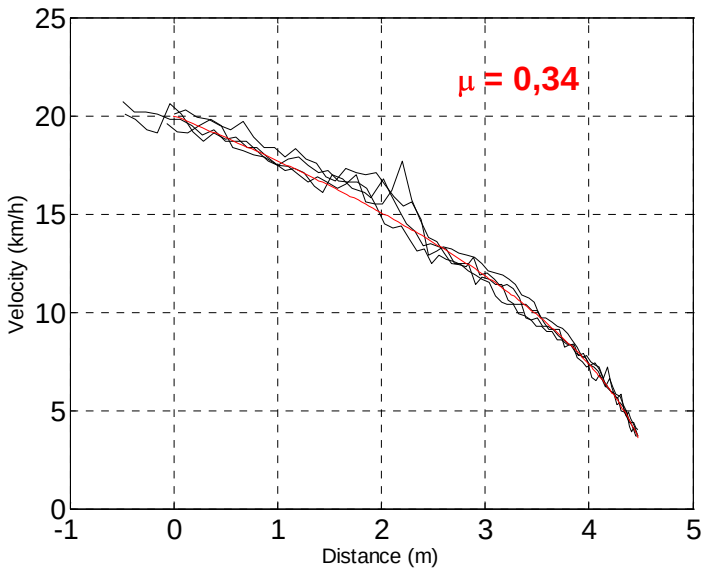


Figure 39. Four different brakings with the NIRA car compared to an estimated curve

Figure title detail: Four different brakings (id 65, 66, 68 and 69) with the NIRA car on snow from approximately 20 km/h are displayed with the velocity/distance curves shifted so that the end up in the same point at velocity 1 m/s. A reference line (red) indicates the expected stopping distance if a constant deceleration -μg is used. In this case μ=0,34.

By using the estimated values of γ_{abs} shown in TABLE 6 for every measurement, t_s, γ_{peak} could be determined through regression using the speed versus time data. The best way to do this is to use a constrained optimisation process, forcing $0 < t_s < 0{,}3s$ and $|\gamma_{peak}| > |\gamma_{abs}|$.However, as can be seen in Figure 39, the initial speed for each braking is rather unclear due to rapid oscillations in the speed signal from the Correvit sensor (probably due the difficult surface conditions). We have argued that small differences in the initial speed result in large differences of the braking distance. This implies that since the initial speed is not known with enough precision for each braking measurement, the initial speed itself must be part of the optimisation. The initial speed, denoted v_0, will of course be constrained so that $19 < v_0 < 21$ for brakings from 20 km/h, $48 < v_0 < 52$ for brakings from 50 km/h, and $68 < v_0 < 72$ for brakings from 70 km/h.

However, with relatively few data points per braking (the sampling frequency 50 Hz results in 15 recorded data points after 0,3 seconds), individual curve fitting of each braking using three independent optimisation parameters results in a large spread of the optimised parameter values. Instead, it is better to do a simultaneous curve fitting of all brakings within a category, using the same value of t_s. It is also reasonable to assume an upper limit for γ_{peak}. We have used the constraint $|\gamma_{peak}| \leq 1.2|\gamma_{abs}|$ The results of this optimisation is shown in TABLE 8.

TABLE 8. VALUES OF V_0, t_s AND γ_{peak}

Table title detail: The optimised parameters v_0, t_s and γ_{peak} from the curve fitting with constraints described in the text. Values of t_s within parentheses are the resulting values if no constraint for this parameter is used.

Attempted Speed (km/h)	Surface	Measurement id	v_0	t_s	γ_{abs}	γ_{peak}	$\gamma_{peak}/\gamma_{abs}$
20	Snow	65	19,9	0,22	-3,27	-3,92	1,20
20	Snow	66	19,4	0,22	-3,45	-3,98	1,15
20	Snow	68	19,9	0,22	-3,75	-4,17	1,11
20	Snow	69	20,1	0,22	-3,48	-3,49	1,00
50	Snow	71	49,0	0,30 (0,61)	-3,37	-3,37	1,00
50	Snow	73	50,1	0,30 (0,61)	-3,26	-3,26	1,00
50	Snow	74	51,5	0,30 (0,61)	-3,20	-3,20	1,00
50	Snow	75	50,5	0,30 (0,61)	-3,26	-3,26	1,00
70	Snow	76	69,6	0,30 (0,41)	-3,49	-3,49	1,00
70	Snow	77	71,6	0,30 (0,41)	-3,50	-3,64	1,04
70	Snow	78	69,6	0,30 (0,41)	-3,61	-3,61	1,00

70	Snow	79	69,3	0,30 (0,41)	-3,43	-4,12	1,20
20	Ice	81	19,0	0,03	-1,17	-1,41	1,20
20	Ice	82	21,0	0,03	-0,98	-0,98	1,00
20	Ice	83	19,5	0,03	-1,01	-1,01	1,00
50	Ice	84	48,0	0,18	-1,03	-1,24	1,20
50	Ice	85	48,5	0,18	-1,16	-1,16	1,00
50	Ice	86	48,8	0,18	-1,01	-1,01	1,00
20	Snow	90	19,9	0,21	-3,40	-4,08	1,20
20	Snow	91	19,5	0,21	-3,54	-4,24	1,20
20	Snow	92	21,0	0,21	-3,47	-3,47	1,00
50	Snow	93	50,2	0,20	-3,72	-4,46	1,20
50	Snow	94	49,1	0,20	-3,75	-3,75	1,00
50	Snow	95	49,6	0,20	-3,60	-4,15	1,15
70	Snow	96	69,4	0,29	-3,64	-3,64	1,00
70	Snow	97	68,0	0,29	-3,82	-4,58	1,20

No coherent behaviour of t_s and γ_{peak} when the velocity is altered can be seen on snow, nor on ice, as evident from TABLE 8. For the high friction surfaces, we concluded that t_s is proportional to the initial speed. The winter tests suggest that t_s is between 0,2-0,3 seconds on snow, and crude fitting of the data would result in even higher values if the upper constraint of 0,3 s would be removed. On ice the value is 0,03 seconds for braking from 20 km/h and 0,18 seconds from 50 km/h. Unfortunately we could not perform brakings from higher speed on ice, and in retrospect, brakings from a speed in between would have been useful for the analysis. However, we believe that the main reason no coherence could be found for these parameters when different speeds were used is because of the relatively poor quality of the velocity data. Ideally, acceleration data should be used for deriving the proper values of the parameters, and since the acceleration data obtained from numerical differentiation of the speed data was so poor, it could not be used.

Based on these findings, we propose a simple model which distinguishes between snow and ice only in that t_s have different values. We let $t_s = 0{,}25$ seconds for braking on snow, and $t_s = 0{,}10$ seconds for braking on ice. Furthermore, we let γ_{abs} and γ_{peak} be the same.

Now, a relation between γ_{abs} and the friction coefficient determined from a reference vehicle, μ_{ref} via the constant parameters *a* and *b* must be determined (*a*=*b* since $\gamma_{abs} = \gamma_{peak}$) . We have used the NIRA car and the BV12 as reference vehicles, and since the ROADSTAR were not used during the winter tests, parameters for the ROADSTAR on snow and ice could not be established. In contrast to the Nantes measurements on dry surface, where *a* and *b* parameters for 5 different surfaces with friction values ranging between 0.69 – 0.92 were determined, the winter measurements only comprised two different surfaces, ice and snow, and hence only two values of a (=b) must be determined for each reference vehicle. With only two values of the parameter it is quite pointless trying to interpolate parameter values for winter surfaces with friction in the range between pure ice and pure snow.

The friction measurements with the NIRA car and the BV12 are presented in Section 6.2. On snow, the NIRA car reported friction values μ_{Nira} in the range 0,32-0,50 and it makes sense to use a value in the middle of that interval to represent NIRA friction on snow. Thus, we use $\mu_{Nira} = 0{,}41$ on snow. For the BV12 we chose a slip value of 15% as a reference value. The measured friction values was in the range 0,35-0,39 at 15% slip, and we use $\mu_{BV12} = 0{,}37$ on snow. (There is no need in choosing a specific velocity for the reference tests with the BV12 as no evident speed dependence of the friction could be seen.) On ice, the NIRA car did not perform as expected, probably because the test track was too short, and there is no point in estimating parameters for NIRA on ice. The BV12 measured ice friction values in the interval 0,095-0,125 at 15% slip. We use $\mu_{BV12} = 0{,}11$ on ice.

The average value of γ_{abs} on snow is -3,53, which can be deduced from Tab. 7.2.2.2. On ice the average value is γ_{abs}=-1,06. Since $\gamma_{abs} = b\mu_{ref} g$, we have the following relations show in TABLE 9.

TABLE 9.

The a and b parameters for the NIRA car and the BV12 on snow and ice, determined from the Arjeplog measurement campaign. (*: The *a* parameter for the BV12 on ice was -0,98, but for simplicity we used the same value as for snow.)

Reference Vehicle	**Surface**	μ_{ref}	*a=b*	t_s (s)
NIRA	Snow	0,41	-0,88	0,25
NIRA	Ice	-	-	-
BV12	Snow	0,37	-0,97	0,25
BV12	Ice	0,11	-0,97 *	0,10

As the BV12 *a* parameters are almost identical for ice and snow, it is a useful simplification to use the same value, 0,97. By using the parameters in TABLE 9, the estimated braking distances could be calculated for all measured brakings, using the initial velocities v_0 from TABLE 8, and compared with the measured distances. We have the following results:

- By using the μ_{Nira} value 0,41 for braking on snow, the relative error of the calculated braking distances compared to the measured values was on average 4%
- By using a μ_{Nira} in the range 0,32-0,50 for braking on snow, the relative error of the calculated braking distances compared to the measured values was on average 28%
- By using the μ_{BV12} value 0,37 for braking on snow, the relative error of the calculated braking distances compared to the measured values was on average 4%

- By using a μ_{BV12} in the range 0,35-0,39 for braking on snow, the relative error of the calculated braking distances compared to the measured values was on average 10%
- By using the μ_{BV12} value 0,11 for braking on ice, the relative error of the calculated braking distances compared to the measured values was on average 7%
- By using a μ_{BV12} in the range 0,095-0,125 for braking on ice, the relative error of the calculated braking distances compared to the measured values was on average 20%

However, since the stopping distance is the sum of the reaction time distance and the braking distance, and because the first entity is known with high precision, the relative errors for the stopping distance are smaller than those for the braking distance. If we assume a reaction time of one second before the driver pushes the brake pedal, we obtain stopping distances with the following accuracy

- By using the μ_{Nira} value 0,41 for braking on snow, the relative error of the calculated stopping distances compared to the measured values was on average 3%
- By using a μ_{Nira} in the range 0,32-0,50 for braking on snow, the relative error of the calculated stopping distances compared to the measured values was on average 17%
- By using the μ_{BV12} value 0,37 for braking on snow, the relative error of the calculated stopping distances compared to the measured values was on average 3%
- By using a μ_{BV12} in the range 0,35-0,39 for braking on snow, the relative error of the calculated stopping distances compared to the measured values was on average 6%
- By using the μ_{BV12} value 0,11 for braking on ice, the relative error of the calculated stopping distances compared to the measured values was on average 5%
- By using a μ_{BV12} in the range 0,095-0,125 for braking on ice, the relative error of the calculated stopping distances compared to the measured values was on average 16%

8 Conclusions

A procedure to estimate the braking distance of a passenger vehicle using a reference friction value as input has been worked out. The procedure have been tested and validated on both high and low friction surfaces (summer and winter conditions) using two different types of reference vehicles. Arsenal's ROADSTAR and VTI's BV12 represent the first type, which uses a 5th wheel to monitor the tyre/road friction. The second type, represented by an Audi A3 equipped with NIRA

Dynamics micro slip solution for estimating the available tyre/road friction using only the standard components of the vehicle's ABS and ESP system.

The braking distance is defined as the distance travelled by the vehicle from the moment when the driver starts pushing the brake pedal until the vehicle is at complete stand still. The braking distance is obviously driver dependent since applying different pressures on the braking pedal yields different braking distances. The model developed and validated in this report concerns a panic braking situation where maximum possible brake pressure is applied on the brake pedal. It is also important to realise that the total stopping distance, comprising both the distance travelled during the time it takes for the driver to react to an emergency and start hitting the brakes and the braking distance, can be much longer than the actual braking distance.

The proposed braking distance model is based on a simplification of the deceleration curve in two regions: a transient and a stabilised region. Key values of the model are transient time t_s, and coefficients *a* and *b*, where the two coefficients represent the link between the vehicle and the reference vehicle. The transient time t_s is affected by the choice of brake system of the vehicle, but could also depend on the vehicle's weight and the tyres.

Due to the restricted budget of the INTRO WP 2.1 we could only use one tyre for determining the parameters of the model. We chose an all season tyre, the Vredestein Quatrac. It was also not possible to distinguish between the individual effects on the parameter values from using different braking systems, or different vehicle weights. Instead, complete parameter sets for three different cars were determined to see how sensitive the model is to different vehicle properties. Three cars belonging to three different vehicle classes were chosen: the Renault Clio, the Peugeot 306 and the Peugeot 406. The effect tyre wear has on the tyre/road friction has not been targeted in this study.

INTRO WP2 deals with slippery risks due to water, snow or ice. The model has then two components: "summer" and "winter". Theoretically, both components must use the same inputs. However, their development was executed as two separate sub-tasks since the physical phenomena during tire/wet-road and tire/snowy- or icy-road contacts are not the same. This difference can have significant consequences on *a, b* and t_s determination. The "summer" part covered wet asphalt surfaces with friction values ranging from intermediate to high, while the "winter" part covered icy and snowy surfaces with low to intermediate friction levels. Ideally, there should have been a crossover between the intermediate friction intervals of "summer" and "winter" surfaces to see if wet surfaces and snow surfaces with the same friction coefficient results in identical parameter values, or if there exist a fundamental difference. Unfortunately this was not possible.

The "summer" braking tests were performed on 5 sections with various friction levels, using the three test vehicles, the Renault Clio, the Peugeot 306 and the Peugeot 406. The ROADSTAR and the NIRA car was used as friction measuring reference vehicles. The friction levels as reported by the ROADSTAR at 80 km/h were in the range 0,69-0,92. The NIRA car failed to distinguish between the different surfaces, and hence no model parameters using NIRA friction values as input were determined.

The “winter” braking tests were performed on two different surfaces: polished ice and packed snow using the NIRA car. The BV12 and the NIRA car was used as friction measuring reference vehicles. The friction level as reported by the BV12 at 15% slip at various speeds, was on average 0,11±0,015 on ice and 0,37 ±0,02 on snow. The NIRA car reported a friction level of 0,41±0,09 on snow, but failed to measure the friction of the ice, possibly because the ice track was too short. Hence no model parameters for braking on ice using NIRA friction values as input were determined.

The results of the parameter fitting to measured braking distances can be summarised as

High friction tests (“summer”):

- It was possible to obtain *a* and *b* coefficients of the proposed model for each of the three tested vehicles, so that together with ROADSTAR friction levels the braking distance could be estimated within 10% accuracy on the five tested high friction (“summer”) surfaces.
- The *a* and *b* coefficients, different for each vehicle, are proportional to the reference friction value, but they are independent on vehicle speed.
- The t_s parameter, different for each vehicle, are proportional to vehicle speed, but they are independent on the reference friction value.

This suggests that other vehicles than the tested ones can be used with the proposed braking distance model, and the procedure to be followed for determining the parameters on “summer” conditions is:

1. select a least 3 sections of different friction coefficient (low, medium, high);
2. perform three emergency braking for two speeds;
3. from the deceleration curves evaluate t_s versus speed and the coefficient a and b;
4. check out the estimator on another section.

If different loads are possible these tests have to be preformed for each load case.

It should be noted that the NIRA car failed to distinguish between the different surfaces, and hence no model parameters using NIRA friction values as input were determined. One possible reason for this could be the relatively short test tracks for measurements on wet surfaces giving the NIRA algorithm not enough values for a good estimation. As this algorithm is knowledge belonging to the subcontractor NIRA it is not possible to verify this assumption.

Low friction tests (“winter”):

- It was possible to obtain *a* and *b* coefficients of the proposed model for braking with the NIRA car on ice, so that together with BV12 friction levels at 15% slip the braking distance could be estimated within 20% accuracy.
- It was possible to obtain *a* and *b* coefficients of the proposed model for braking with the NIRA car on snow, so that together with BV12 friction levels at 15% slip the braking distance could be estimated within 10% accuracy.
- It was possible to obtain *a* and *b* coefficients of the proposed model for braking with the NIRA car on ice, so that together with NIRA friction levels at the braking distance could be estimated within 28% accuracy.

- The best fit is obtained with using the same value for *a* and *b*. This value is the same for both ice and snow, which suggests that it is not friction dependent (at least for low friction).
- No dependence on vehicle speed was found for the t_s parameter.
- Since only two different test surfaces were available, no friction dependence on the t_s parameter could be established, although t_s takes a low value on ice and a higher one on snow.

.

The values of the parameters for low and high friction can not be directly compared since different test vehicles have been used, so it is not possible to draw the conclusion that a common set of parameters can be used with the model for estimating the braking distance on both “summer” and “winter conditions with only a reference friction value as input. Additional input regarding the road conditions (ice, snow or wet/dry) is needed. It would take more testing using surfaces with friction in between pure polished ice and packed snow, as well as really low friction asphalt surfaces for a conclusion whether a reference friction value is enough for braking distance estimation.

9 References

[1] INTRO Milestone M2.1, Final Specifications for Micro-Slip Measurement Subsystem Including Data Communication Interfaces.

[2] INTRO Milestone M2.2, Mutual Exchange of Pre-Processed Measurement Data from Test Site.

[3] WAMBOLD J.C., ANTLE C.E., HENRY J.J., RADO Z., DESCORNET G., SANDBERG U., GOTHIÉ M., HUSCHEK S., International PIARC Experiment to Compare and Harmonize Skid Resistance and Texture Measurements, PIARC Publication n°01,04,T, Paris, 1995.

[4] DESCORNET G., SCHMIDT B., BOULET M., GOTHIÉ M., DO M-T., FAFIÉ J., VAN DEN BOL M., ALONSO M., ROE P., FOREST R., VINER H., (2004), HERMES Final Report, FEHRL Report 2004/1, 358 pages.

[5] KAHANE C.J., Preliminary Evaluation of the effectiveness of Antilock Brake Systems for Passengers Cars, NHTSA Report Number DOT HS 808 206. December 1994.

[6] SCHULTZ G.A, BABINCHAK M.J., Final report for the methodology study of the consumer braking information initiative, Report N° ATC -8170 US Army, September / November 1998.

[7] FORKENBROCK G., FLICK M. GARROTT W.R., NHTSA Light Antilock Brake System Research Program Task 4 – A Test Track Study of Light Vehicle ABS Performance Over a Broad Range of Surfaces and Maneuvers – DOT HS 808 875 January 1999.

[8] HOGT R.M.M.,. JORDENS R.A.P, GERRITSEN W., WENNINK P.M.: Will we be able to predict the braking distance?, PIARC World Road Congress; Kuala Lumpur (Malaysia); October 1999.

[9] HOGT R.M.M.,. JORDENS R.A.P, GERRITSEN W., WENNINK P.M.: From texture to braking deceleration, SURF 2000 congress; Nantes; May 2000.

[10] HOGT R.M.M., VAN OOSTEN J.J.M., Road - scaled Magic Formula for braking performance of cars; 3rd International Tyre colloquium; Darmstadt; October 2000.

[11] NEPTUNE J. A., FLYNN J. E., CHAVEZ P. A., and UNDERWOOD H. W., Speed from Skids: A Modern Approach, J2 Engineering, Inc SAE paper 950354 J2 Engineering, Inc.

[12] NORDSTRÖM, O., The VTI flat bed tyre test facility – A new tool for testing commercial tyre characteristics. Reprint from SAE Technical paper series, SP 1003 – The influence of tire, axle and brake characteristics on truck braking and steering performance, paper 933006, pp. 13-23 (International truck and bus meeting and exposition, Detroit, Michigan, November 1-4, 1993).

[13] GARROTT, R.W, MAZZAE, E.N., An Overview of the National Highway Traffic Safety Administration's Light Vehicle Antilock Brake Systems Research Program. SAE technical paper 1999-01-1286, 1999.

[14] GUSTAFSSON, F., Slip-based tyre-road friction estimation, Linköping University, 1995.

[15] INTRO Task 2.1, Measurement CD, 2006.

[16] GILLESPIE, T.D., Fundamental of vehicle dynamics, SAE, Warrendale, 1992.

[17] FORKENBROCK G., FLICK M. GARROTT W.R., A comprehensible Light Vehicle Antilock Brake System Test Track Performance Evaluation, Paper SAE 1999-01 -1287.

[18] GRACE R, WISSJ.W., AUDAK J.J., EUBANKS C.N., Technology Review for Electronically Controlled Braking Systems, DOT HS 808 803 sept 1998 NHTSA USA

[19] CARLEY L., All About ABS, 2005 CarleySoftware
http://www.aa1car.com/library/abs1.htm

[20] JIANG F., Z. GAO, An Adaptive Nonlinear Filter Approach to Vehicle. Velocity Estimation for ABS, Applied Control Research Laboratory - Cleveland State University.

[21] ELTING D., FENNICH M., KOWALCZYK R. and B. HELLENTHAL B., Fuzzy Anti-Lock Brake System Solution, http://www.intel.com/design/mcs96/designex/2351.htm

[22] DENNY M., The dynamics of antilock brake system, European Journal of Physics 26 (2005) pp; 1007-1016.

[23] EL HADRI A., CADIOU J.-C., M'SIRDI N., DELANNE Y., Wheel-Slip Regulation based on sliding mode approach, SAE 2001, Transactions journal of passenger cars - Mechanical systems.

[24] MAURER, P. ET AL., Straßenzustandserfassung mit dem ROADSTAR – Messsystem und Messgenauigkeit; Research Report; Vienna 2002.

[25] CEN / TC 227 / WG5 /TG2, Procedure for determining the skid resistance of pavements using the Road Surface Tester of arsenal research (ROADSTAR) with longitudinal controlled slip – Technical specification.

[26] GRUBER, J., MAURER P., Zustandserfassung der Straßenoberfläche auf Bundesstraßen B – Messungen mit dem ROADSTAR in den Jahren 2001 und 2002; Bundesministerium für Verkehr, Innovation und Technologie, Straßenforschung Heft 452, Vienna 2004.

10 Appendices

10.1 Tire/ground relationship

10.1.1 Slip rate

Slipping is due to the difference between the local speed of the wheel and the longitudinal speed of the vehicle. During braking, the local speed of the wheel of the contact tyre-ground : $\omega.\mathrm{Re}\,ff$ becomes lower than the longitudinal speed of the vehicle V . The wheel does not make a complete turn, it has to slip in order to follow the motion of the vehicle. This is explained by Figure 40.

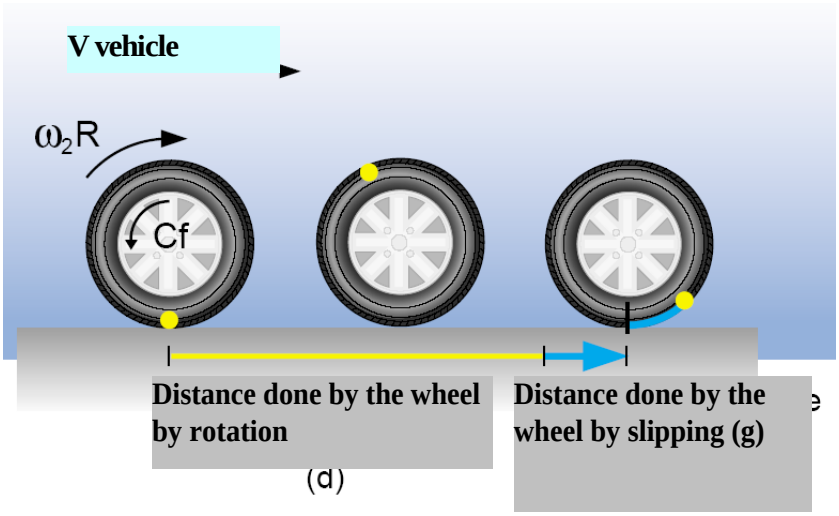


Figure 40. Slipping of the wheel

In the following, we define the slip rate κ according the experimental environment:

F		
(23)	$\kappa = 100.\dfrac{\mathrm{Re}\,ff.\omega - V}{\mathrm{Re}\,ff.\omega}$	For longitudinal acceleration
(24)	$\kappa = 100.\dfrac{V - \mathrm{Re}\,ff.\omega}{V}$	For longitudinal braking.

Table 1 : definition of slip rate

With :

- V is the longitudinal speed of the vehicle (m/s).
- $\mathrm{Re}\,ff$ is the effective radius of the wheel (m).
- ω is the angular velocity of the wheel (rad/s).

According to this definition

- $0 < \kappa < 100\%$ *or* $0 < \kappa < 1$ is positive.
- $\kappa = 100\%$ *or* 1, implies
  - o either the wheel spins, in the case of acceleration
  - o or the wheels are blocked in the case of braking

10.1.2 Braking force and longitudinal friction coefficient

We got the global longitudinal friction force thank to the equation (2). In order to get the friction force for a wheel, we have to take into account the wheel dynamic. Figure 41 shows the external forces applied to the wheel.

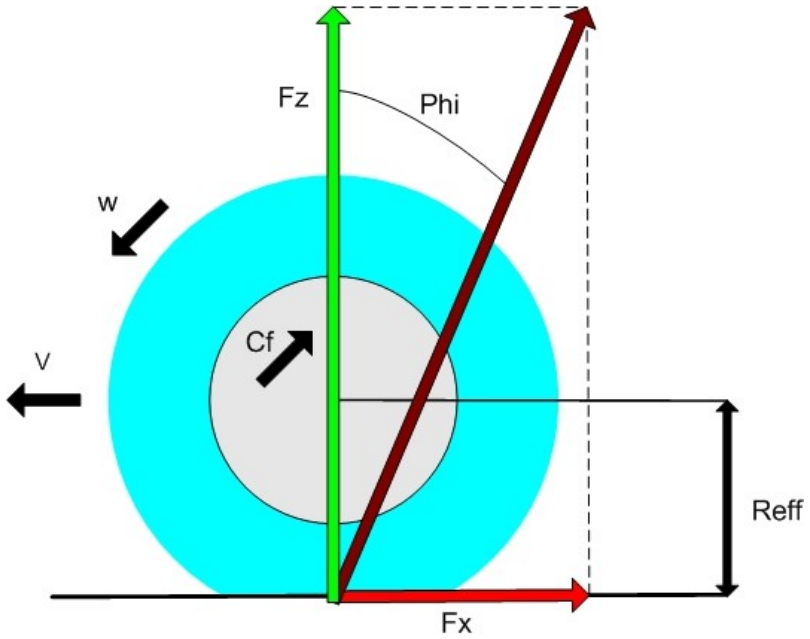


Figure 41. External forces applied on the wheel during braking

The braking torque Cf acts against the moment due to the friction force.

(25) $$Fx = \frac{J_r.\dot{\omega} - Cf}{\mathrm{Re}\ ff}$$

With :

- J_r = moment of inertia of the wheel (kg.m^2).
- $\dot{\omega}$ = angular acceleration (rad/s^2).

The Coulomb's second law defines the longitudinal friction coefficient μ as

(26) $$Fx = \mu.Fz$$

and :

(27) $$\mu = \frac{Fx}{Fz} = \tan(\varphi)$$

μ varies with

- the surface of the road
- Speed
- Tyre : temperature, pressure, geometry, worn.

Figure 42 shows evolution of μ according to slip and speed. The red curve and the cyan curves shows the difference between a braking with and without ABS.

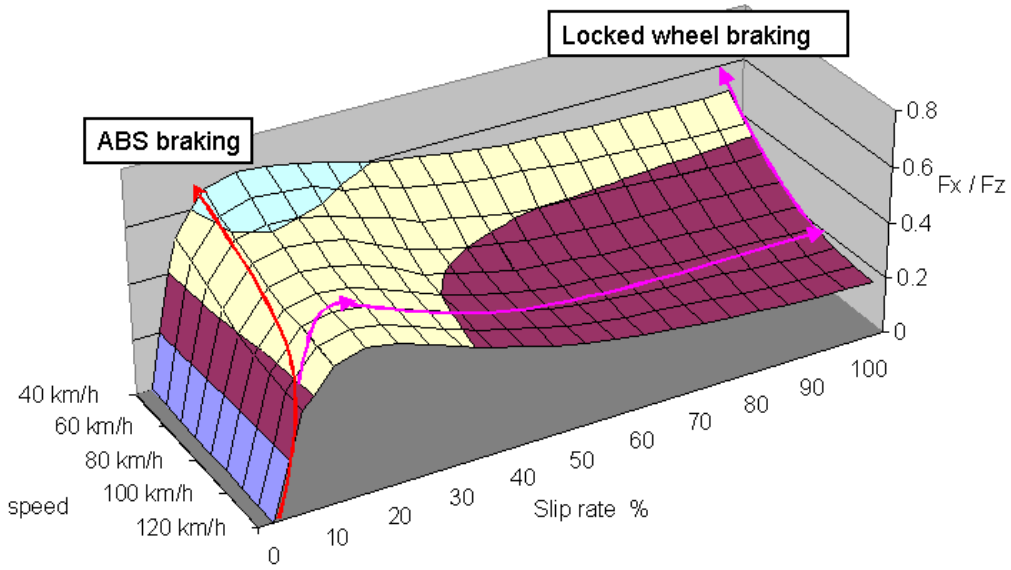


Figure 42. 3D braking curves

10.2 Vehicle dynamics during longitudinal braking

The purpose of this section is to give the equations which are used in order to compute the variables which are plotted in the section concerning the experiments. The objective of this section is to present a report which can be understood by itself. A detailed presentation of the dynamic of a car is out of the scope of this section and can be found in [16].

Here, we derive the longitudinal equations of motion for a car during braking from the external forces, a dynamic model of the car and a tire-ground model. These different models are presented in the following subsections.

10.2.1 External forces

Considering a 2D vehicle on a plan with slope, Figure 43 show the external forces applied to this vehicle.

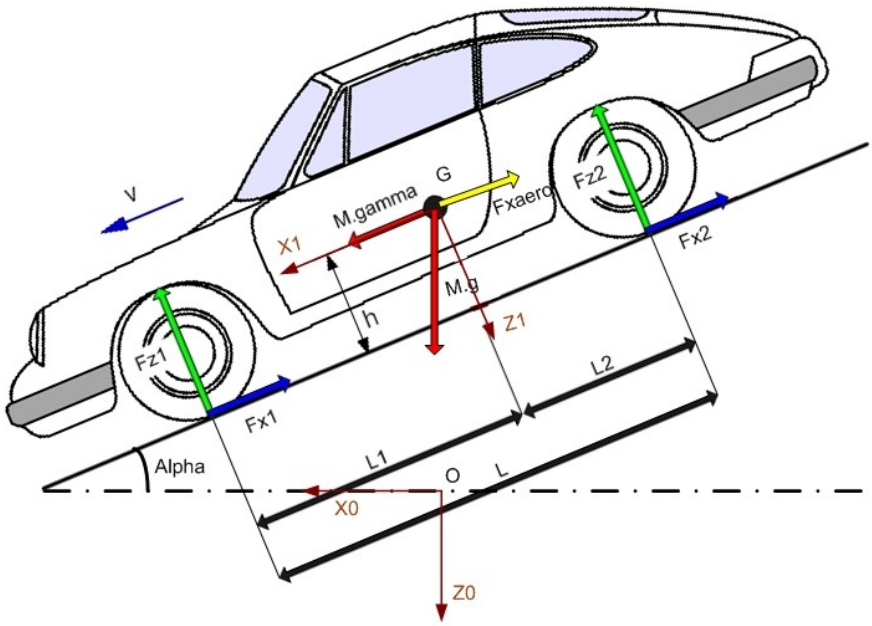


Figure 43. External forces acting on the braking longitudinal car

- G = Center of gravity
- L = Wheelbase (m)
- L_1 = Distance between the center of gravity to the front axle (m).
- L_2 = Distance between the center of gravity to the front axle (m).
- h = Height of the center of gravity to the ground (m).
- m = mass (kg).

- $R_1(G; X1, Z1)$ = frame linked to the chassis of the vehicle.
- $R_0(O; X0, Z0)$ = frame linked to the ground.

- $Fx1$ = longitudinal friction force at the bottom of the front wheel (N).
- $Fx2$ = longitudinal friction force at the bottom of the rear wheel (N).
- $Fz1$ = normal reaction of the ground a the bottom of the front wheel (N)
- $Fz2$ = normal reaction of the ground a the bottom of the rear wheel (N)
- $P = m.g$ = weight of the vehicle.
- F_{xaero} = drag force, for simplicity, we assume that the drag force acts on the center of gravity of the car body(N).
- V = vehicle longitudinal speed (m/s).
- γ =acceleration (m/s2).

10.2.2 Dynamic model

We apply the Newton' s Second Law :

(28) $$\sum \mathrm{F_{ext}} = \mathrm{P} + \mathrm{Fz1} + \mathrm{Fz2} + \mathrm{F_{xaero}} = \mathrm{M}.\gamma$$

The projection of this equation to the axis $\mathrm{R_1(G;X1)}$ gives the global longitudinal friction force of the vehicle.

(29) $$\mathrm{Fx} = \mathrm{Fx_1} + \mathrm{Fx_2} = \mathrm{M}.(\gamma + \mathrm{g}.\sin\alpha) - \mathrm{F_{xaero}}$$

If we consider momentums, we get $\mathrm{Fz_1}$ and $\mathrm{Fz_2}$

(30) $$\mathrm{Fz_1} = \mathrm{M.g.}\frac{\mathrm{L_2}}{\mathrm{L}}.\cos\alpha + \mathrm{M}.(\gamma + \mathrm{g}.\sin\alpha).\frac{\mathrm{h}}{\mathrm{L}} - \mathrm{F_{xaero}}.\frac{\mathrm{h}}{\mathrm{L}} = \mathrm{P_{1stat}} + \Delta\mathrm{P} - \Delta\mathrm{P_{aero}}$$

(31) $$\mathrm{Fz_2} = \mathrm{M.g.}\frac{\mathrm{L_1}}{\mathrm{L}}.\cos\alpha - \mathrm{M}.(\gamma + \mathrm{g}.\sin\alpha).\frac{\mathrm{h}}{\mathrm{L}} + \mathrm{F_{xaero}}.\frac{\mathrm{h}}{\mathrm{L}} = \mathrm{P_{2stat}} - \Delta\mathrm{P} + \Delta\mathrm{P_{aero}}$$

with :

$\Delta\mathrm{P} = \mathrm{M}.(\gamma + \mathrm{g}.\sin\alpha).\frac{\mathrm{h}}{\mathrm{L}}$: the load shift front the rear axle to the front axle

$\Delta\mathrm{P_{aero}} = \mathrm{F_{xaero}}.\frac{\mathrm{h}}{\mathrm{L}}$: the aerodynamic load shift from the front to the rear.

10.3 Antilock Braking Systems

More than two-thirds of all new vehicles are fitted with four-wheel ABS.

10.3.1 Principle

Typical ABS systems have speed sensors at each wheel that continuously feed information to a centrally located ABS computer. The computer uses this data to determine overall vehicle speed, and to detect when a wheel begins to lock. Since

each wheel is independently controlled (in a four-channel ABS system), pressure is automatically limited or reduced to only the wheel that is locking [17][18][19].

10.3.2 Hydraulic phases

Virtually all ABS systems use three phases of hydraulic control during a panic stop. The first phase is referred to as pressure maintain. If the controller senses that wheel slip approaches a programmed value (tire max slip) based on the wheel's deceleration rate, it will enter the pressure maintain phase. This means that the modulator will block off any additional fluid pressure from the master cylinder (driver pedal pressure) to the affected wheel(s). If the wheel slip continues to rise in the pressure maintain phase, hydraulic pressure to the wheel(s) is then released until a min tire slip. This is the second phase of operation, known as pressure decrease. The final phase is referred to as pressure increase. If wheel slip drops low during the pressure maintain phase, hydraulic pressure to the wheel(s) is increased until wheel braking begins. This pressure increase is actually maximum master cylinder pressure that is applied to the wheels.

10.3.3 ABS Electronic Control Unit

The way the electronic controller monitors system operation in acting on the hydraulic depends on the trademark and the generation of ABS controllers. The ECU and control algorithm are partially responsible for how well the ABS system performs. Since December 1970 when Daimler-Benz introduced the first-generation anti-lock braking system progressive improvements of the code were carried out and this subject remains of current interest [20][21].

10.3.4 Simulation of ABS

In [22] a very simple algorithm is described to explain the dynamics of ABS. A more complicated algorithm but simply based on the first generation control code, is presented in [23]. Figure 44 shows a basic structure for ABS control. Accurate slip estimation is a key of ABS control; the tire slip regulation seeks to get the highest deceleration.

Recent algorithms have become more and more complicated to account for the pneumatic time delays, the non-linearity in brake torque due to temperature variation and dynamics of brake fluid viscosity and system components aging, the influences of tire wear, changes in frictional coefficient and road surface. The remaining difficulty is the estimation of the absolute vehicle speed during braking and the wheel angular velocity and acceleration. As the model becomes increasingly complex equations required to control ABS also become increasingly complicated.

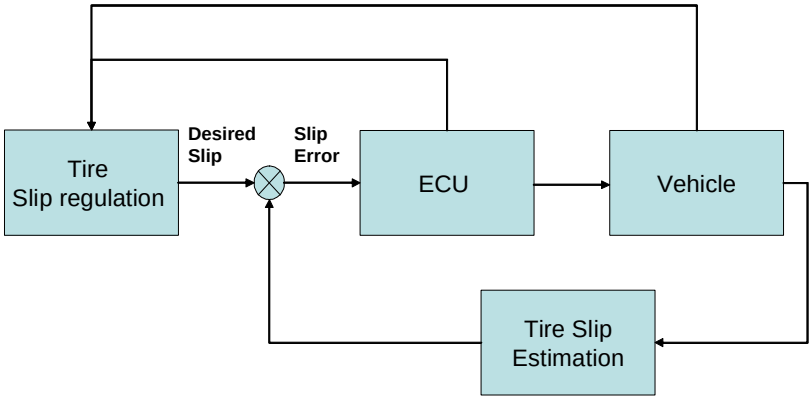


Figure 44. Basic structure for ABS control

10.4 Device descriptions

10.4.1 ROADSTAR

10.4.1.1 Principle of measurements

ROADSTAR's skid resistance measuring unit allows the simulation and investigation of different braking states. The system supports measurements with different slip ratios as well as ABS (antilock braking system) measurements and measurements with blocked wheel.

Skid resistance measurements are done using the "modified Stuttgart skiddometer". The new design of the loading unit - a pneumatic cylinder keeping the tyre contact pressure of the measuring wheel constant - and the additional acquisition of current wheel loads have resulted in a significant increase in the measuring accuracy of friction coefficients. ROADSTAR´s skid resistance measuring unit allows different braking states to be simulated and investigated. The system supports slip measurements as well as ABS and measurements with blocked wheel.

The wetting function enables the specification of a defined water film thickness for all measurements. The amount of water required is adjusted depending on the specified measuring speed [24].

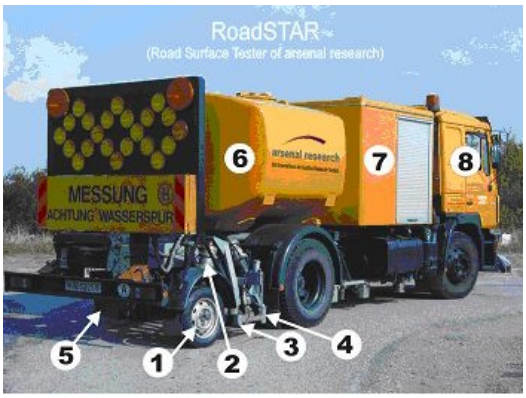


Figure 45. Overview of the ROADSTAR



Figure 46. Skid resistance device

①	Measuring wheel including braking torque measurement	⑤	Gearbox
②	Pneumatic cylinder	⑥	Water tank
③	Wetting unit	⑦	Device storage
④	Prewetting system	⑧	Drivers cabin - digital data acquisition

The actual μ is measured every five millimetres; online averaging results in a minimal section length of five meters.

The measuring wheel at the rear of the vehicle is mounted in such a manner that it runs freely around bends without being subjected to lateral forces. The test wheel arrangement comprises a pneumatic controlled loading cylinder, a torque axle, a gear box and an e-coupler to provide a constant slip ratio, an incremental encoder to record the speed of the test wheel, an electrical load cell to measure the vertical load and a strain gauge to measure the torque caused by the horizontal load in the contact area tyre/pavement. The pneumatically controlled loading unit and the additional registration of current (static and dynamic) wheel loads allow uniform and accurate wheel loading, thus resulting in a significant increase in measuring accuracy. A mechanism raises and lowers the test wheel arrangement from and to the ground [25][26].

During measurements, the current wheel load and braking torque are recorded. Using the known radius of the measuring wheel, the actual μ is calculated. Braking force between tyre and road surface is calculated as described below:

$$F_B = M_B / r$$

F_B ..... Braking force [kN]
M_B .... Braking torque [kNm]
r ..... Radius of measuring wheel [m]

From braking force F_B and measured wheel load F_N the friction coefficient μ is derived (see Figure 47)

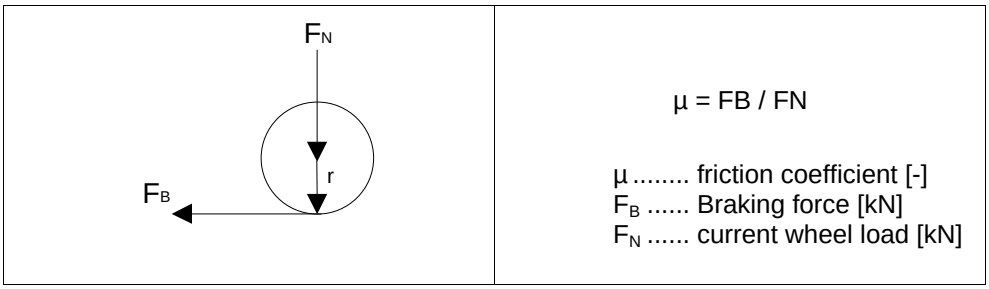


Figure 47. Calculation of friction coefficient μ

The following measurement values are collected during friction measurements:

- station in [m]
- static wheel load in [N]
- dynamic wheel load [N]
- actual speed in [km/h]
- braking torque in [Nm]
- surface temperature in [°C]
- wheel temperature in [°C].

10.4.1.2 Measured data

Figure 48 to Figure 50 show examples of the measured data

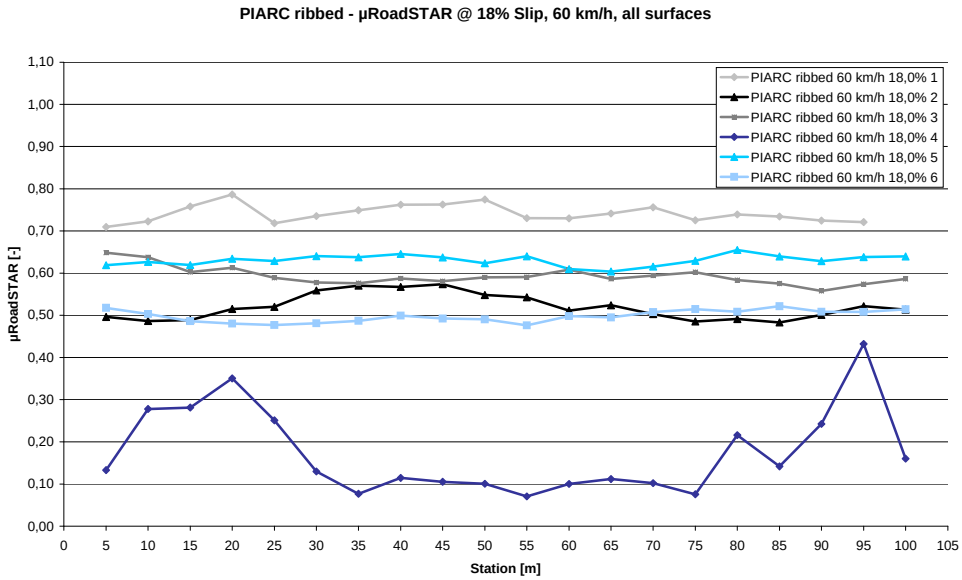


Figure 48. One tyre at one speed and slip, different surfaces

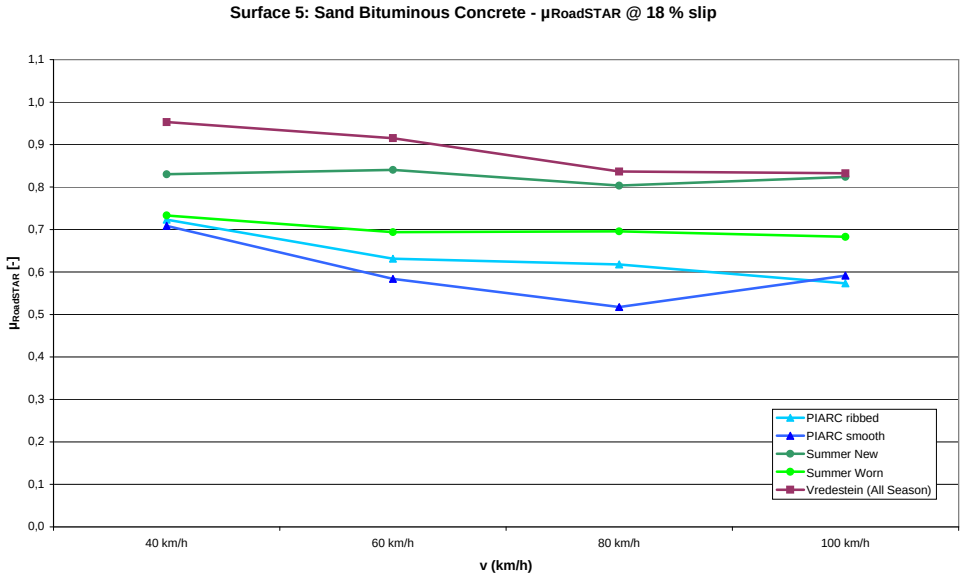


Figure 49. One surface, different tyres and speeds

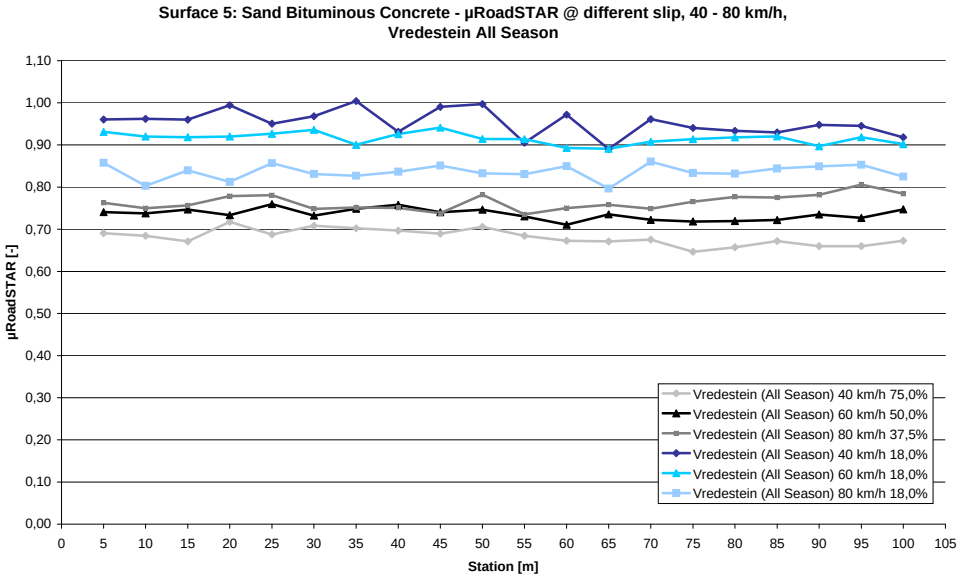


Figure 50. One tyre, one surface, different slips and speeds

10.4.2 BV12

The VTI friction test vehicle BV12 shown in Figure 51 and Figure 52 is a specially equipped truck with a test wheel suspension for passenger car wheels. The test wheel can be forced to rotate at the constant slip that produces maximum braking performance by means of a cardan shaft connected via a chain drive to a gearbox with continuously variable slip up to about 50 % braking slip and about 10 % traction slip. There is also a setting that produces 100% traction slip. (Slip is usually given in percent and is defined as 100 times the ratio between the difference between the

free rolling rotational velocity (w_r) and the rotational velocity during braking (w_b) and the free rolling velocity (Slip = 100 (w_r - w_b)/ w_r).

However, for complete tire friction characterization, full braking slip curves are required. To accomplish such measurements, the gearbox can be decoupled and the test wheel can be continuously braked from zero to 100 % slip by a disc brake system connected to the wheel via the cardan shaft. This hydraulic disc brake is actuated from an electro-hydraulic power unit controlled from a PC. Both application start and release time, application rate and maximum pressure can be remotely controlled by a computer program.



Figure 51. The VTI BV12 measurement vehicle for passenger tyre friction characterisation.



Figure 52. The VTI BV12 measurement vehicle from the rear.

10.4.2.1 The vertical load and the side slip angle

The vertical load can be controlled by a double acting air spring cylinder. When loads lower than the dead weight of the suspension and measuring system of 2850 N is required, the air cylinder is producing a lifting force. The pressure in the spring can be set from the drivers cabin by a manually adjustable pressure regulator. In order to lift the test wheel from the ground between measurements there is a separate system consisting of an electrically driven linear actuator.

The side slip angle is set by an electric steering cylinder which is controlled from a PC program. All PC control signals enter a specially developed electric power control system in a box at the rear of truck. This system then actuates the power units.

10.4.2.2 Force measuring system

Forces acting on the wheel in all three directions are measured by rear mounted force measuring hub constructed at VTI. The system contains standard Bofors KG1 force transducers for longitudinal and transversal forces, while the vertical force is measured by a standard Bofors KIS 1 cylindrical shear force transducer, sensitive to forces only in one direction. The basic construction of the measuring hub is shown in Figure 53.

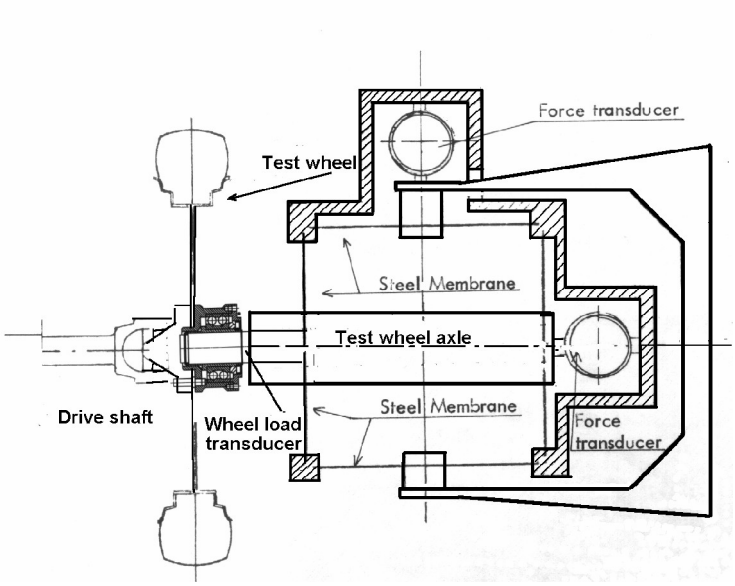


Figure 53. Triaxial force measuring hub principle drawing.

10.4.2.3 Side slip angle and speed measuring system

The side slip angle is measured both relative to the vehicle and relative to the ground.
The angle relative to the vehicle is measured by a potentiometer with a spring-loaded wire/pulley actuation system. The wire is attached to the cylindrical rotating upper end of the steering shaft (see figure). The angle relative to the ground is measured by a fifth wheel with a potentiometer connected to the vertical suspension hinge

The speed of the vehicle is measured by means of the original Leine Linde digital pulse encoder at the left front wheel of the truck. A similar device is used for measuring the rolling speed of the test wheel.

10.4.2.4 On board vehicle water film application system for aquaplaning tests

The BV12 carries an on board water supply system. It consists of a pump driven by a Volvo B18 120 HP petrol engine taking water from the original 3 m^3 water tank and letting the water out through a long tapered nozzle with an opening 200 mm wide and a variable height up to 10 mm. The maximum performance is a nominal water film height of 8 mm at 100 km/h outflow speed which is the maximum obtainable speed of the BV12. The last 100 mm of the nozzle is U-beam shaped open to the ground with the upper wall at a height over ground corresponding to the water film height. The front end of the nozzle is hinged close to the rear axle of the truck and the rear end supported by four roller skate wheels in bogie arrangement. The rear end is also connected to the test wheel suspension by a wire so that it is lifted from the ground when the test wheel is lifted. The nozzle ends about 200 mm in front of the contact area of the tyre. At a speed of 20 m/s the water hits the wheel 0.01 s after leaving the nozzle. The outflow through the nozzle is started by opening two

computer controlled electro-pneumatically activated valves, one on each of the two flexible tubes, between the pump and the nozzle.

The water flow is controlled both by the orifice height and the engine RPM which can be set from inside the cabin, and by manually adjusting the outlet valves from the pump. The system is calibrated by measuring time for the outflow of a given volume of water from the tank for several specific combination of control settings.

The water system is completely removed for winter measurements.

The system is illustrated in Figure 54.



Figure 54. The water nozzle supplying the water film for wet measurements

Figure title detail: The water is pumped from the 3000 litre tank through the water pipe below the tank to the fire engine and from there through two flexible pipes that pass under the rear axle of the truck to the nozzle that is sliding wit its orifice on the ground.

10.4.2.5 VTI test vehicle BV12 specifications

Test vehicle data
Test vehicle type: Scania LB80 1973
Test vehicle maximum weight: 12 000 kg
Water Tank capacity: 3000 litres
Maximum test speed: about 100 km/h

Tyre friction force measuring system

Vertical load: 1000 N to 6000 N
Lateral force: +/- 8000 N (Nominal 5000 N transducer range)
Longitudinal force: +/- 8000 N (Nominal transducer range 5000 N)
Static calibration error: less than 10 N on all transducers
Disk brake capacity: 8000 N

Slip range
Longitudinal slip range in constant slip mode: 0-50 % + locked wheel braking and about 10% traction (spin) + 100% traction.

Side slip angle

Side slip angle range: +/- 15 deg with brake cardan shaft connected. +/- 20 deg without brake cardan shaft connected.
Static calibration error less than 0.03 deg

On board watering system
Water film width: 200 mm
Nominal water film thickness: continuously variable from about zero to 8 mm at 100 km/h outflow speed.
Maximum flow rate: 45 litres/s

10.4.2.6 Software for Measurement Control

An electronic control and data acquisition system has been developed by VTI. Signals from the sensors in the measuring system are sampled at 200 Hz, filtered by a 25 Hz analog low pass filter, and collected in a PC by a measuring program. The program also controls the measuring sequence and presents preliminary data on the screen both during and after the measurement. Parameters recorded by the system are longitudinal, lateral and vertical forces, speed of measuring wheel, vehicle speed, test wheel angle in relation to vehicle, side slip angle, water pressure in the nozzle and time.

The measurement is started from the main menu of the program, see Figure 55, where also all sensor data is presented live during the measurement.

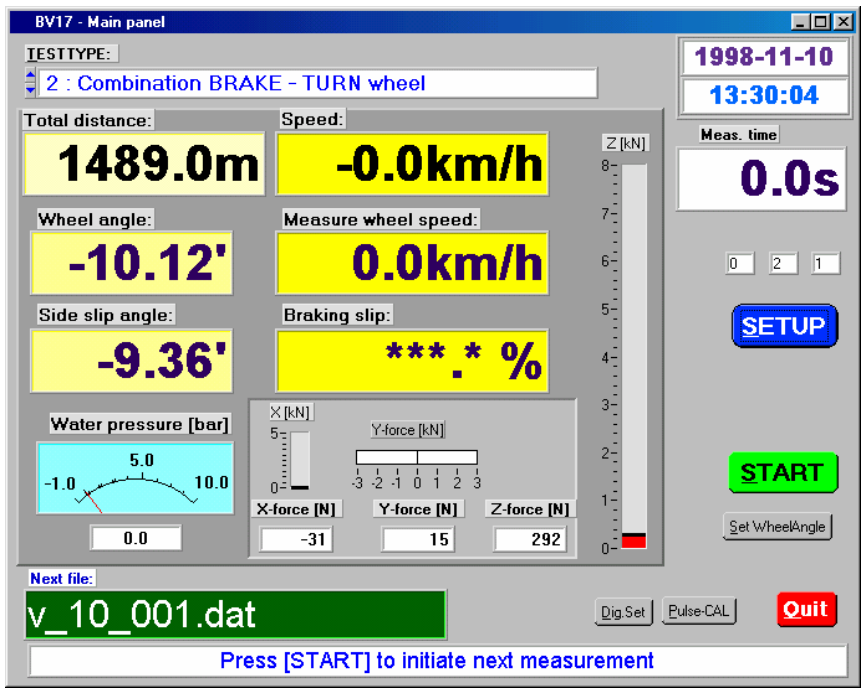


Figure 55. The main menu of the measuring program.

In the program several possible measuring sequences has been prepared. One of the more advanced measurements are the “Combination BRAKE – TURN Wheel”, see also Figure 55. For this measuring sequence a number of measuring parameters can be adjusted. An example of possible settings is shown in Figure 56.

Adjustable parameters are for example used wheel angles during each measuring sweep, delay times for brake application, wheel positioning and water on/off. The braking torque is applied following a ramp function where time constant and maximum value can be adjusted. The wheel is braked once for each chosen wheel angle, e.g. six times according to Figure 56, also seen on the forces in Figure 57. Each time the brake is applied, one friction/slip curve is generated. Each measuring sweep can then produce friction/slip curves for several slip angles as the wheel is sequentially turned and the break is applied once at each slip angle.

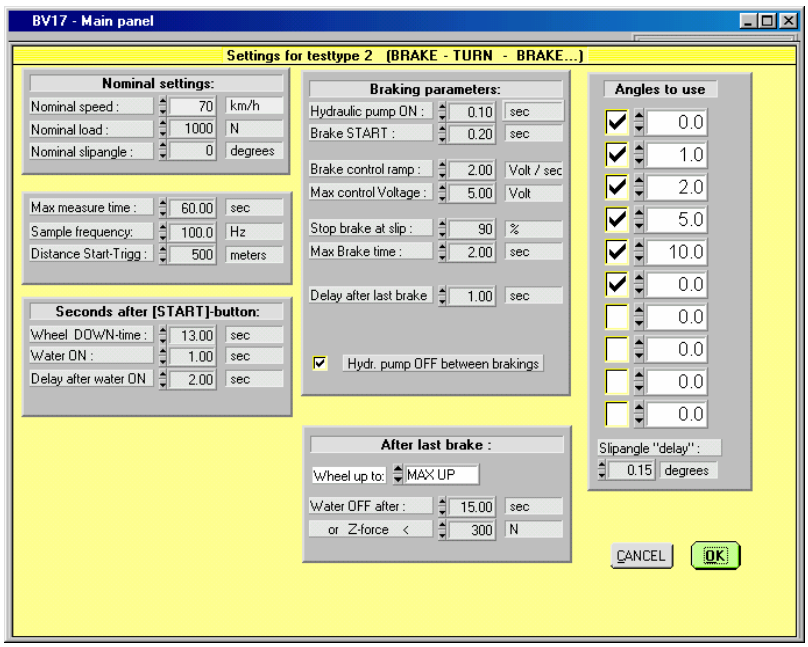


Figure 56. Menu for setting parameters for the brake/turn wheel measuring sequence.

When the measurement is finished, the program automatically raises the measuring wheel, turns off the water etc, and present graphs showing the measured parameters. An example of these graphs is seen in Figure 57.

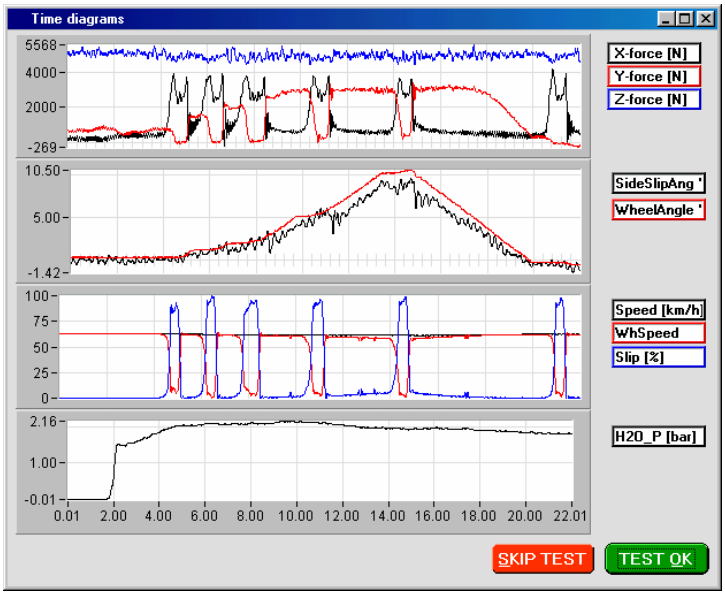


Figure 57. Graphs of forces, speeds, and wheel angles shown after completion of the measuring sequence.

10.4.2.7 Data acquisition and analysis

In the INTRO project the data collected from the measuring program was further treated using Matlab to extract the interesting combinations of variables. Typically, 4-6 complete brakings with zero slip angle were carried out during each test run. By performing two test runs per speed and load, about 10-12 separate slip curves was recorded for each setting. Due to mainly variations of the vertical load during a measurement, but also from variations of the surface friction, this is typically the number of slip curves needed to produce a good average slip curve. The effect of vertical load oscillations is illustrated in Figure 58, where six consecutive brakings are presented. The average of these six curves is shown in Figure 59. This average was constructed by dividing the x-axis into small segments and for each segment calculating the vector average of all measurement points contained in the segment. This averaging method was used in the INTRO project with no measurement curve, nor measurement point, excluded from the average process for each set of measurement condition.

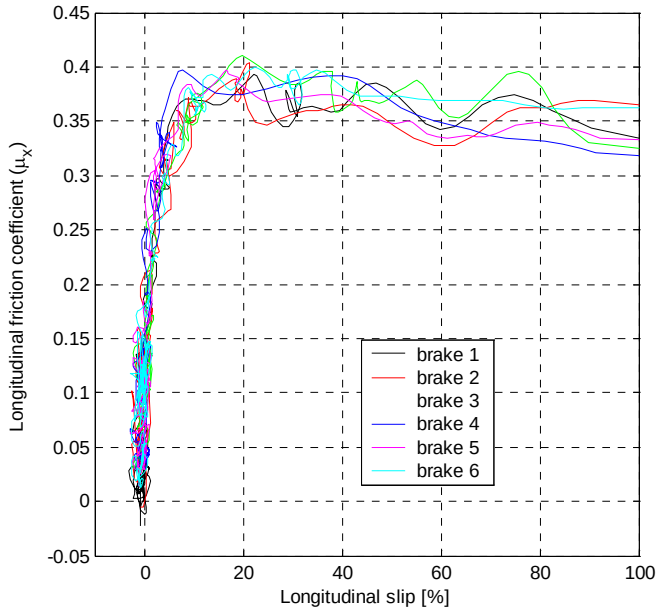


Figure 58. Example of six consecutive brakings with the BV12 on snow at 20 km/h.

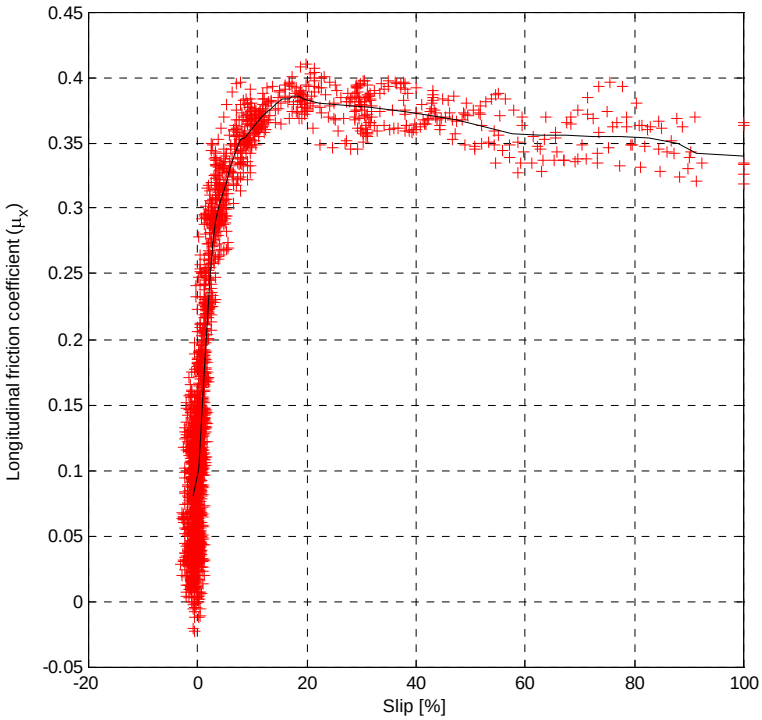


Figure 59. An average slip curve constructed from the six brakings in Figure 58.

10.4.2.8 Contact

Questions about the equipment and measuring services can be directed to the National Swedish Road and Transport Research Institute (VTI).
581 95 Linköping Sweden.
Fax + 46 13 14 14 36
Tel. + 46 13 20 40 00
Contact person: Dr Mattias Hjort

10.4.3 ADHERA

ADHERA 2 is the mlpc equipment designed to measure the Longitudinal Friction Coefficient (LFC) with blocked wheels, on wet pavement.

Combination of the test results at different speeds allows quantifying the skid of the pavement. A car type wheel, on which a fixed vertical load is applied, is pulled at constant speed by a tractor vehicle also ensuring water spraying of the pavement. The tire is the standard PIARC smooth tyre. The wheel being prevented from rotating along a distance of 20 m or so, the average torque ensuring balance with the friction torque exerted by the pavement on the tire is then measured.



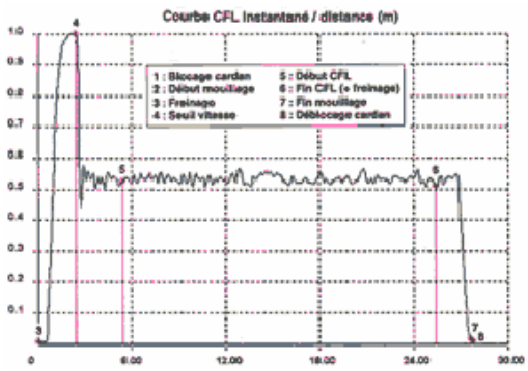


Figure 60. View of ADHERA 2 device and example of data recording

The measuring wheel and its servo-brake are carried by a rigid girder the mode of which is close to that of the components of a private car. The 250 daN load on the wheel consists of a structure attached to the girder through an original suspension/shock-absorber system. The service equipment units, designed as modules which can be readily installed on board different types of tractor vehicles, consist of a water tank, a water spraying module (variable spraying flow rate), and an electronic control and measurement module. Power supply to the assembly is ensured by a separate thermal unit.

During the tests, the tractor vehicle and trailer are rigidly connected together through a universal joint brake. The measurement can be performed in the traffic flow. The control station, fully computerized, provides guidance to the operator for the performance of the tests, while displaying the information collected, and providing the possibility of editing hard copies of the results.

10.4.4 NIRA car (Audi A3) and Toyota Verso

10.4.4.1 Internal Sensors (Audi A3)

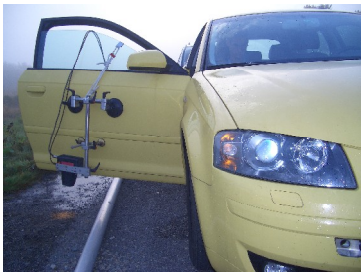


Figure 61. NIRA Car (Audi A3) with external Sensors

The NIRA Car Audi A3 is equipped with a micro slip measurement device (NIRA DYNAMICS) and CAN-Bus reader interface. The internal car sensors for ESP/ABS are connected to the CAN communication bus. The relevant data readout is listed in table - .

Tabelle 10-1: CAN-Bus list of internal sensors and microslip measurements

	Time in hour:minute:second,millisecond
t:	format
v:	Speed in m/s
ax:	Longitudinal acceleration in m/s^2
ay:	Lateral acceleration in m/s^2
w_xx:	Angular velocity for wheel xx in rad/s
tau:	Engine tourque in Nm
RPM:	Engine RPM
Beta:	Steering wheel angle in degrees
Psidot:	Yaw-rate in degrees/s
brake:	1 if brake is active 0 otherwise
clutch:	1 if clutch is active 0 otherwise
myMax:	Estimated friction coefficient
Te:	Engine temperature in degrees Celsius
Ta:	Ambient temperature in degrees Celsius
my_xx:	Normalized traction force for wheel xx
s_xx:	Wheel slip for wheel xx in rad/s
mark:	Current pavement mark
k:	slip slope
off:	1 if system is inactive 0 if the system is active

xx: Two-letter wheel identifier, FL = FrontLeft, FR = FrontRight, RL = RearLeft, RR = RearRight

10.4.4.2 Applied (External) Measurement Systems (Audi A3 / Toyota Verso



Figure 62. The Toyota Verso with mounted external measurement device

The external measurement system consists of an accelerometer and an optical velocity sensor:

- Capacity triaxial-accelerometer Typ 8393A2 (Kistler)
- Correvit L-CE CORRSYS Datron optical velocity Sensor
- DT BNC-Box USB of DT 9800-EC (A/D-conversion)
- Signal amplifier for accelerometer
- Laptop

10.4.5 Peugeot 406

In this section, we present our vehicle : a Peugeot 406, systems of measurements embedded in the car and the signal processing.

10.4.5.1 Vehicle

The vehicle used is a Peugeot 406 (year 1998) (see Figure 63)



Figure 63. Peugeot 406

- The suspension is a pseudo Mc-Pherson with triangle and stabilizer bar.
- The rear suspension is a multi arm one.
- ABS is a 5th generation Bosch
- Mass is 1435 kg (without passengers with all tank full).
- Wheelbase is 2,70 m.

10.4.5.2 System of measurement

• **inertial system**
The used gyroscope is an inertial central Crossbow VG700AA-201 d. This system is dedicated to car test. Its technology is MEMS



Figure 64. Inertial system Crossbow VG700AA-201

The performance are :

- Longitudinal acceleration: ± 2g, accuracy <± 1%.
- Transversal acceleration: ± 2g, accuracy <± 1%.
- Vertical acceleration: ± 2g, accuracy <± 1%.
- Yaw velocity: ± 200°/s.
- Roll velocity: ± 200°/s, angle : ± 180°.
- Pitch velocity: ± 200°/s, angle : ± 90°.

• **Longitudinal speed sensor**
The Correvit DLS1 from Datron is used for speed measurements.

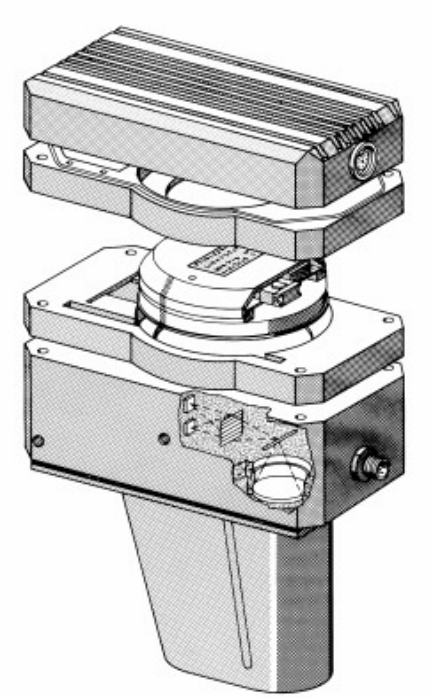


Figure 65. Correvit Datron DLS1

The speed measurement is based on an optical sensor. It analyzes the variation of the spatial frequency induced by the motion. A signal processing delivers the longitudinal speed.

Its performances are :

- Linearity : 0.2%.

• Wheel encoders.

We use two types of encoders : encoders Hengstler RI-58 with 10000 pulses by turn. This encoder is very accurate. It gave very sound information during braking procedure. However, we had too much outliers data and we cannot use the signal delivered by this sensor during all the tests. It is the reason why, we uses less precise and more robust sensor : encoder IVO GI 355



Figure 66. Encoder 10 000 pulses/turn Hengstler RI-58

• **Torque sensor:**
Two torque sensors are mounted on the two transmission shaft. They deliver the torque during traction.

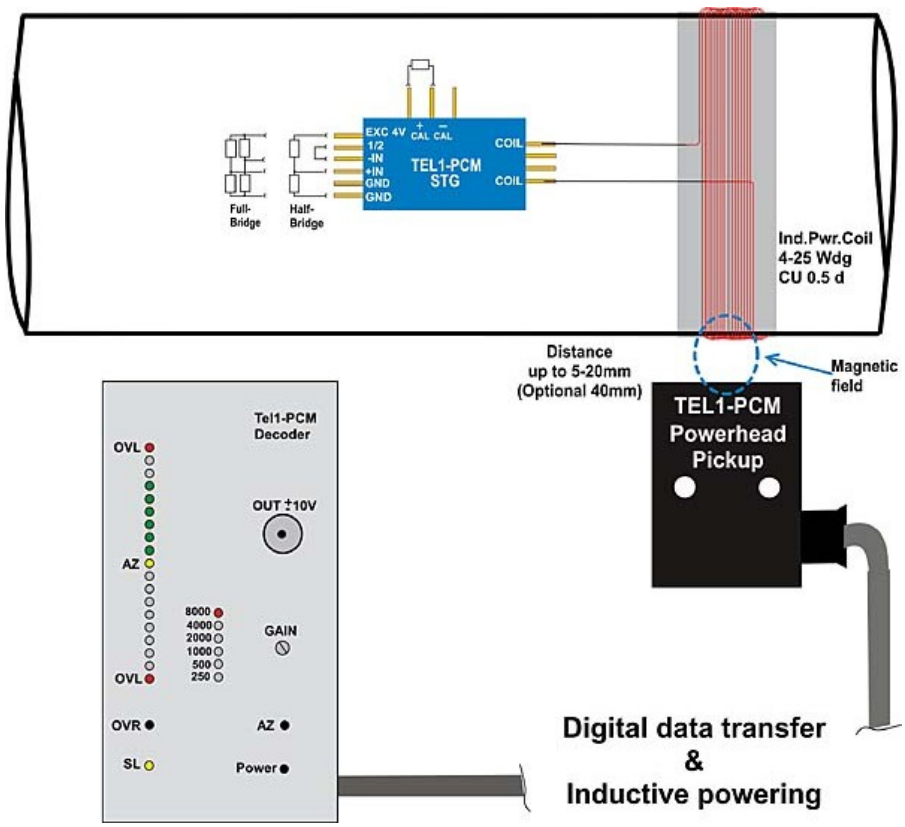


Figure 67. Torque sensor

The evaluation of this system is still in progress. However, the accuracy is very good and seems to be below 1%.

• **Tyre radius measurement :**

The tyre radius ($\mathrm{Re}\ ff$) is given by a laser : Optmess M_PSD 3040. r.



Figure 68. Laser sensor for tyre radius measurement

10.4.5.3 Data acquisition

A PC with two national instruments cards was used during the test (located in the car's boot) :

- An analogic card : NI 6071 E, 12 bits, 64 voies d'acquisitions
- A count card NI 6602, 32 bits, 8 voies d'acquisitions

The software Labview drives these cards and saves the data. The sampling time was 1 millisecond.



Figure 69. PC with Labview

10.4.5.4 Estimation of wheel slip (κ)

In order to compute κ, according to equation (6), we need to know the longitudinal speed V , the angular speed of the wheel and the effective radius tire($\mathrm{Re}\ ff$).

- Angular speed

We use the encoders in order to compute this angular speed. We need a very high accuracy. For example, one of the specifications was to have the maximum information during the braking process with ABS before the action of the ABS. It means that we are looking for some information when κ moves from about 0 to about 0.15. This evolution is very quick : less than 0.2s.

With an encoder at 1000 pulses/turn, it implies that the evolution of the speed is from about 11 pulses/ms to about 10 pulses/ms. It is clear that we have a problem of resolution. In order to improve the resolution, there is two ways either we use an encoder with a better resolution or we filter the signal. We tried to use a more accurate encoder but it was not enough robust. So, we filtered the signal with a butterworth filter under Matlab at 15 Hz (15 Hz = about 100 samples are required to compute a enough accurate angular speed).

Moreover, during the test when the high resolution encoder was available, we observed sinusoid in the angular speed which seems to be due to the mechanical link between the encoder and the suspensions as explained below.

Figure 70 to Figure 73 show the difference between two sampling time of the information given by the encoders, just after braking: about 0.2s after the first deceleration due to the braking action. Oscillations at about 20 Hz are observed. These oscillations are detected at different speed (see Figure 70: test at 40 km/h and Figure 72: test at 80 km/h) and with or without ABS : (see Figure 71 and Figure 73). It is the reason why, we analyze these oscillations as a transient part of the response of the mechanical link between the encoder and suspension. For mechanical reason, this link has to be elastic. The braking force excites this link which noises the encoders signal. However, this is simply an assumption. This serves as an additional argument to use a low pass filter (5 Hz).

- Longitudinal speed

The delay of the Correvit sensor is too significant compared to the small duration of the most interesting part of braking (before reaching μ_{max}). That is the reason not to use this signal directly. The longitudinal speed is computed by using the encoder signals of the rear wheel.

Kommentar [S1]: Skip most important - transient instead?

- Tire radius

As the signal of the laser sensor was too noisy, we prefer to use a simplified model of tire which is considered as an elastic body. We compute the normal force as explained below and after estimating a stiffness of the tire, we deduced a tire radius.

10.4.5.5 Estimation of friction coefficient (μ)

For simplicity, we compute a global front normal reaction of the ground : F_z for the two wheel and a global longitudinal friction force F_x . We divide these quantities by two in order to get it for one wheel. The computation of F_x and F_z is mainly based on the signal delivered by the longitudinal accelerometer of the inertial central

F_x is computed with the equation (2) by using the longitudinal accelerometer and the longitudinal speed given by the rear wheel (as explained above)

F_z is computed with the equation (3) and (4) by using the longitudinal accelerometer.

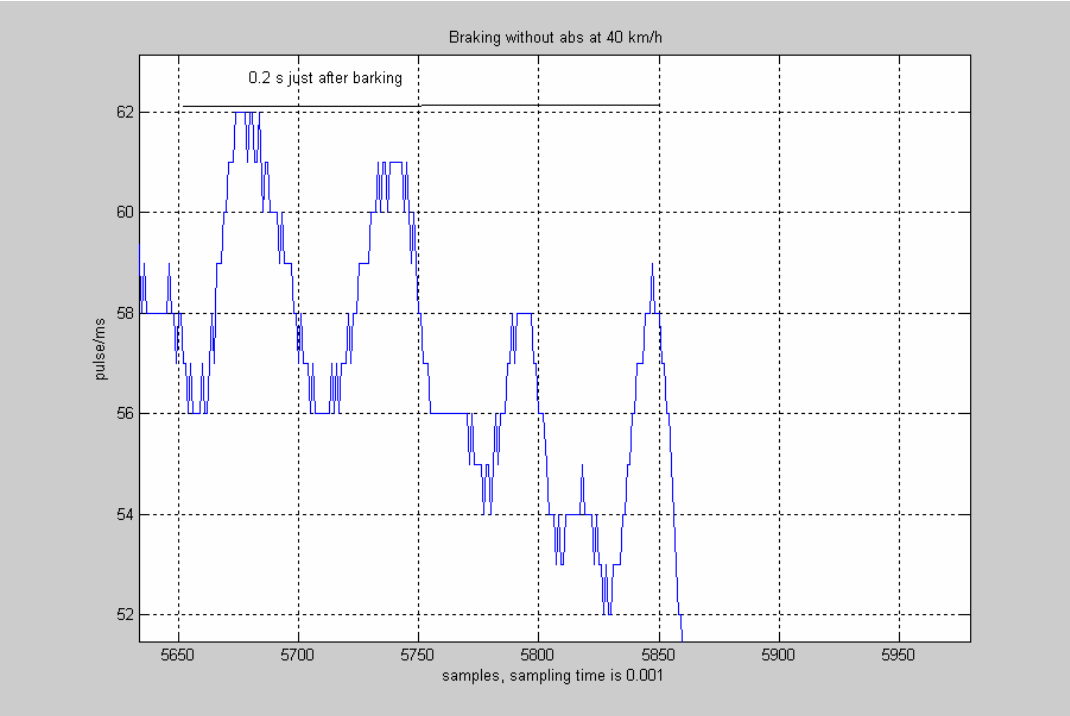


Figure 70. Braking without ABS at 40 km/h – Analysis of encoders signal just after braking

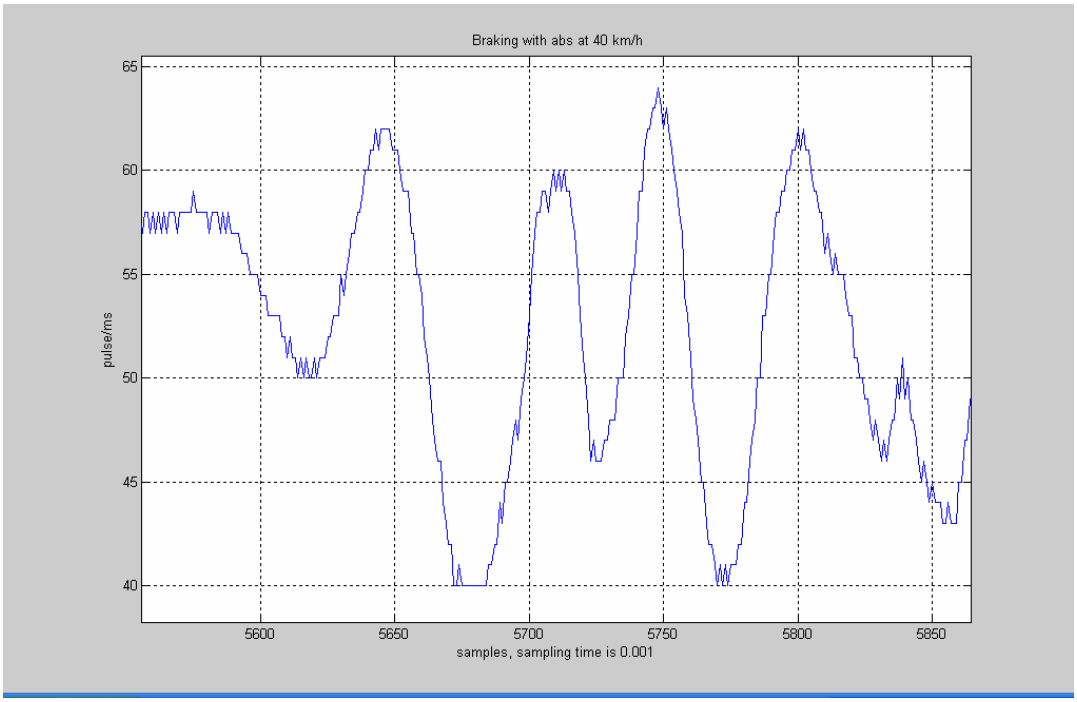


Figure 71. Braking with ABS at 40 km/h – Analysis of encoders signal just after braking

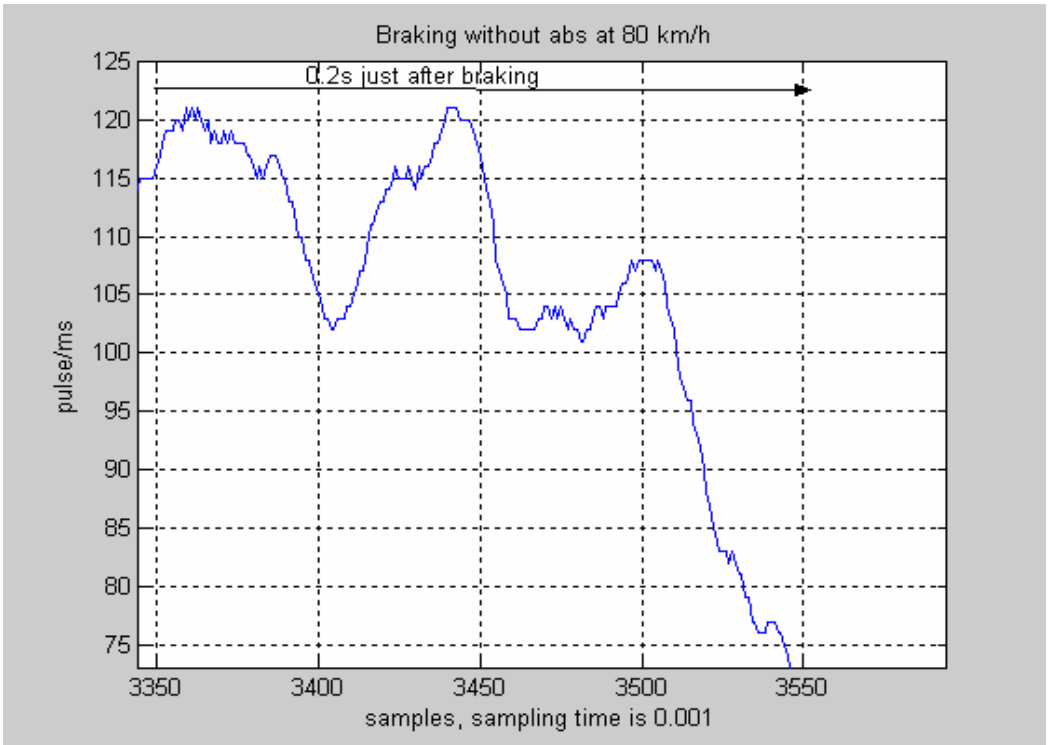


Figure 72. Braking without ABS at 80 km/h – Analysis of encoders signal just after braking

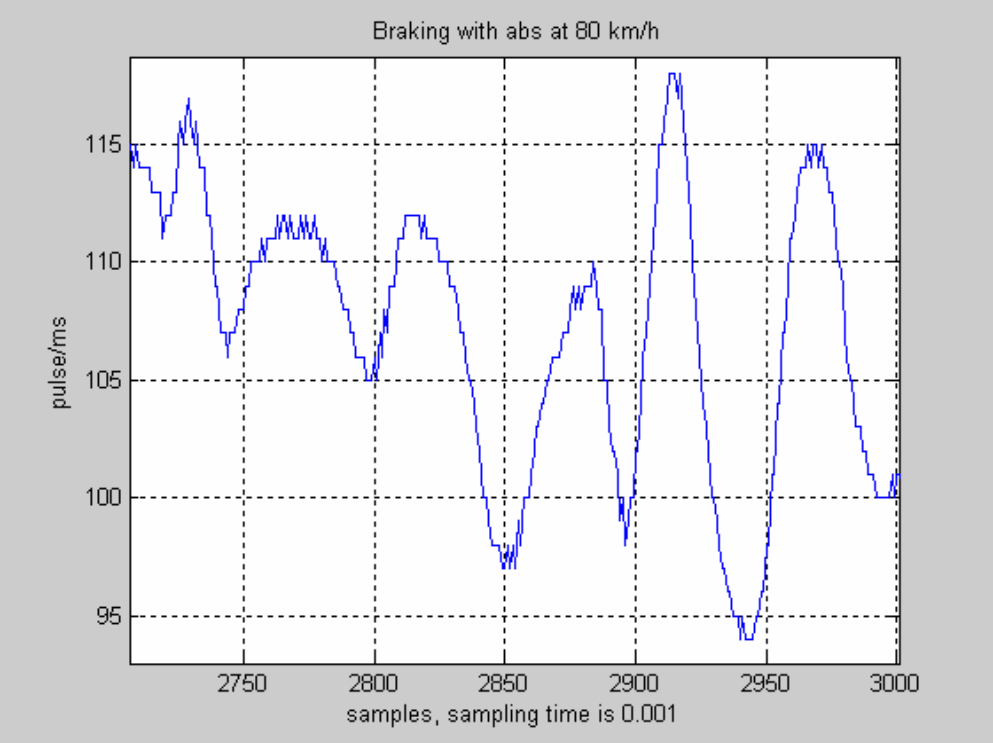


Figure 73. Braking with ABS at 80 km/h – Analysis of encoders signal just after braking